5-2017

Quantification and Evaluation of Long-term Draindown and Its Influence on the Raveling Susceptibility of Open-graded Friction Course

Kimberly Renee Lyons
Clemson University, krlyons@g.clemson.edu

Follow this and additional works at: https://tigerprints.clemson.edu/all_dissertations

QUANTIFICATION AND EVALUATION OF LONG-TERM DRAINDOWN AND
ITS INFLUENCE ON THE RAVELING SUSCEPTIBILITY OF OPEN-GRADED
FRICTION COURSE

A Dissertation
Presented to
the Graduate School of
Clemson University

In Partial Fulfillment
of the Requirements for the Degree
Doctor of Philosophy
Civil Engineering

---

by
Kimberly Renee Lyons
May 2017

Accepted by:
Dr. Bradley J. Putman, Committee Chair
Dr. Prasad R. Rangaraju
Dr. Julie P. Martin
Dr. Amir Poursaee

ABSTRACT

A porous pavement is a type of sustainable pavement that allows stormwater to infiltrate through the pavement into the natural soil bed. An open-graded friction course (OGFC) is a type of porous asphalt mixture that is commonly used as a wearing course typically having a thickness less than 1.5 inches that is constructed over a conventional asphalt surface. This porous wearing course is used to improve the frictional resistance of pavements and minimize hydroplaning on highways.

Raveling is a defect commonly seen in OGFC because of the limited amount of fine aggregates in the mix. This reduction in fine particles from the aggregate matrix causes a reduction in the number of contact points between aggregate particles. This reduction in contact points limits the amount of asphalt binder that is able to bind coarse aggregate particles together. The fewer the contact points between aggregate particles; the more likely raveling is to occur on the surface of the pavement (Shaowen and Shanshan, 2011).

Previous studies have been conducted on the draindown that occurs during production and hauling of the asphalt binder due to gravitational forces. However, only a few studies have been conducted on the draindown of asphalt binder after installation, over the service life of the pavement. For the purpose of this research study, "long-term draindown" is defined as the downward migration of asphalt binder through the pore structure of an open graded friction course over the service life of the structure after construction.

OGFC can also exhibit clogging of the pore structure caused by the gravity-induced draindown (long-time draindown) of asphalt binder from the top to the bottom of the OGFC pavement layer over the life of the pavement. This can cause a reduction in the binder film thickness surrounding the aggregate particles near the surface and potentially lead to an increase in the raveling susceptibility of the OGFC mix design while clogging the accessible air voids of the structure. The decrease in binder thickness surrounding the aggregate particles and oxidation of the remaining binder film near the surface of the pavement can lead to an increase in raveling susceptibility of OGFC.

This research study evaluated and quantified long-term draindown and its influence on the raveling susceptibility of OGFC. In order to effectively evaluate the effects of long-term draindown on the raveling susceptibility of OGFC and identify the underlying mechanism; new laboratory test methods were designed and compared to the existing test method that is currently used to evaluate the raveling susceptibility of OGFC.

The new laboratory test methods focused on simulating the forces commonly applied to the surface of OGFC during its service life and showed more of a correlation to the direct shear and indirect tensile strength tests. This indicates that the two new test methods show more of a cohesive failure with minimal fracturing of the aggregate particles compared to the existing test method (Cantabro). The long-term draindown was quantified using image analysis and a Draindown Factor [D_F] was calculated. The D_F indicated that long-term draindown does have an influence on the raveling susceptibility

of the surface of OGFC mixture. The mixture becomes more susceptible to raveling as

draindown increases (i.e., higher the D_F).

DEDICATION

I would like to dedicate this dissertation to:

My parents, Tony and Pamela Lyons

For earning an honest living for me and my brother, and teaching me to believe in hard work, education, and to be an honest, hardworking, driven person who does what is right above all else. Your constant love and support throughout my entire education is truly one of a kind.

My grandparents, Francis and Patricia Bessinger

For supporting me through this whole, hard process and encouraging me to believe in myself. I am very lucky to have whom I consider the coolest, most generous and loving grandparents around.

My dearest and closest friends, George Lyons, Ellen Ross and Matthew Shuler

For their constant support throughout my entire education, both the good and bad times. I have been fortunate enough to have been blessed with the best friends anyone could ask for. We share a special love from above that will always leave a mark embedded deeply within my heart.

Thank you all for standing by my side and supporting every decision I have made. It is wonderful to know that I have such a great support system and love from all of you.

ACKNOWLEDGEMENTS

To my advisor, professor, and committee chair, Dr. Bradley J. Putman, for his inspiration and guidance throughout my time at Clemson University. I appreciate all of his contributions of time, funding, and ideas that made this research project possible.

To my committee members Dr. Julie Martin, Dr. Prasad Rangaraju, and Dr. Amir Poursaee, for their instructions and assistance with developing and completing this dissertation. I would also like to thank the graduate students (Venkat Kothala, Eric Kim, and Behrooz Danish) and Gordon Wright from Lane Construction that helped me complete my research. Their assistance, words of encouragement and efforts in the lab were appreciated.

To my parents, Tony and Pamela Lyons for their love and financial support throughout this whole process. To my grandparents, Francis and Patricia Bessinger, for their love and support. Without their unconditional love and support throughout my academic career, none of this would have been possible.

To Scott Black and Danny Metz for their help and efforts in the lab, and the building and design of the lab equipment necessary for completion of this research. Without this support, the completion of this research study would have been impossible.

TABLE OF CONTENTS

Table of Contents (Continued) Page

Table of Contents (Continued) Page

LIST OF FIGURES

xiii

List of Figures (Continued) Page

LIST OF TABLES

CHAPTER ONE

INTRODUCTION

Raveling Susceptibility of Open-Graded Friction Course

Open graded friction course (OGFC) helps improve the frictional resistance of

pavements by removing water from the surface of the pavement. This is achieved by

allowing the water to flow through the internal structure of the OGFC layer by way of

interconnected air voids. OGFC pavements are important especially for use on high speed

roadways such as interstate highways because the increase in permeability improves the

frictional behavior during wet weather while reducing the dangers of splash and spray

and hydroplaning due to increased drainage from the pavement surface.

The design of OGFC mixtures have to be modified from the traditional mix

design in order to meet the high air void content requirement. The high air content, while

necessary for OGFC mixes, leads to an increased potential for raveling and accelerated

aging, as oxygen has access to a higher surface area of the mixture (Kandhal and Mallick,

1998). Raveling is the dislodgement of aggregate particles from the surface of the

pavement. This can result from the loss of asphalt binder from the surface, oxidation,

traffic loads, weather conditions, asphalt mix design, and inadequate compaction of the

asphalt during construction (Porous Pavement 2012).

OGFC can also exhibit clogging of the pore structure caused by the gravity-

induced draindown of asphalt binder from the top to the bottom of the OGFC pavement

layer. Additionally, this binder draindown can result in a reduction in the binder film thickness surrounding the aggregate particles near the surface that could potentially lead to an increase in the raveling susceptibility of the OGFC mix design while clogging the accessible air voids of the structure.

In a study conducted by Putman and Lyons (2015), the long-term draindown of OGFC specimens was evaluated by measuring the permeability of mixes throughout an 84-day conditioning period at 140°F (60°C). Even though the study showed evidence of long-term draindown based on the permeability reduction of the specimens over time, the question of what is happening to the binder on the internal structure of the specimens still needs to be quantified and explained (Putman and Lyons, 2015).

Abrasion resistance of compacted asphalt specimens is commonly measured by the Cantabro abrasion loss test (ASTM D7064). For comparative measurements, the Cantabro test is simple, inexpensive, and quick; however, the stress exerted on the specimens (impact resulting from rotating in a drum) is not representative of the stress caused by traffic (Herrington et al 2005).

OGFC has an increase in raveling susceptibility when compared to other asphalt mixture pavements; therefore, there is a need for further investigation into the test method used to quantify the raveling susceptibility of an OGFC mix as well as what causes premature raveling. The development of a new test method that is more representative of the frictional forces being applied to the OGFC pavement surface over its service life needs to be investigated. Additionally, an investigation into the long-term draindown of

OGFC and how it effects the raveling susceptibility of the surface of the pavement needs to be conducted. This is important because it directly effects the performance of OGFC over its service life. This study will provide information that will be helpful in improving the mix design of OGFC to reduce the raveling susceptibility of OGFC. Reduction in the raveling susceptibility will improve the frictional resistance of the pavement, which will minimize hydroplaning, thus making them safer during rainy weather. This study will also provide useful information to transportation agencies related to cost and maintenance of OGFC.

Research Objectives and Scope

The primary objective of this study was to evaluate and quantify long-term draindown, and investigate how long-term draindown influences the raveling susceptibility of OGFC. In order to effectively evaluate the effects of long-term draindown on the raveling susceptibility of OGFC and identify the underlying mechanism(s); new laboratory test methods were designed and compared to the existing test method that is used to evaluate the raveling susceptibility of OGFC. The new laboratory test methods focused on simulating the forces (stresses) commonly applied to the surface of OGFC during its service life. To accomplish this objective, the following tasks were completed:

1. A detailed review of literature related to porous asphalt, the raveling susceptibility of OGFC, and long-term draindown of OGFC.

2. Prepared specimens with plant-mix asphalt.

3. Evaluated the volumetric properties and the abrasion resistance of both un-aged and aged asphalt specimens using different abrasion test methods.

4. Evaluated and quantified long-term draindown using image analysis and direct measurement of binder content using the ignition oven.

<u>Organization of Dissertation</u>

This dissertation is divided into five chapters. The first chapter is the introduction, which provides background information on the research topic as well as the research objectives. The second chapter is an extensive literature review, which includes information on porous asphalt, open-graded friction course (OGFC), warm mix technologies and long-term draindown of OGFC. The third chapter describes the experimental materials and procedures used to complete the research. The fourth chapter of this dissertation discusses the results of the research. Finally, the fifth chapter completes the manuscript and presents the conclusions of the research project while providing recommendations for implementation and future research.

CHAPTER TWO

LITERATURE REVIEW

<u>Porous Asphalt</u>

Asphalt is a composite material that consists of mineral aggregates bound together with a black, oily, viscous material known as bitumen. Bitumen is a mixture of hydrocarbons obtained naturally or as a residue from petroleum distillation that is made up of 83% carbon, 10% hydrogen, and smaller amounts of oxygen, nitrogen, and other elements. Bitumen has a low molecular weight and its rheological properties change based on temperature: at lower temperatures it is brittle and rigid, room temperature it is flexible, and at higher temperatures, it flows as a liquid (Hirst, 2016).

Porous asphalt, also known as permeable asphalt, is standard hot mix asphalt with reduced sand or fines. Porous asphalt mixtures generally consist of high amounts of coarse aggregate with gap gradations, and small amounts of fine aggregate and asphalt binder (Shaowen and Shanshan, 2011). The reduced amount of fines leaves interconnected, stable air pockets in the asphalt mix that allow stormwater to flow through the asphalt. The stormwater then enters a crushed stone aggregate bedding layer and base. The aggregate storage bed will retain the water until it can soak into the native soil below. A representative cross-section of porous asphalt can be seen in Figure 2.1. Porous asphalt has a higher air void content (18-22%) compared to conventional asphalt (Shaowen and Shanshan, 2011).
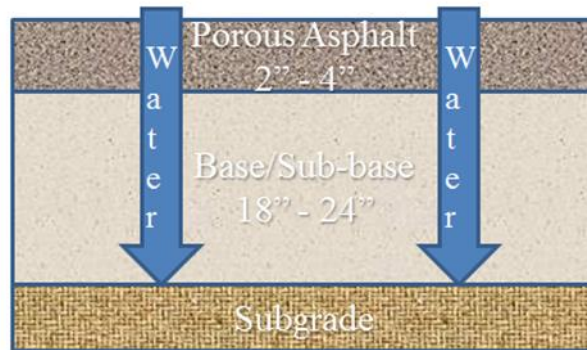
Figure 2.1- Typical Porous Asphalt Pavement Section

Open Graded Friction Course

Open graded friction course (OGFC) is a type of porous pavement that is used as a sacrificial wearing course to improve the frictional resistance of pavements and minimize hydroplaning on highways (Figure 2.2). OGFC is normally used as a 1 to 1 ½ - inch thick surface course over normal dense graded pavements in areas that experience high traffic volumes and moderate to heavy rainfall (Caltrans, 2006). The porosity in porous asphalt and OGFC is a function of the gradation and quantity of the coarse aggregate in the mixture**.** By increasing the proportion of coarse aggregate and reducing the amount of fine aggregate in the mix design, the porosity can be increased (Hardiman 2005). The higher porosity allows water to run through the aggregate matrix and away from the surface of the pavement (Shaowen and Shanshan, 2011), making it safer for drivers during wet conditions (Poulikakos and Partl, 2009).

Figure 2.2- Typical OGFC Pavement Section

Higher pavement temperatures occurring in summer months can cause two kinds of pavement failure in OGFC due to long-term gravity induced binder draindown: clogging of the pore structure and raveling of the pavement surface. Clogging is when the pore structure of the pavement becomes filled with surface debris and binder, and can occur due to "long-term draindown" of the asphalt binder during high temperatures in the summer months. It has been speculated that thick films of unmodified asphalt binder liquefy due to the increase in pavement temperature during hot summer months, then drain down due to gravity. The remaining thin films of asphalt binder coating the aggregates then age more rapidly, becoming brittle (Huber, 2000).

Effects of Long Term Draindown

Many studies have been conducted on draindown during production and hauling, but there have been limited research on the draindown of asphalt binder after installation over the life of the pavement. Draindown is a term that is used to describe the downward migration of asphalt binder from around the aggregate particles while warm, during both production and installation of the material (Ferguson, 2005). For the purpose of this research study, "long-term draindown" is defined as the downward migration of asphalt binder due to gravitational forces through the pore structure of an open graded friction course over the service life of the structure.

In a study conducted by Putman and Lyons (2015), the long-term draindown of OGFC specimens was evaluated by measuring the permeability of mixes every 14 days over a 84-day conditioning period at 140°F (60°C). The study showed a steady decrease in the permeability of the conditioned specimens for the first 56 days of conditioning. This showed evidence of long-term draindown based on the permeability reduction of the specimens over time due to the internal air voids becoming clogged over the conditioning period (Putman and Lyons, 2015).

In order to explain what was happening to the binder internally in the structure of the specimens, Putman and Lyons conducted an additional study on the specimens that were aged for 84-days. Each specimen was sliced into four sections horizontally, and the percent binder content was determined for each slice. The study found that the binder content for the top slice was less than that of the original binder content of the asphalt

mix design, where the bottom slice had a higher binder content. This indicated that the binder was draining downward over time (Putman and Lyons, 2015).

<u>Asphalt Binder Modifications</u>

Several techniques can been used to minimize the occurrence of draindown such as the use of modified asphalt binders, addition of cellulose fibers, the use of warm mix asphalt technologies, and the addition of ground tire rubber. The following is a list of the different types of modifiers used for asphalt modification: block copolymers (SBS), SBR latex, Polyolefins, crumb rubber, chemical additives, and engineered binders (Kluttz, 2012). Martinez-Boza et al stated that in order to increase the service life of pavements over a wide range of temperatures, especially higher temperatures, the addition of polymers to bitumen are important. Copolymers such a styrene-butadiene-styrene (SBS) are used to improve bitumen and have proven to be very effective modifiers for bitumen (Martinez-Boza et al 2001).

Polymer modified binders are less susceptible to higher temperature changes than unmodified asphalt binders which helps to improve the performance of the pavement over its lifetime. Polymer modified asphalt binders are widely used to help withstand increased traffic volumes and loads in higher temperature areas and locations (Yildirim, 2007). A study conducted by Mogawer et al showed that modified asphalt binders had higher elastic recovery and better resistance to fatigue cracking than unmodified binder (Mogawer et al, 2011). The performance of polymer modified binders depends upon the stiffness of the base binder, cross-linking between the base binder and polymer, type of

polymer, and the quantity of the polymer (Shirodkar et al. 2012). In a study conducted

by Lu and Isacsson, the results indicated that SBS modified bitumen present better

rheological properties than equivalent base bitumen, which increases the long-term

durability of asphalt pavements (Lu and Isacsson, 1998).

Warm mix technology is another modification used to alter the properties of

asphalt mixtures. Warm mix asphalt (WMA) is a type of asphalt that is produced using

warm mix technologies that allow producers of hot mix asphalt (HMA) to lower

production and construction temperatures by 30 to 120 degrees Fahrenheit. WMA

technologies reduce the viscosity of the asphalt binder so that aggregates can be coated at

lower temperatures. Reducing the viscosity also makes the mixture easier to manipulate

and compact at the lower temperature (Warm Mix Asphalt, 2016).

<div align="center">Effects of Aging on Bitumen</div>

Aging of asphalt binders occurs during the mixing, placement and over the

service life of the asphalt pavement. The aging of asphalt binders primarily occurs due to

the volatilization of light oils present in the chemical makeup of the binder and oxidation

caused by the air surrounding the asphalt pavement. Oxidation of asphalt binders occurs

at a relatively slow rate. Oxidation and loss of light oils leads to an increase in stiffness

and a reduction in the flexibility of the binder (Lavin, 2003). Aging of the asphalt binder

is one of the primary factors behind the deterioration of asphalt pavements.

Lu and Isacsson found that there are two primary effects of aging on the behavior

of asphalt binder. The first mechanism is the impact that aging has on the rheological

<div align="center">10</div>

properties of the asphalt binder such as oxidation, loss of volatile components, and migration of oily components from the bitumen into the aggregate. The second mechanism is physical hardening, a reversible process in which the stiffness of the asphalt binder increases at constant low temperatures. In a study on bitumen aging by Lu and Isacsson, they found that aging influences the chemical and rheological properties of the bituminous binder and that the chemical and rheological changes are generally not consistent (Lu and Isacsson, 2002).

The decrease in binder thickness around aggregate particles and oxidation of the remaining binder film near the surface of the pavement can lead to an increase in raveling of OGFC. Raveling occurs on the surface as a result of the dislodgement of aggregate particles; it is a loss of fine and coarse aggregates from the asphalt matrix (Mathaven et al 2014). In addition to high and low temperatures, there are several factors that contribute to raveling. Raveling can be caused by inadequate compaction during construction, ingress of water, aggregate segregation, and high traffic loads (Mitchell, 2014). An asphalt pavement requires a high density during construction in order to develop sufficient cohesion between aggregate particles. Inadequate compaction during construction reduces this cohesion, thus resulting in raveling of the pavement surface. Mechanical wear by studded tires, snowplow blades and tracked vehicles can also occur especially in colder regions (Raveling, 2009).

<u>Raveling of OGFC</u>

Raveling is commonly seen in porous asphalt mixtures such as OGFC because of the reduction in fine aggregates. Figure 2.3, shows raveling of OGFC on Interstate-20 in Lugoff, SC. If fine particles are missing from the aggregate matrix, then the asphalt binder is only able to bind coarse aggregate particles at relatively few contact points. The fewer the contact points between aggregate particles; the more likely raveling is to occur on the surface of the pavement (Shaowen and Shanshan, 2011). The fine aggregate usually wears away first but as the erosion continues, larger particles are broken free from the matrix. Over time the pavement has a rough and jagged appearance typical of surface erosion (Mathaven, 2014). This reduction in surface aggregates leads to a decrease in the ride quality of the pavement and eventually leads to more severe problems.

Figure 2.3- Raveling of OGFC on I-20 in Lugoff, SC

Laboratory studies have shown that a better performing OGFC pavement can be achieved by using a coarser gradation for OGFC mixes. Mixes with 15% or less of aggregate passing the 4.75 mm sieve are vulnerable to significant binder draindown and it is recommended to provide a suitable stabilizer such as polymer-modified binders or fibers in the mix to prevent excessive drain-down. The use of both polymer-modified binder and fiber can minimize the abrasion loss and thus increase the durability of OGFC (Mallick et al 2000).

The durability of asphalt pavements is extremely important from both ride quality and safety aspects. Durability is one of the most important properties of asphalt as pavements are expected to perform over longer periods of time. Raveling and loss of material eventually leads to potholes which reduces the durability of the pavement (Mitchell et al, 2014). Raveling of an asphalt pavement can result in loose debris on the pavement, roughness of the pavement surface, water collecting in the raveled locations resulting in vehicle hydroplaning and stripping, and loss of friction, which reduces the skid resistance of the pavement. Stripping is the loss of bond between aggregates and asphalt binder due to moisture or poor aggregate-to-asphalt binder chemistry. When stripping begins at the surface and progresses downward, it usually results in raveling (Raveling, 2009).

Abrasion resistance of compacted asphalt specimens is commonly measured using the Cantabro abrasion test (ASTM D7064). The test is conducted by recording the initial weight of the specimen, then placing the specimen in the Los Angeles abrasion apparatus

for 300 revolutions without the steel charge at room temperature. Once the 300 revolutions are complete, the specimen is removed and the final weight is recorded. The percent mass loss is then calculated by dividing the mass loss by the initial mass of the specimen. For comparative measurements, the Cantabro test is simple, inexpensive, and quick; however, the stress exerted on the specimens (impact resulting from rotating in a drum) is not representative of the stress caused by traffic (Herrington et al 2005).

Abrasion loss is used to evaluate the resistance to disintegration of porous asphalt mixes (Hardiman, 2005). Hardiman found that polymer modified binder (SBS) mixes were found to be more resistant to disintegration compared to conventional (penetration grade 60/70) asphalt mixes. The permeability and resistance to abrasion loss decreases when the maximum aggregate sizes in porous asphalt decreases (Hardiman, 2005). In a study conducted by Putman, a decrease in the abrasion loss was seen when the binder content of the mix design was increased. As the binder content increases, a thicker and stronger film of binder is holding the aggregate together, thus increasing the abrasion resistance of the pavement structure (Putman, 2012).

In a study conducted by Mansour and Putman, the Cantabro abrasion test was used to characterize the durability of the compacted specimens. A maximum loss of 20% is specified for unaged conditioned specimens and 30% for aged specimens (Kandhal 2002). The results indicated that abrasion resistance was influenced by the mixture porosity and air voids. The gradation with the highest porosity exhibited the highest

abrasion loss and the mix with the lowest porosity experienced the lowest abrasion loss (Mansour and Putman 2013).

Hamzah et al. found that the abrasion loss for all mixes decreased as the initial conditioning temperature (ICT) and binder content were increased. The specimens were conditioned at a specific temperature for 4 hours. The specimens were placed in the Los Angeles drum and tumbled for 300 rotations without a steel charge. An infrared thermometer was used to determine the temperatures of the specimen skin and the internal walls of the Los Angeles drum during testing. Using the abrasion loss at an ICT of 15ºC as the baseline, the abrasion losses of specimens initially conditioned at 20, 25, 30, and 35ºC decreased by 16.7%, 39.9%, 57.9% and 65.0%, respectively (Hamzah, 2012).

The initial conditioning temperature (ICT) had a distinct effect on the abrasion loss of porous asphalt. At lower temperatures, binder becomes brittle and more prone to disintegrate when exposed to external forces. A statistical analysis of the binder types showed that the modified binder (PG76 SBS) resulted in a higher resistance than the conventional binder (60/70). This study also showed that the higher binder contents (5.0% and 5.5%) and higher initial ICT (above 30ºC) yielded the lowest abrasion loss values (Hamzah, 2012).

CHAPTER THREE

EXPERIMENTAL MATERIALS AND METHODS

This chapter summarizes the materials and methods used to satisfy the objectives of this research. For Phase 1A, the materials used in the preparation of the mixes consisted of aggregate (single source, one gradation), cellulose fibers (0.3% by mixture weight), one grade of asphalt binder (PG 76-22), and hydrated lime (1% by aggregate weight). The main component of each mix that was varied was the binder content (5%, 6%, and 7%). For Phase 1B and 2, the materials used in the preparation of the specimens consisted of a plant-mixed OGFC that consisted of aggregate (single source, single gradation), one grade of asphalt binder (warm-mix asphalt using Evotherm technology), and hydrated lime (1% by aggregate weight).

Table 3.1, shows the mix design data for the material. For Phase 1A, the only component varied was the binder content (5%, 6%, and 7%) for each set of specimens. Fifteen specimens were compacted per a binder content and tested for the porosity, indirect tensile strength, direct shear strength and the raveling susceptibility.

For Phase 1B and 2, the only component that varied per set of specimens for the raveling susceptibility portion of this study was the type of aging that the specimen endured. One set of specimens (n=24) were tested un-aged, one set of specimens (n=25) were aged for 56 days at 60°C, and one set of specimens (n=11) were inverted (flipped) every 2 days for 56 days while being aged at 60°C. For the evaluation and quantification of long-term draindown in OGFC pavements portion of this study; one set of additional

specimens (n=3) were aged for 56 days at 60°C, and one set (n=2) were inverted (flipped) every 2 days for 56 days while being aged at 60°C.

This research study was divided into two different phases: (1) comparison of existing and new laboratory test methods to evaluate and identify the underlying mechanism of the raveling susceptibility of OGFC pavements and (2) evaluation and quantification of long-term draindown in OGFC pavements. The specimens were tested to evaluate the porosity, long-term draindown, indirect tensile strength, direct shear strength, modulus of toughness and the abrasion resistance (using several test methods).

Table 3.1- Mix Design Information

Mix Design Properties	Phase 1A Lab Produced	Phase 1A & 2 Plant-Mix
Gradation		
1 ½ in.	-	100
1 in.	-	100
¾ in.	100	100
½ in.	94.0	93.8
⅜ in.	69.0	67.9
No. 4	19.0	23.1
No. 8	6.0	-
No. 30	4.0	-
No. 100	2.3	10.7
No. 200	1.0	1.72
Binder Type	PG 76-22	PG 76-22
Viscosity @ 135°C	0.87 Pa-s	1.138 Pa-s
$G^*/\sin\delta$ @ 76°C	-	1.11 kPa
δ @ 76°C	-	74.8°
Binder Content	5.0, 6.0, & 7.0	6.03
Anti-Strip Additive	Hydrated Lime (1% by aggregate weight)	Hydrated Lime (1% by aggregate weight)
Production Temperature	325°F	270°F
Additives	Cellulose Fibers (0.3% by mixture weight)	Evotherm™ added at the terminal at a rate of 0.5% by weight of binder.

Plant-Mix Asphalt (Phases A1 and B)

OGFC mix was sampled at the plant during one night of production. The sampling corresponded with the quality control (QC) check samples. A haul truck was sampled after loading and prior to delivery to the construction location. By sampling at the same time as the QC check samples, the plant staff tested gradation (SC-T-4) and binder content (SC-T-75). The test specimens sampled for the QC testing were sampled with a small shovel from the truck bed and placed directly into the ignition oven sample basket. For this research project, twelve 5-gallon metal buckets of mix were collected and transported to the lab at Clemson University.

Experimental Methods

To fulfill the objective of this study for Phase 1A, 3800g compacted asphalt specimens were made for testing porosity, abrasion resistance, and indirect tension strength). Fifteen compacted specimens were made for each mix at a specific binder content (5%, 6%, and 7%). The specimens were compacted using a Superpave gyratory compactor at 50 gyrations per specimen and a consolidation pressure of 600 kPa (87 psi). The compacted specimens had a diameter of 150 mm and a height of 115±5 mm.

To fulfill the objective of this study for Phase 1B and 2, 3900g specimens were produced by reheating and weighing the sampled plant mix at the research lab located at Clemson University. The specimens were then compacted at the target temperature of 255°F. The specimens (n= 60) for the raveling susceptibility portion of this study were compacted using a Superpave gyratory compactor at 50 gyrations per specimen and a

consolidation pressure of 600 kPa (87 psi). The specimens prepared for the evaluation

and quantification of long-term draindown in OGFC pavements portion of this study

were compacted at 20 gyrations (n=1), 35 gyrations (n=1) and 50 gyrations (n=3) and a

consolidation pressure of 600 kPa (87 psi). The compacted specimens had a diameter of

150 mm and a height of 115±5 mm. Once the specimens were compacted, the mold was

set in front of a fan to cool for about 25 minutes before removal of the specimen from the

mold to minimize the chance of specimen deformation after demolding.

<center>Porosity</center>

The porosity of each specimen was measured using the procedure first outlined by Montes et al. (2005) and adapted by Putman (2010), which is summarized in the following steps:

1. Recorded the dry mass of the specimen to the nearest 0.1 g (W_{dry}).

2. Measured and recorded the height and diameter of each specimen at three representative locations to the nearest (0.1mm). Then calculated the average height (H_{avg}) and diameter (D_{avg}) of each specimen.

3. Calculated the total volume of each specimen using the Equation 1:

$$V_T = \frac{(D_{avg})^2 * H_{avg} * \pi}{4}$$
<div align="right">Equation 1</div>

Where:

D_{avg} - Average diameter of the specimen

H_{avg} - Average height of the specimen

V_T - Total volume of the specimen

4. The specimen was submerged in 25°C water for 30 minutes.

5. After 30 minutes, while keeping the specimen submerged, the specimen was inverted 180° being careful not to expose the specimen to air.

6. The specimen was kept submerged, then tapped 5 times against the side of the tank without damaging the specimen, then inverted 180°.

<center>21</center>

7. The submerged mass of the specimen was then measured and recorded without exposing it to the air (W$_{sub1}$).

8. The temperature of the water was recorded.

9. The porosity was calculated using the following equation:

$$Porosity\ (\%) = \left[1 - \frac{\left(\frac{W_{dry}-W_{sub}}{\rho_w}\right)}{V_T}\right] \qquad\qquad \text{Equation 2}$$

Where:

W_{dry}- Weight of the dry specimen

W_{sub}- Weight of the submerged specimen

V_T- Total volume of the specimen

ρ_w- Density of water at the water temperature

After the porosity testing was complete, the porosity data was used to group the specimens to ensure that each group was representative of the overall mix design properties. To verify that the test groups were statistically similar with respect to porosity, an analysis of variance (ANOVA) was performed using α=0.05.

After grouping, for Phase 1A of this study, all specimens were tested un-aged. For Phase 1B and 2 of this study, some of the specimens were tested un-aged; some of the specimens were aged for 56 days at 60°C, and some of the specimens were aged for 56 days at 60°C while being inverted (flipped) 180° every two days without removing the specimens from the environmental chamber. Open-graded fiction course specimens are susceptible to deformation at higher temperatures so all the aged specimen were wrapped with wire mesh before placement in the environmental chamber (Figure 3.1). An apparatus was built to flip the aged specimens that had to be inverted every two days to prevent disturbance of the specimens (Figure 3.2). After the specimens were flipped, the top platform of this apparatus was removed so as to not interfere with the aging process.
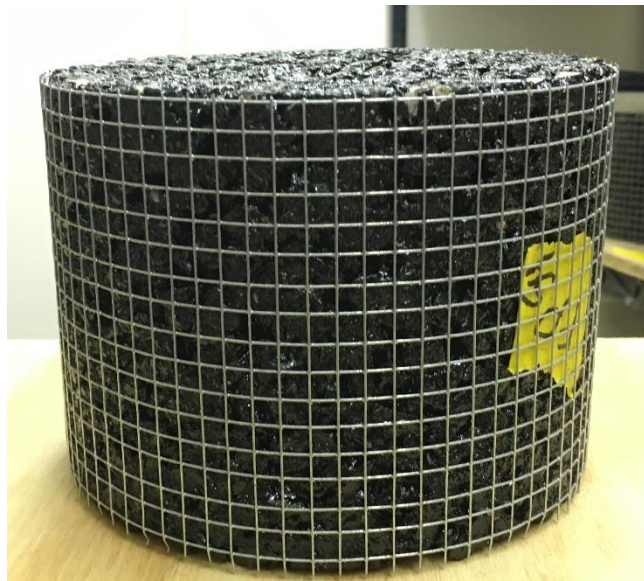
Figure 3.1– Specimen Wrapped in Wire Mesh
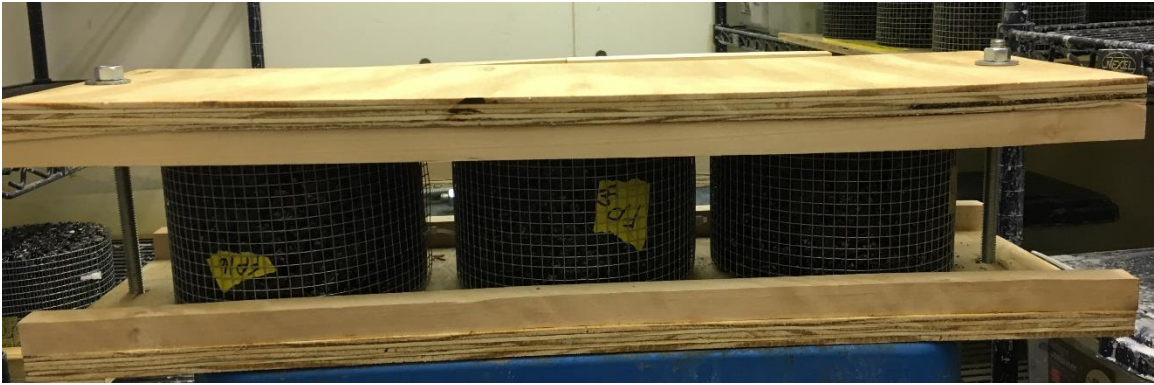
Figure 3.2- Apparatus Used to Flip Aged Specimen

For Phase 1A and 1B of this study, the un-aged and aged specimens were subjected to the following test methods: Cantabro abrasion (ASTM D7064), direct shear strength test, singular motion surface abrasion test, planetary motion surface abrasion test, and indirect tensile strength. Figure 3.3, shows the research plan for the Phase 1A of this research study. Figure 3.4, shows the research plan for the Phase 1B of this research study For the Phase 2 of this study, the grouped un-aged, aged and flipped specimens were evaluated using an image analysis and the standard test method for asphalt content of asphalt mixture by ignition method (ASTM D6307) to evaluate long-term draindown. Figure 3.5, represents the research plan for the Phase 2 of this study.
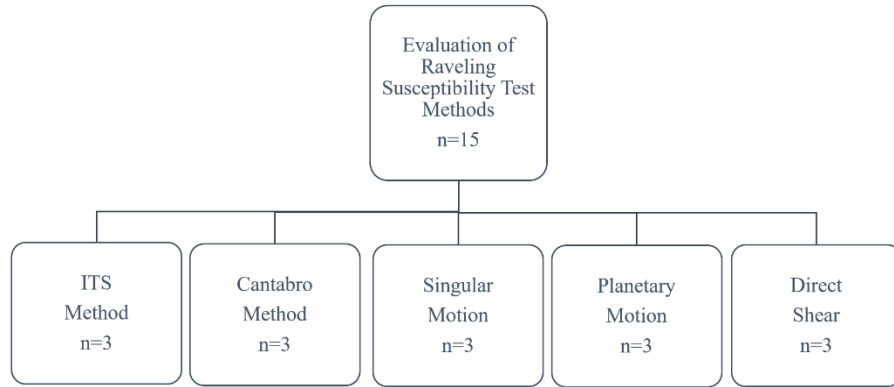
Figure 3.3- Phase 1A Research Plan
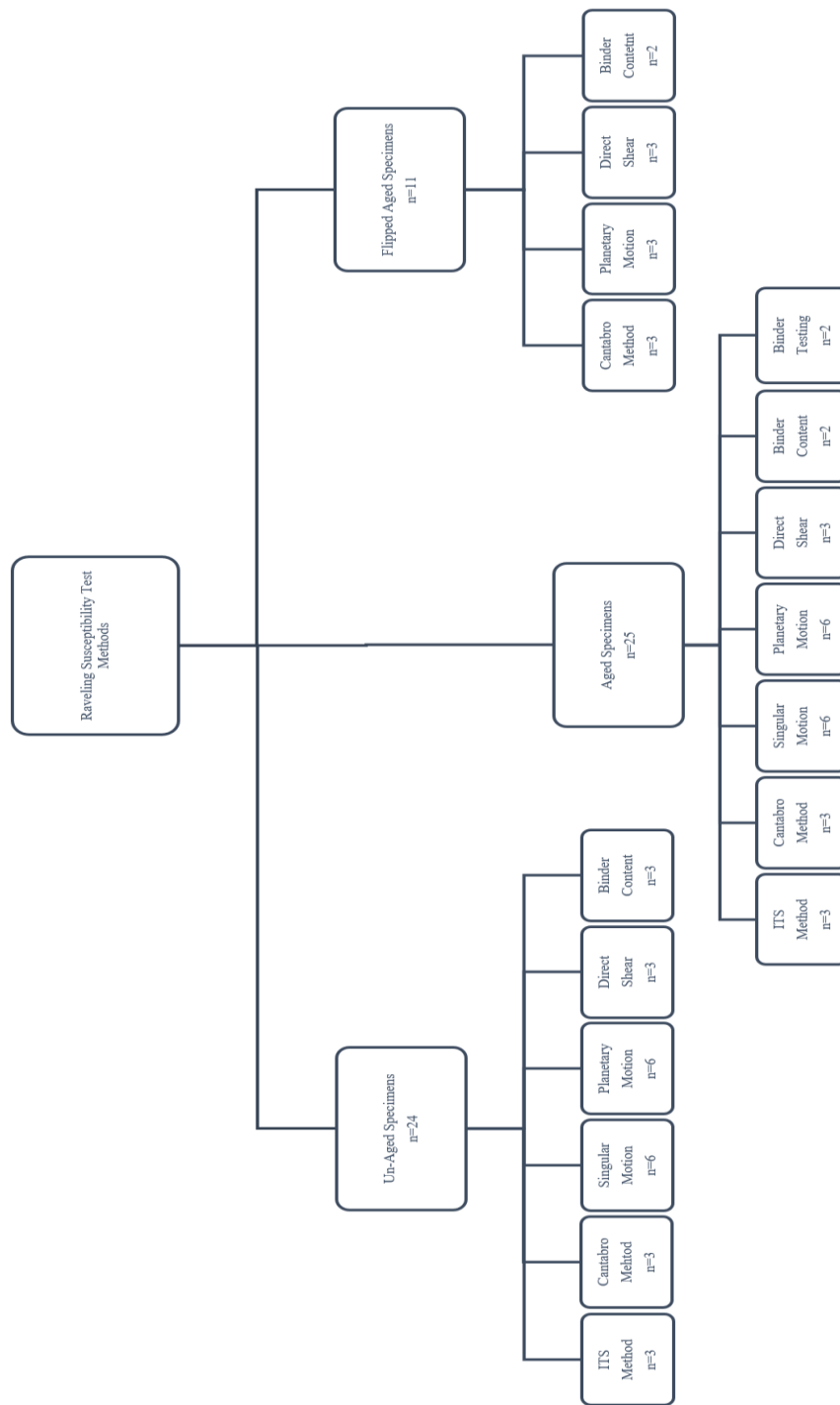
Figure 3.4- Phase 1B: Research Plan
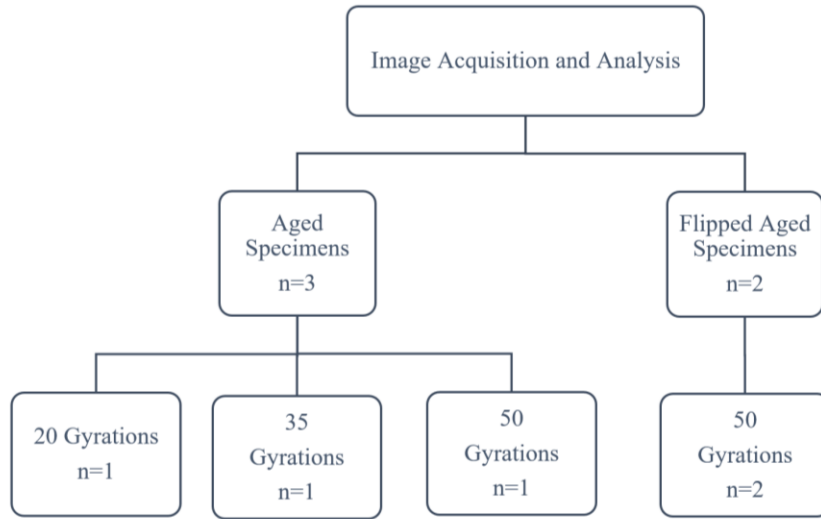
Figure 3.5- Phase 2: Research Plan

Abrasion Resistance

The Cantabro abrasion test was used to measure the abrasion resistance of the OGFC mixtures. Three specimens from each conditioning group (un-aged, aged and flipped) were tested using the procedure outlined in the ASTM D7064 standard. The test was conducted by recording the initial weight of the specimen then placing the specimen in the Los Angeles abrasion (Figure 3.6) apparatus for 300 revolutions without the steel charge at room temperature. Once the 300 revolutions were complete, the specimen was removed and the final weight was recorded. The percent mass loss was calculated by dividing the mass loss by the initial mass of the specimen.

Figure 3.6- Los Angeles Abrasion Machine

<u>Direct Shear Strength Test</u>

The direct shear strength test was conducted on three specimens from each conditioning group (un-aged, aged and flipped) using a universal testing machine (UTM). The shear strength was measured using a procedure developed by Mohammad et al (2012). For Phase 1A, each specimen was placed so that the specimen was sheared directly in the middle of the specimen. For Phase 1B, each specimen was placed into the shear test apparatus so that only the top and bottom 1 inch of each specimen was sheared as shown in Figure 3.7. Load was applied to specimen at a rate of 0.1 in/min until failure of the specimen occurred. The deformation and load was recorded for each specimen along with its peak load. These values were then used to develop stress-deformation and load-deformation curves in Excel. The toughness (energy) of the specimens were calculated by calculating the area under the load-deformation curve using the trapezoidal formula in Excel.
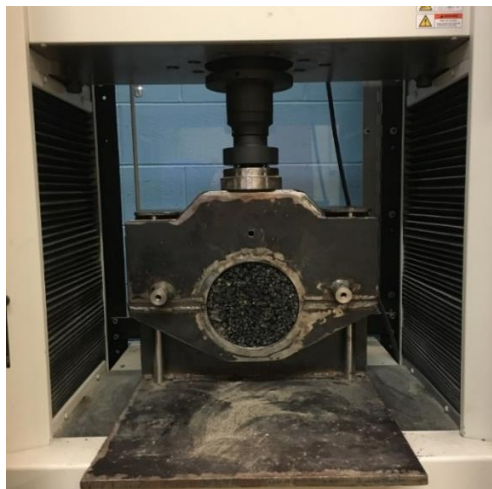
Figure 3.7- Shear Testing Apparatus

Singular Motion Surface Abrasion Test

The singular motion surface abrasion test was used to measure the abrasion resistance of the surface of the OGFC specimens. Three specimens from each conditioning group (un-aged and aged) were tested using the procedure outlined in the ASTM C944 standard as a guideline. The test apparatus consists of two rotating cutter heads (Figure 3.8 and Figure 3.9), specimen adapter base and drill press (Figure 3.10). The difficulty in maintaining a constant load on the abrading cutter when using the lever, gear and spring system of a drill press was addressed by placing a constant load of 98 N (22 lb.) directly upon the spindle that turns the cutter. The cutter rotated at a constant rate of 240 rpm. The specimen was placed into the adapter base so that 10 mm of the specimen was above the raveling test adapter base.

The initial weight of the specimen was recorded. The specimen was placed in the adapter base and tightly secured. The motor of the cutter was started, then slowly lowered until the cutter made contact with the surface of the specimen. The specimen was abraded for five minutes, then removed from the adapter base and the surface was cleaned with a soft brush to remove any loose debris followed by blowing the specimen with an air hose for ten seconds in a circular motion. After recording the mass of the specimen, the specimen was then placed back into the adapter base, and the process was repeated for five more five-minute cycles. The percent mass loss was then calculated after each cycle by dividing the mass loss by the initial mass of the specimen.
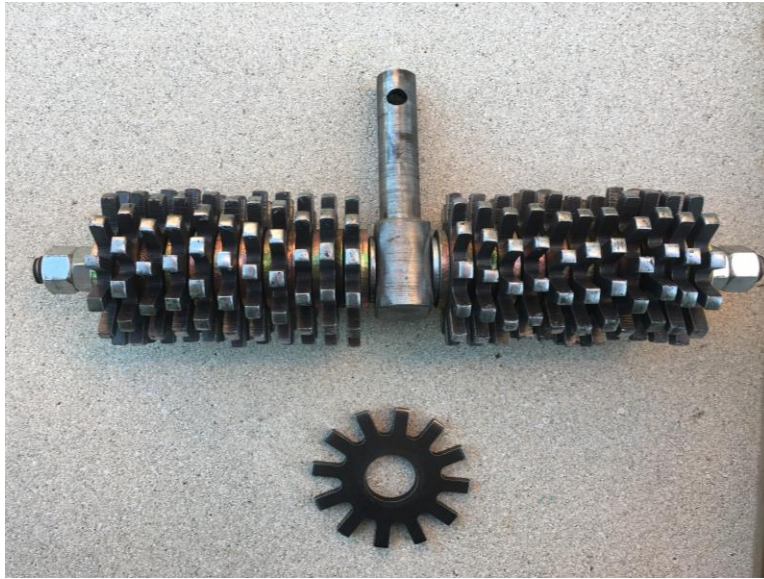
Figure 3.8- Square Rotating Cutter Head (Cutter Head A)

Figure 3.9- Triangle Rotating Cutter Head (Cutter Head B)
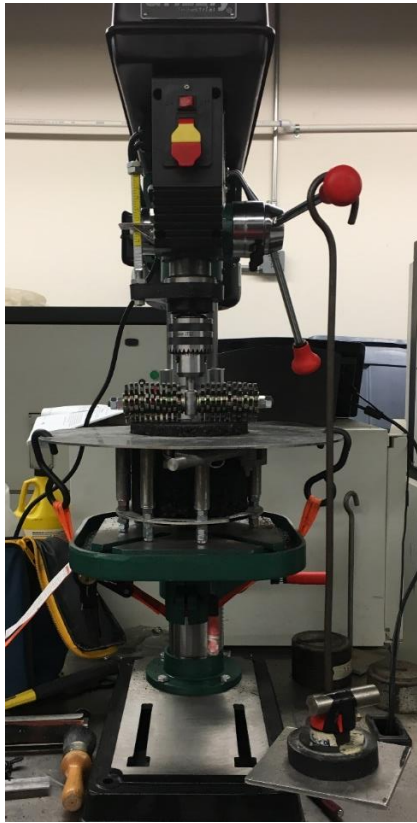
Figure 3.10- Singular Motion Surface Abrasion Apparatus

Planetary Motion Surface Abrasion Test

The raveling test for cold mixed emulsified asphalt sample (ASTM D7196) was used as a guideline to measure the surface abrasion resistance of the OGFC mixtures. Three specimens from each conditioning method (un-aged, aged and flipped) were tested using the planetary motion surface abrasion test method. Instead of using a rubber-testing adapter as per the standard, two rotating cutter heads (A and B) were used (Figures 3.8 and 3.9, respectively). The square rotating cutter head adapter (cutter head A) had a weight of 1832.5g. The triangular rotating cutter head adapter (cutter head B) had a weight of 1339.8g. The mixer rotated at a rate of 72 rpm.

The test was conducted by recording the initial weight of the specimen, then placing the specimen in the raveling test adapter base (Figure 3.11). A minimum of 10 mm of the specimen was exposed above the raveling test adapter base. The sample was abraded for five minutes (one cycle), and then was carefully removed from the base. The specimen was brushed with a fine bristle brush to remove any loose debris followed by blowing the specimen with an air hose for ten seconds in a circular motion, then weighed and the percent mass loss was calculated. The specimen was abraded for a total of six 5 minute cycles (30 minutes total).

Figure 3.11- Planetary Motion Surface Abrasion Apparatus

<center>Indirect Tensile Strength</center>

Three specimens from each conditioning group (un-aged and aged) were subjected to a split tensile test in accordance with SC-T-70. The specimens were placed between two bearing plates in a Marshall load frame machine, then load was applied at a constant rate of 2 inches/minutes (Figure 3.12). The load being applied to the specimen along with the deflection of the specimen were recorded. These values were then used to develop a stress-deformation and load-deformation curves in Excel. The toughness (energy) of the specimens were calculated by calculating the area under the load-deformation curve using the trapezoidal formula in Excel.
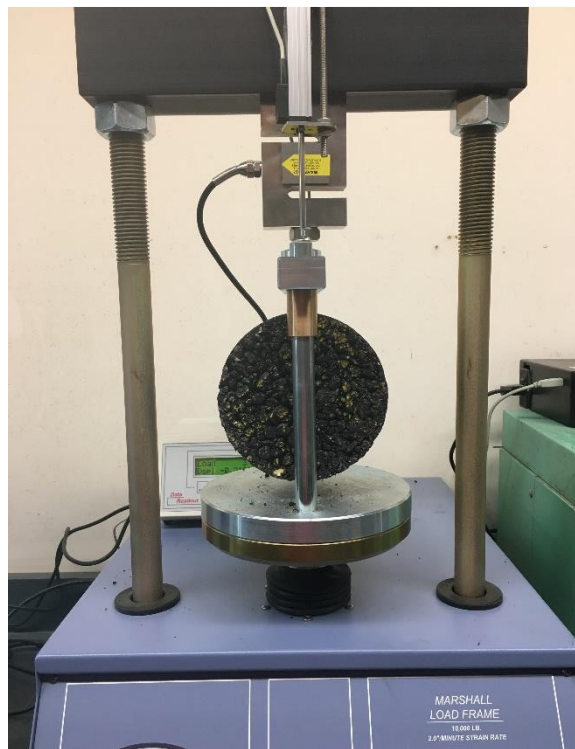
Figure 3.12- Specimen Setup for the Marshall Load Frame

To evaluate the long-term draindown of OGFC, five compacted specimens (one at 20 gyrations, one at 35 gyrations and three specimens at 50 gyrations) sampled from the same lot as those evaluated in Phase 1B were evaluated. After measuring the porosity or each specimen, they cut in half as illustrated in Figure 3.13 using a water cooled masonry saw.

After the specimens were cut, pictures of the cut face of each of the specimens were taken. The specimens were then wrapped in wire mesh (Figure 3.14), then put into an oven to condition at 60°C for 28-day intervals. After each 28-day interval, the specimens were removed from the oven, then allowed to cool to room temperature. Once cool, pictures of the cut face of each specimen were taken. The specimens were then wrapped and placed back into the oven for another 28-day interval.
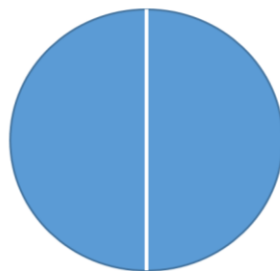
Figure 3.13- Demonstration of Cut Specimens, Halved

Figure 3.14- Specimens Wrapped with Wire Mesh

Image Acquisition and Analysis

The following is a systematic process of how long-term draindown was evaluated and quantified in this study:

1. Specimens were sliced in half and each half was labeled for reference.

2. Images of the cut face of the specimen were taken using a DSLR camera with appropriate lighting before and after aging (Figure 3.15).

3. Pre-processing of the images was done to enhance the contrast and get accurate results. For each specimen, ten percent of the total length and width of the specimen was removed to account for the irregularities of the specimen surface (Figure 3.16 and Figure 3.17).

4. Image processing algorithms were developed to detect the percent of pixels by area of the cut surface for each component (binder, air, aggregate). (air-voids (Figure 3.18), aggregate (Figure 3.19), and binder (Figure 3.20)

5. Each image of a cut surface was divided into four equal horizontal slices (Figure 3.21).

6. A section wise analysis was conducted to quantify the amount of air-voids (Figure 3.22), aggregate (Figure 3.23) and binder (Figure 3.24) in each slice.

7. A comparison of the amount of binder and air voids before and after aging were conducted on each specimen.

Figure 3.15- Un-Aged Specimen Image
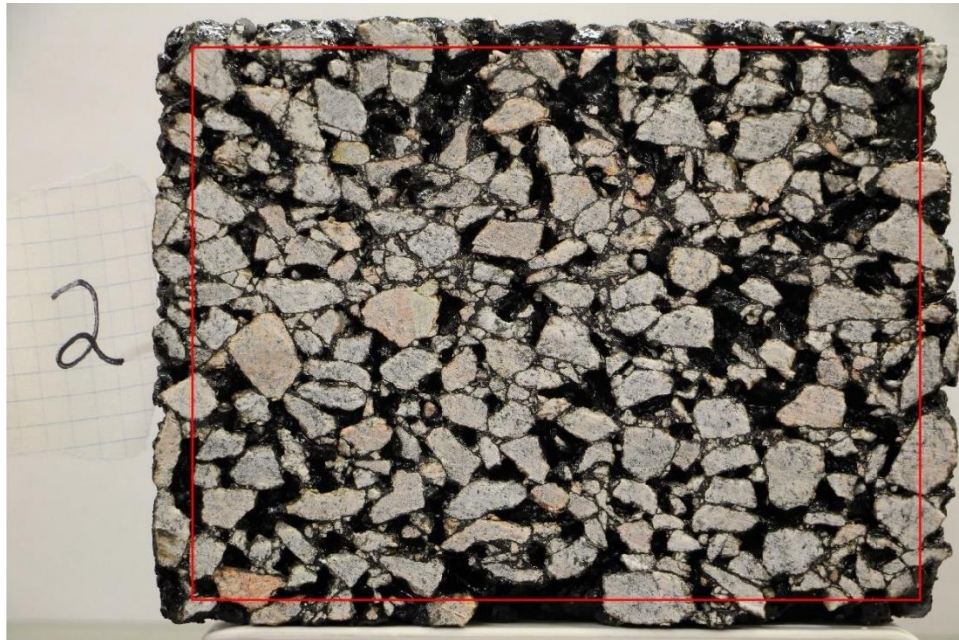
Figure 3.16- Reduction in Length and Width of Specimen

Figure 3.17- Image of Specimen Used for Analysis
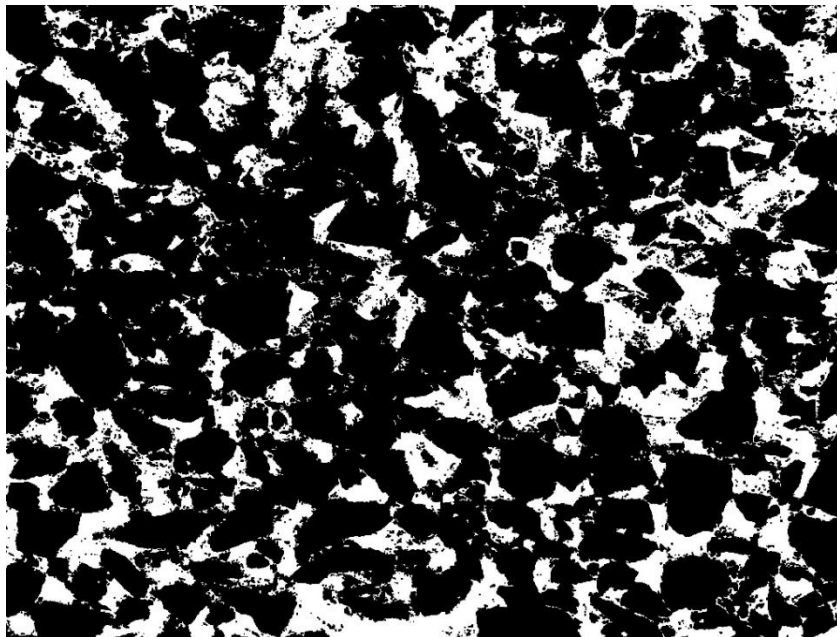
Figure 3.18- Image of the Air Voids (White) in a Specimen
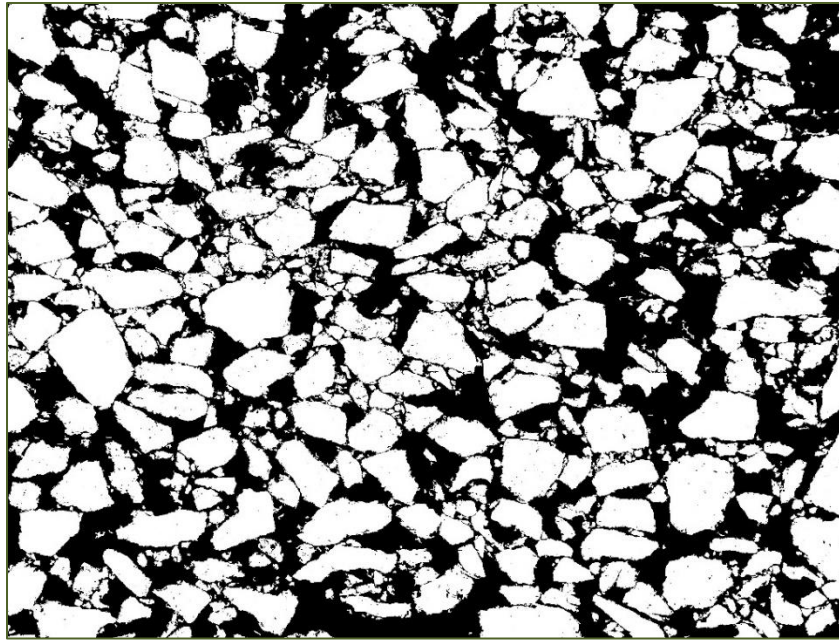
Figure 3.19- Image of the Aggregates (White) in a Specimen
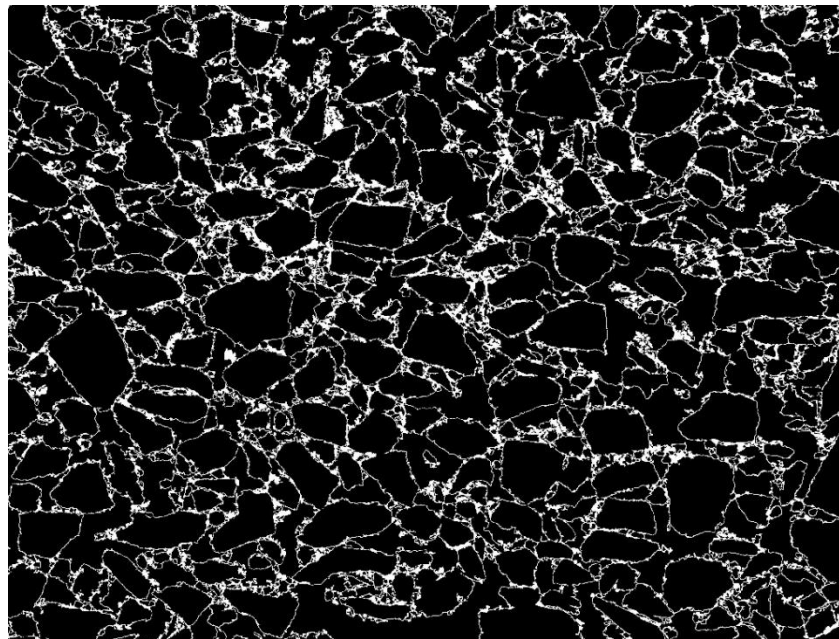
Figure 3.20- Image of the Binder (White) in a Specimen

Figure 3.21- Image Cut into Slices
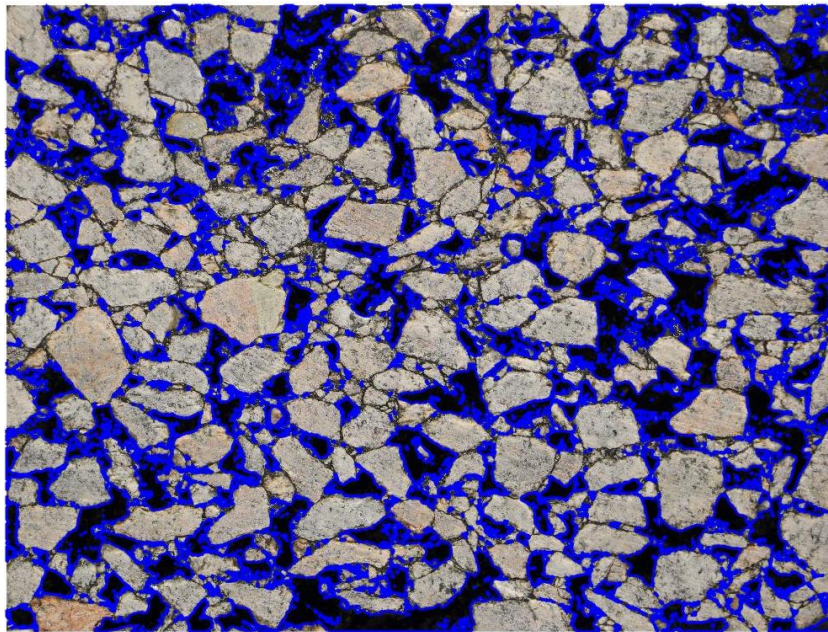
Figure 3.22- Plot of Air Voids (Outlined in Blue) in a Specimen
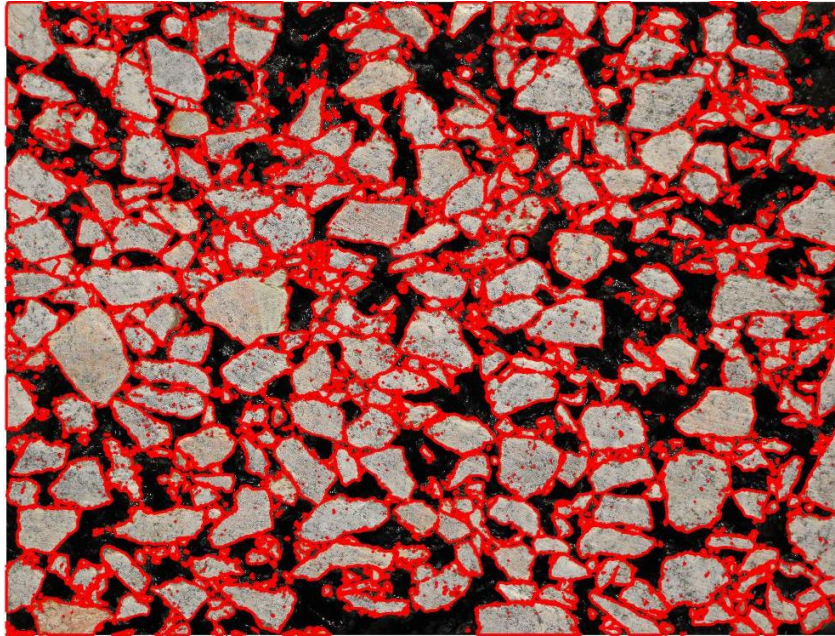
Figure 3.23- Plot of Aggregates (Outlined in Red) in a Specimen
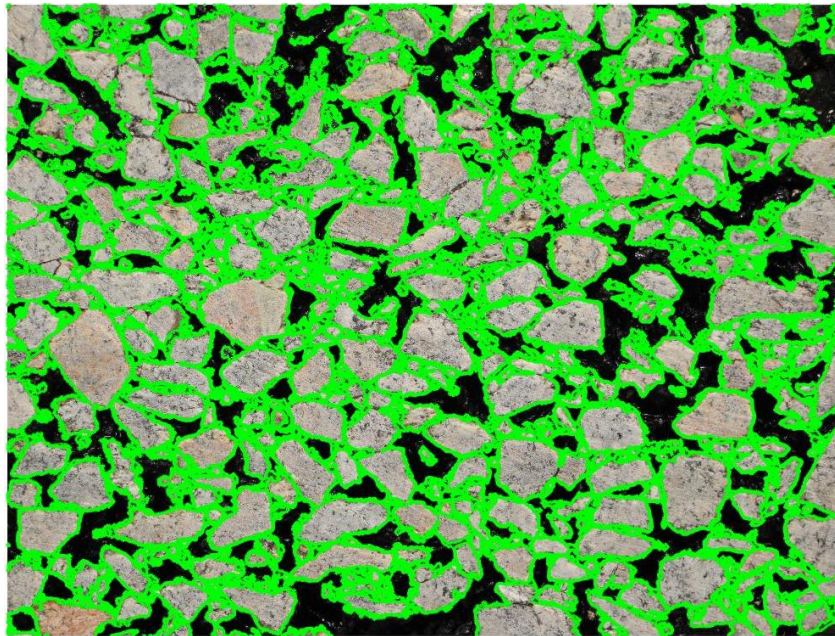
Figure 3.24-Plot of Asphalt Binder (Green) in a Specimen

Binder Content Analysis

To evaluate the long-term drain down of asphalt binder over time, seven specimens (three un-aged, two 56 day aged, and two 56 day aged that were flipped every 2 days) were cut into four equal horizontal slices about 1 inch thick (Figure 3.25). After each specimen was cut into four slices, each slice was cleaned and labeled so that the slices remained in the correct order. Slice one presented the top quarter of the specimen, with slice four representing the bottom quarter of the specimen. After the slices were clean and dry, the binder content of each slice was determined using the standard, ASTM D 6307.

Figure 3.25- Binder Content Cut Specimens

<u>Roughness Stepwise Analysis</u>

To evaluate the surface roughness of the specimens before and after testing using the singular and planetary motion surface abrasion test methods; the following steps were taken:

Image Acquisition:

1. The specimens were prepared, labelled and marked with a gold marker for reference before and after testing (Figure 3.26).

2. An image acquisition setup was arranged as shown in Figure 3.27 and images were acquired using a Canon Rebel T5i DSLR camera mounted on a tripod without disturbing the experimental arrangement.

3. Images were taken using the manual focus mode with zoom level kept constant.

4. 25-30 images were collected for the untested top and bottom surfaces of each OGFC specimen by constantly changing the focus of the camera lens.

5. After testing, another 25-30 images of the tested surfaces were taken for comparison.

6. All the images acquired were stored in respective folders.
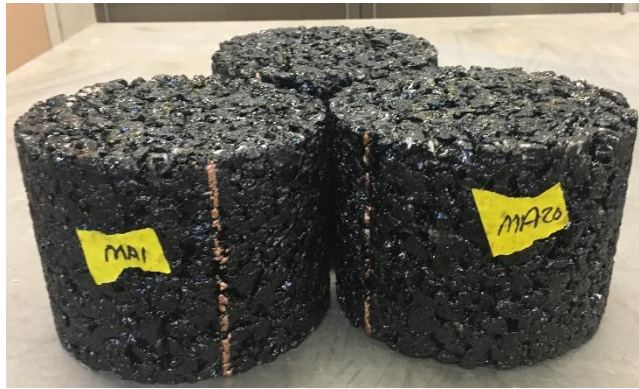
Figure 3.26- Marked Specimens for Roughness Analysis
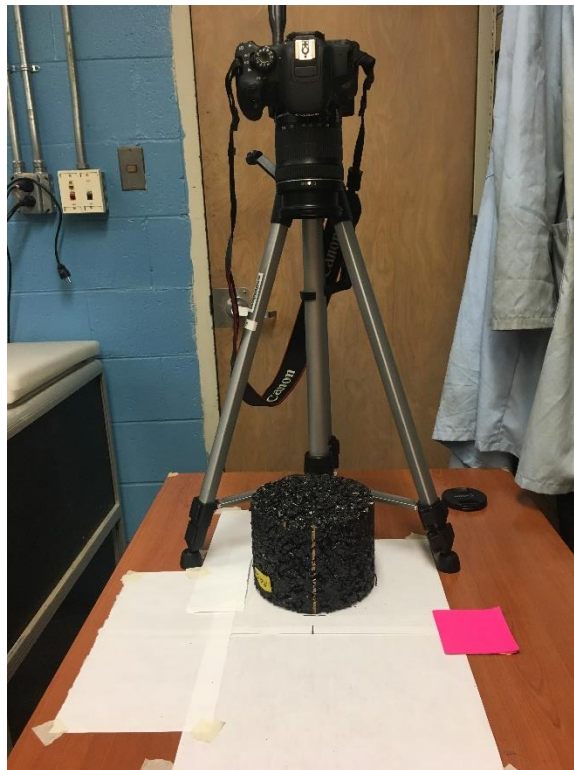
Figure 3.27- Experimental Setup for the Canon Rebel T5i DSLR Camera and Tripod

Image Stacking:

1. Images were stacked vertically after being loaded into the software called **Helicon Focus** to get the depth of each pixel (Figure 3.28).

2. The images were rendered using the Method C (Pyramid) option to get a stacked image of the specimen (Figure 3.29).

3. All stacked images (before and after testing), were created and stored in respective folders.
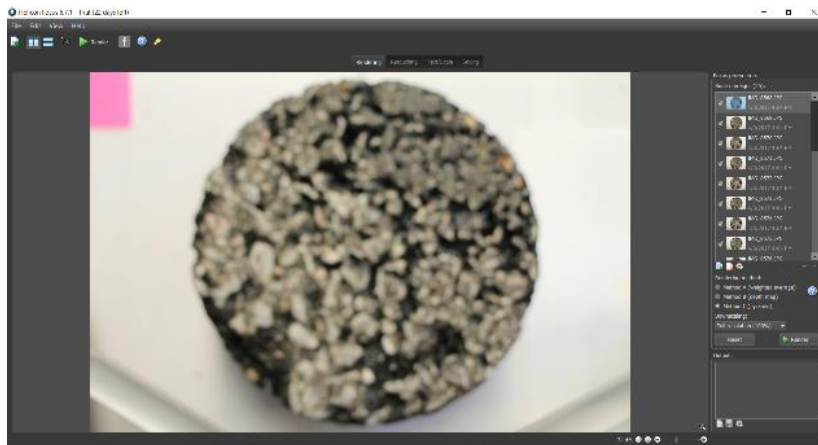
Figure 3.28- Specimen Image Before Vertically Stacking
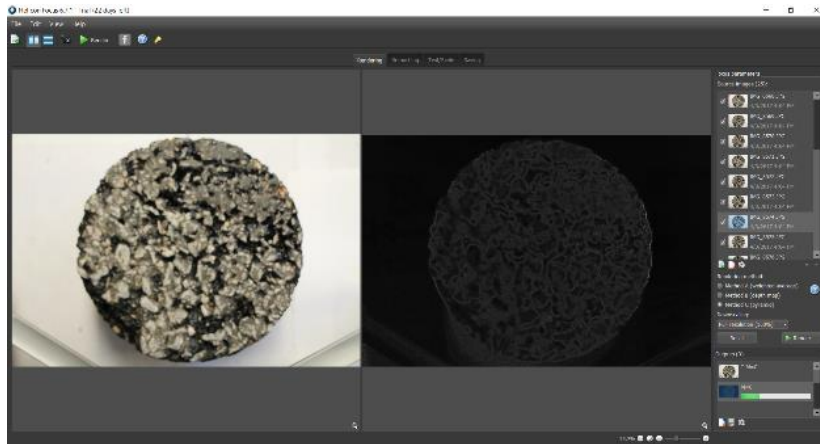
(a)
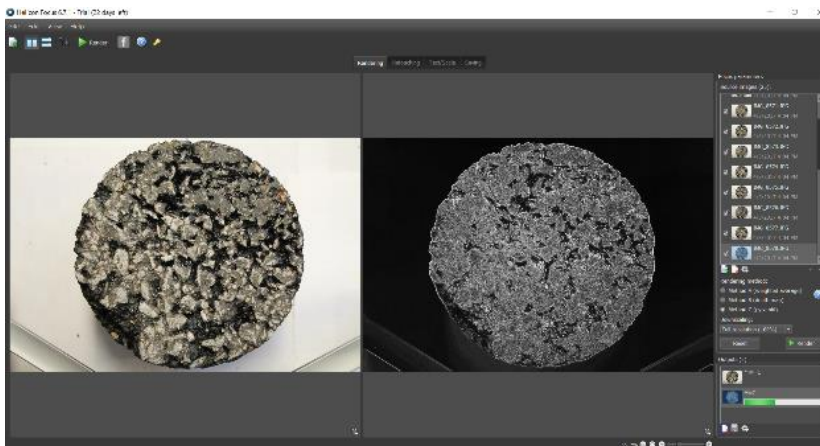
(b)

Figure 3.29- The Start of Image Stacking (a) and the Finished Stacked Image (b)

Quantification of Roughness:

1. Stacked images were loaded into a software called **Image J** to perform roughness calculations (Figure 3.30).

2. To perform a roughness calculation on a certain area of interest in the image, shape tools were used to draw around the Region of Interest (ROI) (Figure 3.31).

3. A duplicate image was created so that just the ROI image would appear without the unwanted area surrounding the image as shown in Figure 3.32.

4. A Roughness Calculator. Jar plugin was used to calculate the roughness of the ROI selected. The Ra value in the results box is considered as roughness value (Figure 3.33). The Ra value is the average roughness (texture deviation) of all the pixel points from the plane to the testing surface of the specimen.

5. Results were saved to Excel, which was used to calculate the percent change in roughness of the specimen after testing.
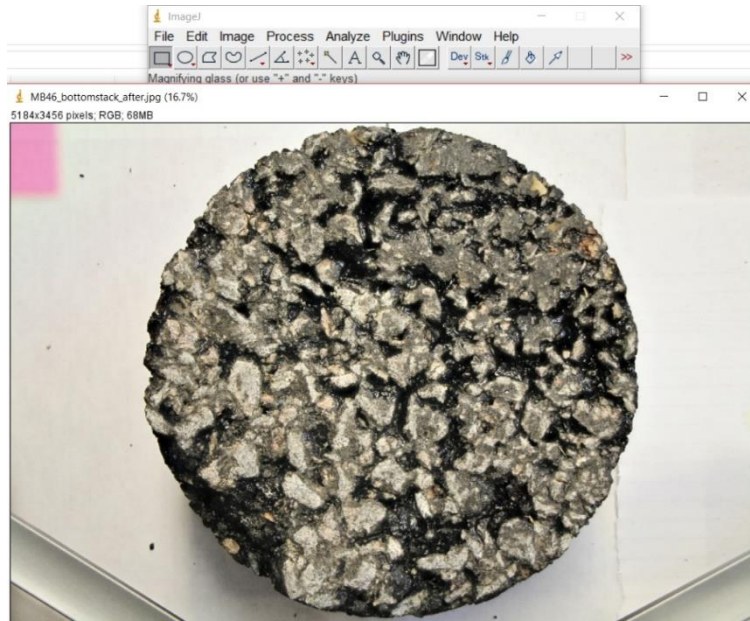
Figure 3.30- Stacked Image Loaded into Image J Program
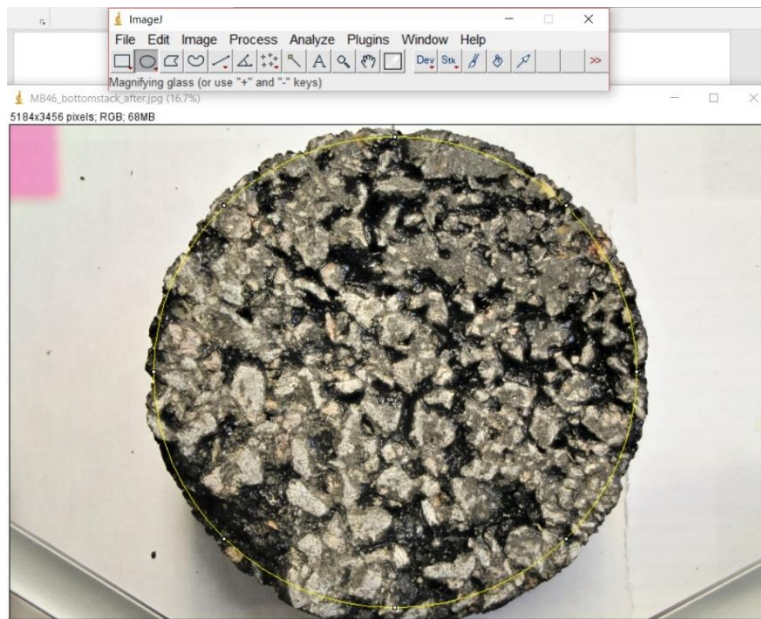
Figure 3.31- Shape Tool used to Draw Region of Interest

Figure 3.32- Cropped Image of the Region of Interest

Figure 3.33- Result Box with Roughness Value (Ra)

CHAPTER FOUR

RESULTS AND DISCUSSION

In this chapter, the experimental results for one lab produced OGFC mix design (Phase A1) as well as one plant produced Warm-Mix Asphalt (WMA) mix design (Phase A2) are presented. The compacted specimens were produced for porosity, Cantabro abrasion, direct shear strength, singular motion surface abrasion, planetary motion surface abrasion, indirect tensile strength testing. In Phase B, the specimens were also evaluated for long-term draindown using image analysis and binder content testing (ignition oven). Three different conditioning methods were used for this study: un-aged, aged for 56 days, and aged for 56 days while flipping the specimen every 2 days. Table 4.1 shows the abbreviations for the tested specimens for this study.

Table 4.1- Legend for the Tested Specimens

Test Specimen Description	Abbreviation
Un-Aged	UA
Aged	A
Aged Flipped	AF
Un-Aged Top of Specimen	UAT
Un-Aged Bottom of Specimen	UAB
Aged Top of Specimen	AT
Aged Bottom of Specimen	AB
Aged Flipped Top of Specimen	AFT
Aged Flipped Bottom of Specimen	AFB

PHASE A: TEST METHOD DEVELOPMENT AND SCREENING

Phase A1

In this section, the development of two new test methods to assess the raveling susceptibility of OGFC were evaluated (singular and planetary surface abrasion). The two newly developed test methods were compared to the Cantabro test method as well as the direct shear strength and indirect tensile strength test methods. The main component of each mix that was varied was the binder content (5%, 6%, and 7%), which was varied to assess the validity of the two new test methods. Multiple studies have shown that as the binder content increases, the cohesive strength of the mix design increases. Therefore, the raveling susceptibility of the OGFC decreases as the binder content increases.

Cantabro Abrasion Resistance

Three specimens for each binder type were tested using the Cantabro abrasion test

method. Figure 4.1 shows each specimen before and after testing using the Los Angeles

Abrasion Machine. As the binder content of the specimen increases, the mass loss of the

specimen after testing decreases. The average percent mass loss for each binder content is

summarized in Figure 4.2, which shows that as the binder content of the OGFC increases,

the percent mass loss decreases. This means that the abrasion resistance of the specimens

increases as the binder content increases.
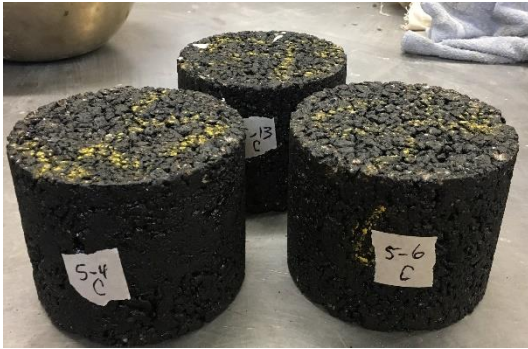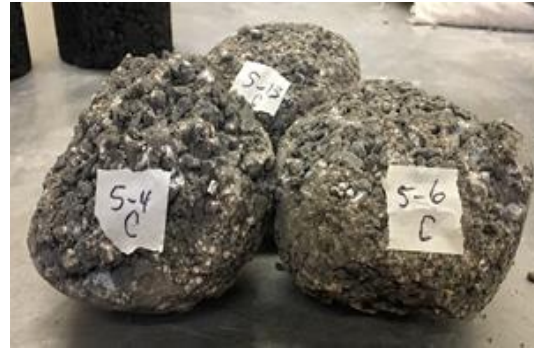
(a)   (b)

(c)   (d)

(e)   (f)

Figure 4.1- Los Angeles Abrasion Machine (a) 5% Before Testing, (b) 5% After Testing, (c) 6% Before Testing, (d) 6% After Testing, (e) 7% Before Testing, and (f) 7% After Testing
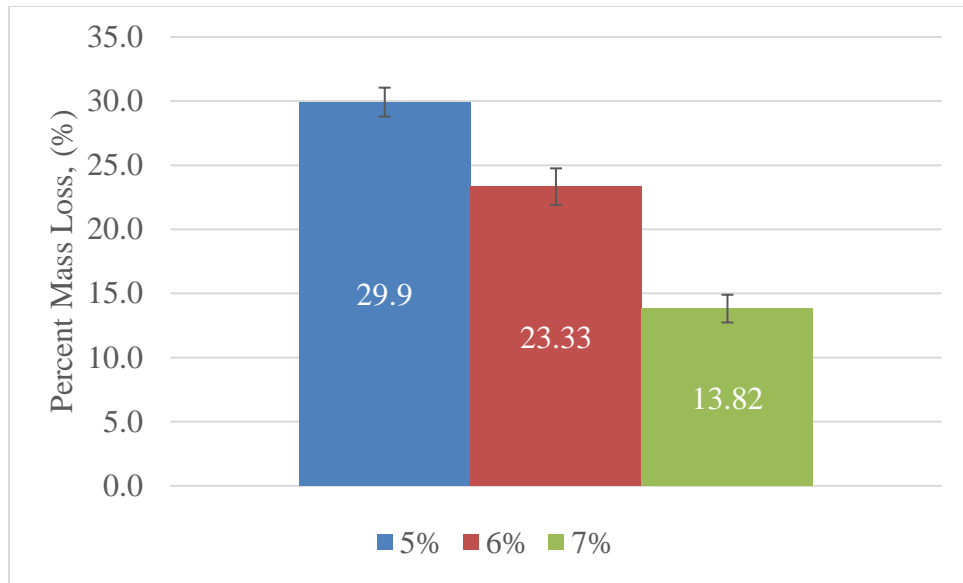
Figure 4.2- Cantabro Abrasion Test Method Data. (Error bars indicate one standard deviation)

<u>Singular Motion Surface Abrasion Test Method</u>

Three specimens for each binder type were tested using the singular motion surface abrasion test method. Figure 4.2 shows each specimen before and after testing using the singular motion surface abrasion test method. The average percent mass loss of the three specimens for each binder content for each cycle (2 minutes per cycle) using cutter head A can be seen in Figure 4.3. For each binder content as the number of cycles increased, the percent mass loss increased in a linear pattern. The 5% binder content specimens exhibited a higher percent mass loss than the 6% and 7% binder content specimens, with 7% being the lowest.

(a)

(b)
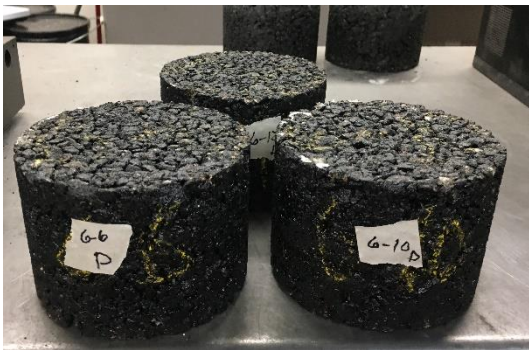
(c)
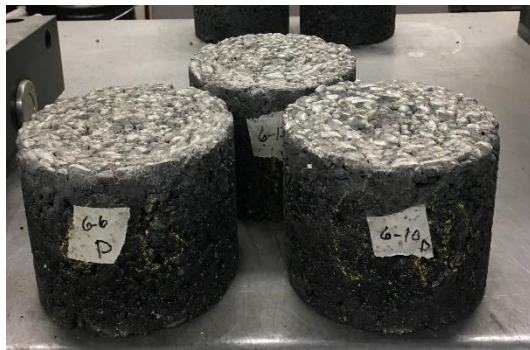
(d)

(e)

(f)

Figure 4.3- Singular Motion Surface Abrasion Test Method (a) 5% Before Testing, (b) 5% After Testing, (c) 6% Before Testing, (d) 6% After Testing, (e) 7% Before Testing, and (f) 7% After Testing
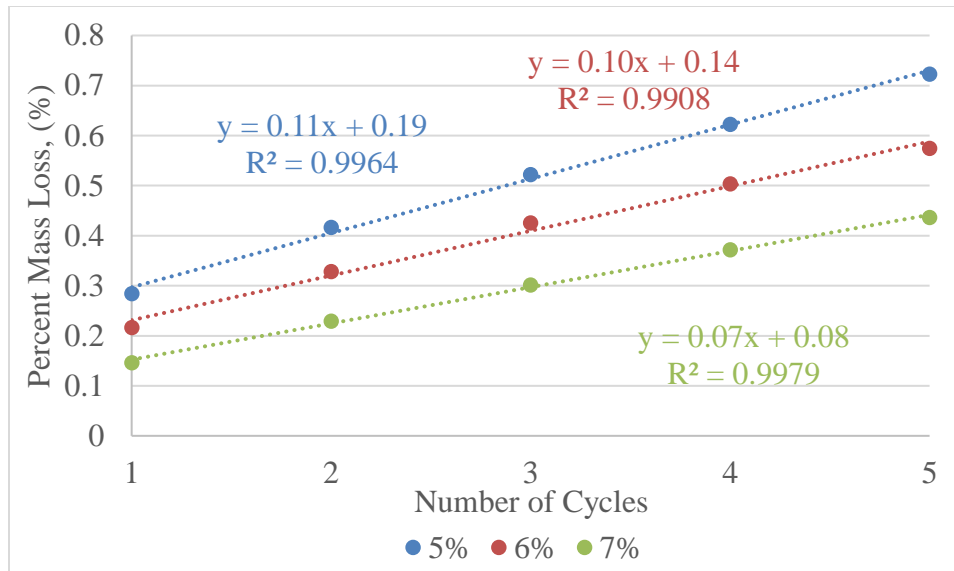
Figure 4.4- Singular Motion Surface Abrasion Test Method Data (Each Cycle was 2 Minutes in Duration)

<u>Planetary Motion Surface Abrasion Test Method</u>

Three specimens for each binder type were tested using the planetary motion surface abrasion test method. The specimens were tested for one cycle of 15 minutes. Figure 4.5 shows each specimen before and after testing using the planetary motion surface abrasion test method. The average percent mass loss of the three specimens for each binder content is summarized in Figure 4.6. The 5% binder content specimens have a higher percent mass loss than the 6% and 7% binder content specimens do with, 7% being the lowest.

Figure 4.5- Raveling Test Using Univex Mixer (a) 5% Before Testing, (b) 5% After Testing, (c) 6% Before Testing, (d) 6% After Testing, (e) 7% Before Testing, and (f) 7% After Testing
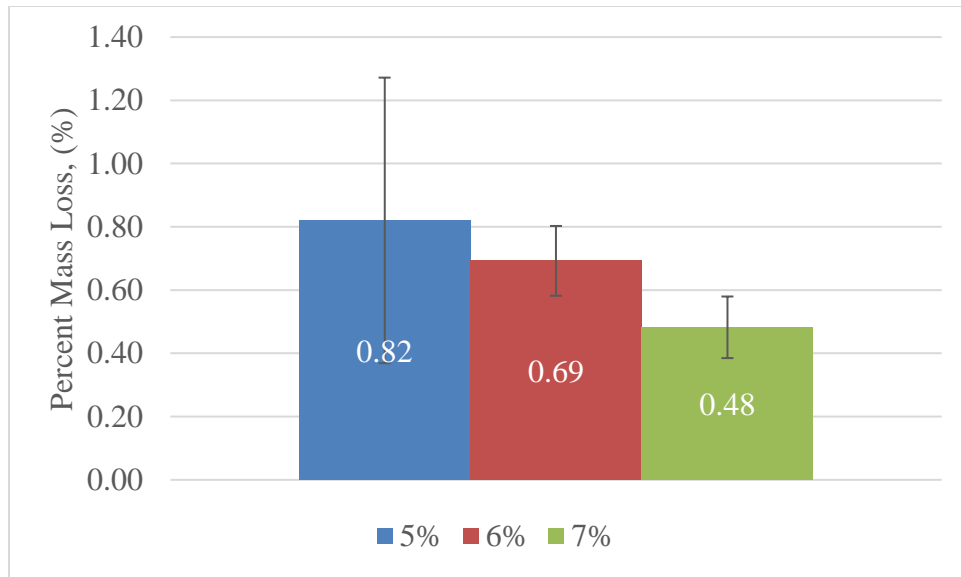
Figure 4.6- Planetary Surface Abrasion Test Method Data

<u>Indirect Tensile Strength</u>

Three specimens for each binder type were subjected to an indirect tensile strength test. The indirect tensile strength (ITS) increases as the binder content increases (Figure 4.7). This shows an increase in the strength of the mix design as the binder content increases. The 7% binder content specimens had the highest indirect tensile strength with the 5% binder content having the lowest indirect tensile strength.

The area under the load-deformation curve between zero load and the peak was calculated (Modulus of Toughness). The average calculated toughness for each binder content can be seen in Figure 4.8. The calculated toughness modulus of the specimens indicated the ability of the specimens to absorb energy and plastically deform without failure. The toughness (energy) of the specimens was determined by calculating the area under the load-deformation curve using the trapezoidal formula in Excel. The modulus of toughness for each binder content increases as the binder content increases. This shows that as the binder content increase, the toughness of the mix design increases.
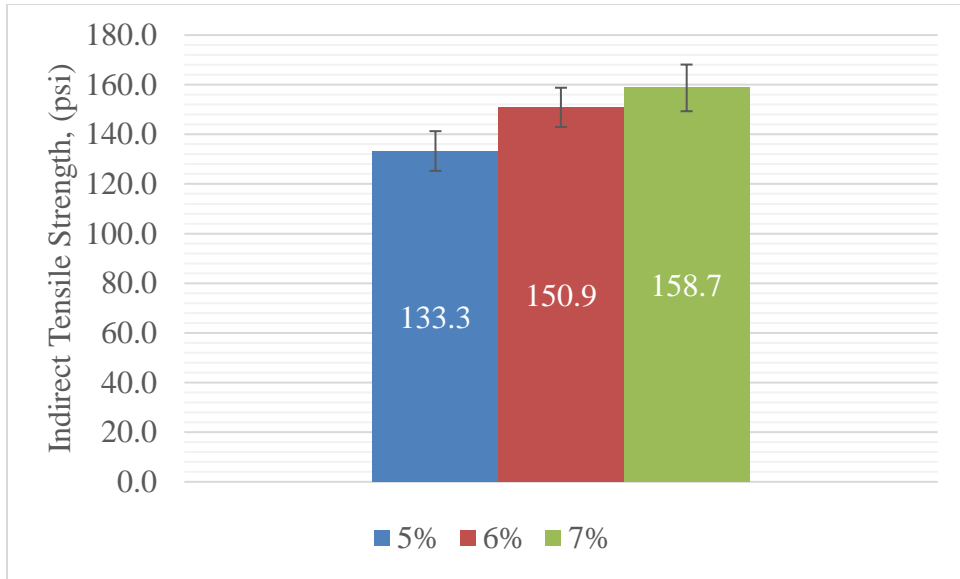
Figure 4.7- Indirect Tensile Strength
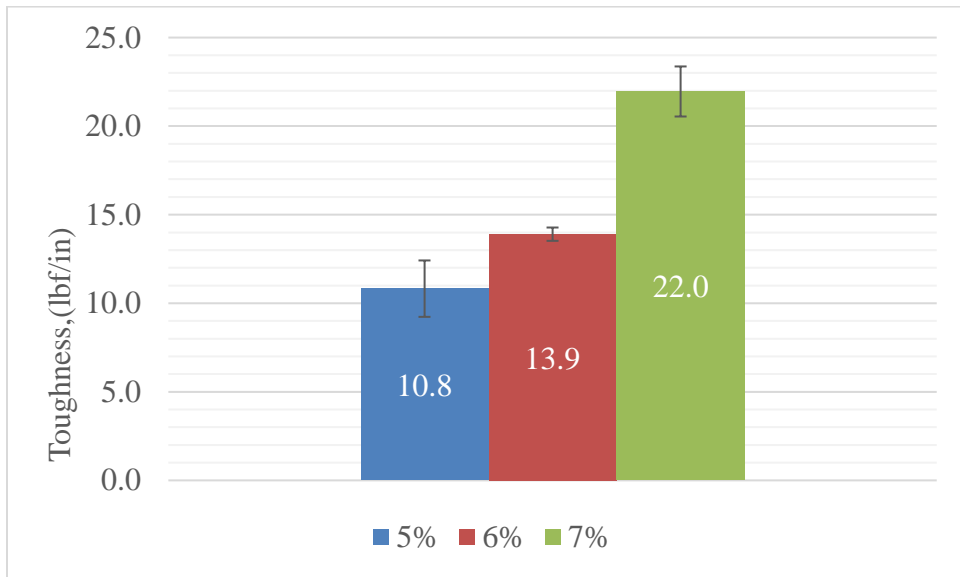
Figure 4.8- Modulus of Toughness Data for the Indirect Tensile Strength Test

Direct Shear Strength Test

Three specimens for each binder type were subjected to a direct shear strength test. The shear strength increases as the binder content increases (Figure 4.9). The specimens with the 5% binder content had the lowest shear strength, with the 7% binder content specimens having the highest shear strength at failure. The area under the load-deformation curve between zero load and the peak was calculated similar to that of the indirect tensile strength specimens. The average calculated toughness for each binder content is summarized in Figure 4.10. The modulus of toughness for each binder content increases as the binder content increases, with the specimens with the 7% binder content having the highest modulus of toughness.
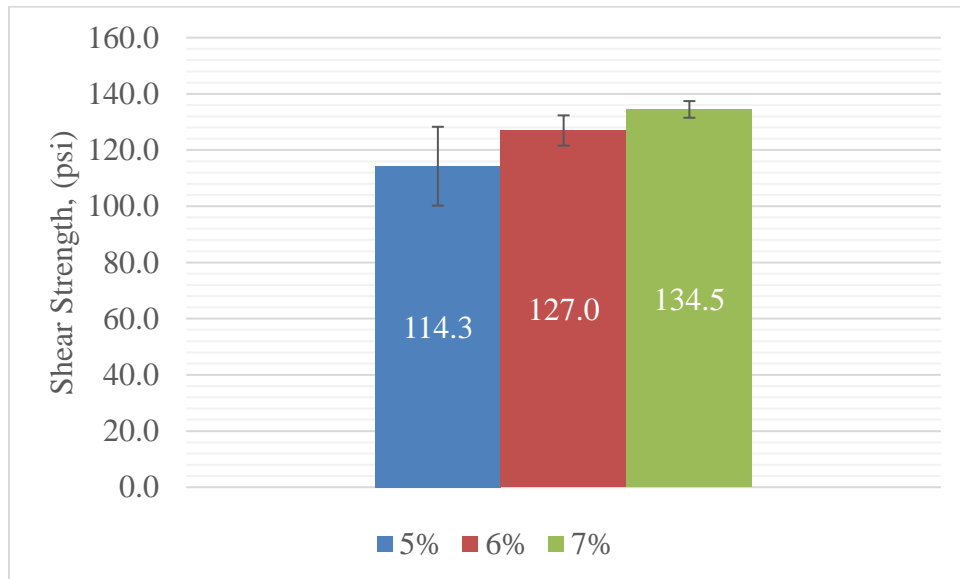
Figure 4.9- Shear Strength Data
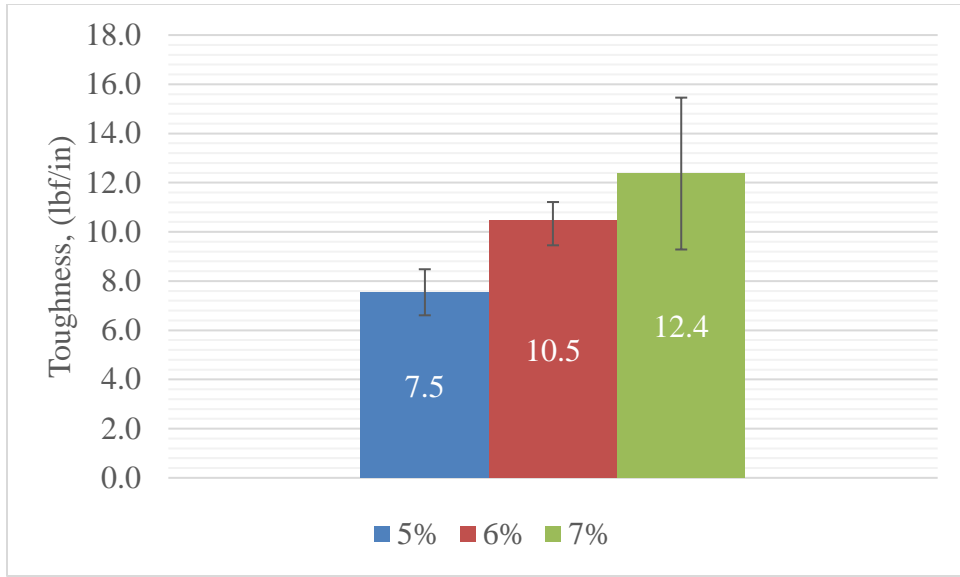
Figure 4.10- Modulus of Toughness Data for the Direct Shear Strength Test

Conclusion of Phase A1

The two new test methods, singular and planetary motion surface abrasion tests, were validated in this phase of the research study through the comparison of the Cantabro test method, shear strength test method, and the indirect tensile strength method. The new test methods showed the same trends as the other test methods. As the binder content increased, the strength (or raveling resistance) of the OGFC mix design increased.

<u>Phase A2</u>

The purpose of this phase was to evaluate the effects of long-term mix aging on the performance using the two new test methods along with the Cantabro test method, direct shear strength test method and the indirect tensile strength test method. The binder properties of the binder used in the mix design for this phase in this study was also tested and evaluated.

Cantabro Abrasion Resistance

Three specimens for each conditioning type, (un-aged, aged, and flipped aged) were tested using the Cantabro abrasion test method. Figure 4.11 presents the average percent mass loss for each aging condition. The un-aged specimens had the lowest average present mass loss (10.5%) and the aged specimens had the highest average percent mass loss (18.4%). The flipped specimens had an average percent mass loss of 16.5%, which is lower than the aged but higher than the un-aged. After the statistical analysis of the Cantabro results comparing the conditioning type, it was determined that the aged and flipped specimens were found to be statistically similar, while the unaged was found to be significantly different than the aged and flipped conditioned specimens.

 Figure 4.12 shows each specimen before and after Cantabro testing. After testing, the aged specimens (Figure 4.12 (d)) were visibly more deteriorated than the un-aged specimens (Figure 4.12 (b)). The aged specimens (Figure 4.12 (d)) and the flipped specimens (Figure 4.12 (f)) look visibly similar after testing, reflecting the mass loss results. The Cantabro test method demonstrates more of an impact test method on the OGFC specimens.

Upon examination of the specimens after testing, the Cantabro test results in a significant amount of aggregate degradation. Based on this observation and how the test procedure works, the Cantabro test is part impact test and part evaluation of cohesive strength of the mix. Being an impact test, this is less representative of the stresses imposed on a pavement surface under traffic.

Figure 4.11 – Cantabro Test Results (The White Letters Represent the Statistical Analysis of the Data as Analyzed by the Letter Report. Alike Letters are Statistically Similar)
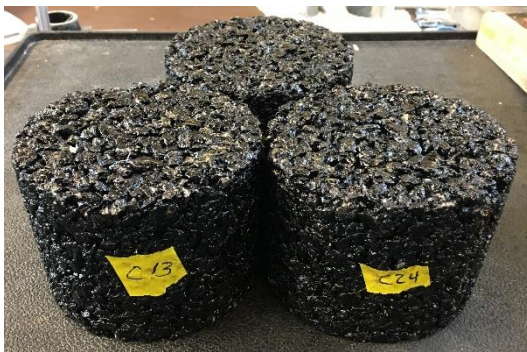
Figure 4.12- Cantabro Abrasion Test (a) Un-Aged Before, (b) Un-Aged After, (c) Aged Before, (d) Aged After, (e) Flipped Aged Before, and (f) Flipped Aged After

Direct Shear Strength Test

Three specimens for each conditioning type (un-aged, aged, and flipped aged) were subjected to a direct shear strength test. Figure 4.13(a) presents the average shear strength (psi) for each aging condition for both the top and bottom of the specimens. Each specimen was tested along two parallel planes, 1 inch from the top and 1 inch from bottom of the specimen. The top of all of the specimens had a higher average shear strength (psi) than the bottom of the specimens. The flipped conditioned specimens had the highest average strength for both top and bottom of the specimen, whereas the un-aged had the lowest average strength (psi).

For each specimen, the modulus of shear toughness (lbf/in) for the top and bottom of the specimens was calculated. The calculated shear toughness modulus of the specimens shows the ability of the specimens to absorb energy and plastically deform without failure. Figure 4.13 (b) summarizes the average modulus of shear toughness (lbf/in) for the top and bottom of the specimens. The top of all of the specimens had a higher shear toughness modulus (lbf/in) than the bottom of the specimens. The flipped conditioned specimens had the highest average modulus of shear toughness (lbf/in) for both top and bottom, whereas the un-aged had the lowest average modulus of shear toughness.

(a)
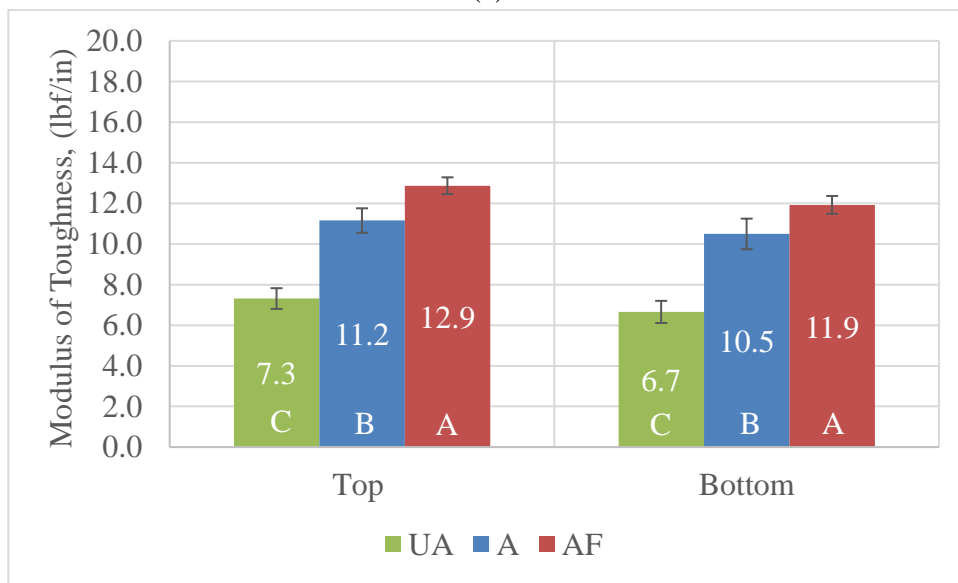
(b)

Figure 4.13-Average Shear Strength (a) and Modulus of Shear Toughness (b) of the Top and Bottom for Each of the Conditioned Specimen Types Using the Direct Shear Strength Test (The White Letters Represent the Statistical Analysis of the Data as Analyzed by the Letter Report. Alike Letters are Statistically Similar)

After the statistical analysis of the direct shear strength test was conducted by comparing the specimens by conditioning type of the top of the un-aged, aged and aged flipped specimens; the analysis found that the top of the aged and flipped specimens were significantly similar. The top of the un-aged specimen were found to be significantly different from the top of the aged and flipped specimens. The same trend can be seen for the bottom of the un-aged, aged and flipped specimens. This can be seen in the letter report on Figure 4.13(a).

Statistical analysis comparing the top of the specimens to the bottom of the specimens for each aging condition (Figure 4.13 (a)) indicated that the top of the specimens for each aging condition were found to be significantly different from the bottom of the specimens. This means that the shear strength of the top of un-aged specimens was significantly different than the bottom of the un-aged specimens, and the same trend was seen for the aged and aged flipped specimens.

The statistical analysis of the modulus of shear toughness (Figure 4.13 (b)) was conducted by comparing the specimens by conditioning type of the top of the un-aged, aged and aged flipped specimens; the analysis found that the top of the un-aged, aged and aged flipped specimens were significantly different. The same trend follows for the bottom of the specimens as well. Statistical analysis comparing the top of the specimens to the bottom of the specimens for each aging condition (Figure 4.13 (b)) showed that the top of the specimens for each aging condition was found to be significantly similar to the bottom of the specimens.

Figure 4.14 includes photos of each specimen before and after shear testing. The after pictures for the tested specimens show a slight horizontal deformation in the top and bottom of the specimens. From visual inspection during testing, the direct shear test showed a cohesive failure of the asphalt binder as there was no evidence of fractured aggregates.
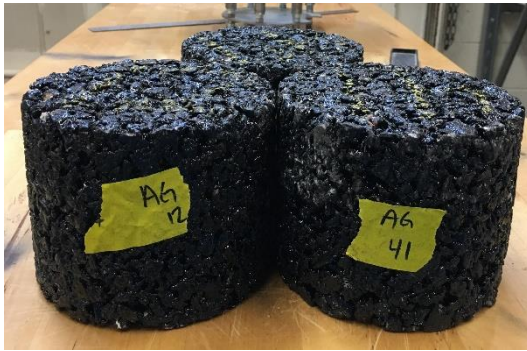
(a)

(b)

(c)

(d)

(e)

(f)

Figure 4.14- Direct Shear Test (a) Un-Aged Before, (b) Un-Aged After, (c) Aged Before, (d) Aged After, (e) Flipped Aged Before, and (f) Flipped Aged After

<u>Singular Motion Surface Abrasion Test</u>

Three specimens for two conditioning types (un-aged and aged) were subjected to a singular motion surface abrasion test on the top and bottom surface of each specimen. Figure 4.15 shows the percent mass loss (%) versus the number of cycles for the top and bottom of each specimen using cutter head A (Figure 4.15(a)) and cutter head B (Figure 4.15 (b)). Cutter heads A and B showed the same trends where the bottom of the aged specimens had the lowest abrasion loss, however, the top of the aged specimens had about the same percent mass loss for the first two cycles. The top of the un-aged specimens had the highest abrasion loss for all six cycles, followed by the bottom of the un-aged specimens for cutter head A and B.
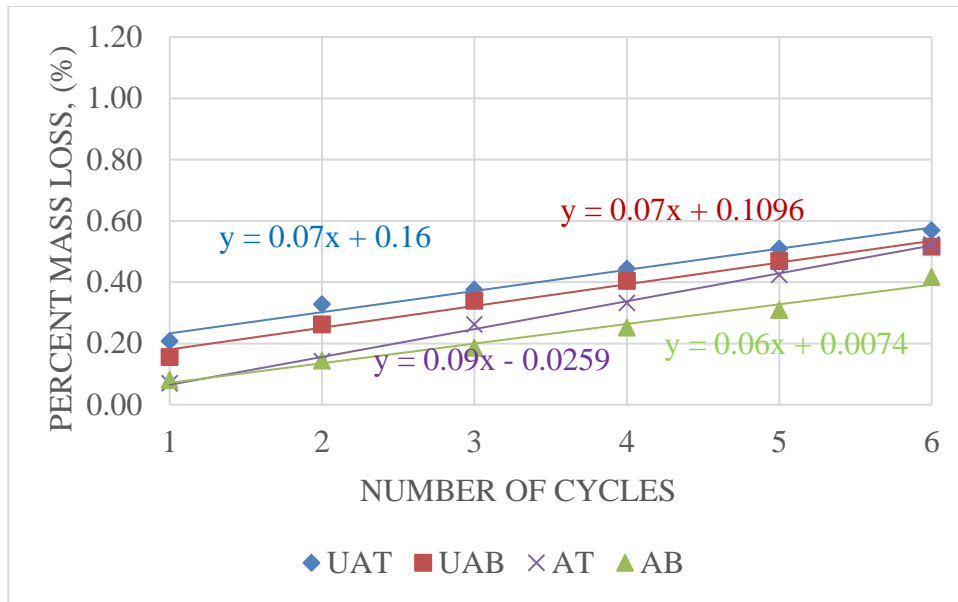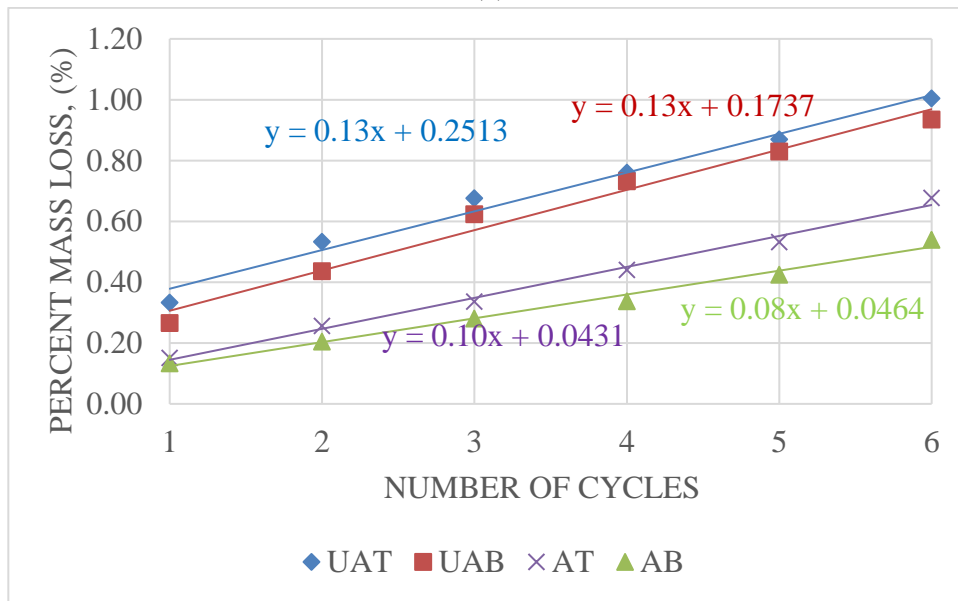
Figure 4.15- Singular Motion Abrasion Test Data for Cutter Head A (a) and Cutter Head B (b) (Ran for Five Minute Cycles)

When comparing the slope of the trendlines for each set of specimens, the top of the aged specimens had the highest slope for cutter head A (Table 4.2). The top and bottom of the un-aged specimens had the highest slope for cutter head B. Cutter head B had higher slope values for all specimen types when compared to cutter head A. This means that the rate of the percent mass loss (%) per cycle of cutter head B is higher than cutter head A; therefore cutter head B is more abrasive than cutter head A. When comparing the top and bottom of the un-aged specimens using cutter head A, the slopes are the same. This means that the top and bottom of the unaged specimens abraded at the same rate. The same trend was seen for the un-aged specimens using cutter head B.

The results show that the top and bottom of the un-aged specimens using the singular motion surface abrasion test method exhibited the same rate of wearing. This pattern was expected in the un-aged specimens because the binder content of the top and bottom of the specimen should be about the same, therefore, should have the same strength. When comparing the top and bottom of the aged specimens, the rate of wear was higher for top of the specimen than the bottom of the specimen. This shows that the bottom of the aged specimens are slightly more resistant to particle loss than the top of the specimens. This could be due to the fact that the bottom had a higher binder content than the top of the specimens due to binder draindown during the aging process.

Table 4.2- Slope of Trendlines of Cutter Head A and B for Singular Motion Abrasion Test

Slope of Trendlines (% Mass Loss/ Cycle)		
Specimen Type	Cutter Head A	Cutter Head B
UAT	0.07	0.13
UAB	0.07	0.13
AT	0.09	0.10
AB	0.06	0.08

The surface roughness of the aged specimens before and after testing was measured using image analysis as outlined in Chapter 3 and a percent difference in roughness between the untested and tested specimens was calculated. The singular motion average percent difference in roughness and average percent mass loss after six cycles for cutter head A and cutter head B of the aged specimens is summarized in Figure 4.16.

Cutter head A had a lower average difference in percent roughness (11.7%) for the top of the aged specimens than cutter head B (15.9%). The bottom of the aged specimens had the same average difference in percent roughness (10.4%) for both cutter heads A and B. This indicates that cutter B was more abrasive for the top of the aged specimens.

When comparing the tops of the specimens, the relationship between the average difference in percent roughness and the average percent mass loss after being tested for six cycles follows the same trend for both cutter heads A and B. The top of the aged specimens for cutter head A (Figure 4.16 (a)) had a higher average difference in roughness (11.7%) and a higher average percent mass loss (0.52%). The bottom followed the same trend, having an average difference in roughness (10.4%) and an average percent mass loss of 0.42%.

The top of the aged specimens for cutter head B (Figure 4.16 (b)) had a higher average difference in roughness (15.9%) and a higher average percent mass loss (0.68%). The bottom followed the same trend, having an average difference in roughness (10.4%)

and an average percent mass loss of 0.54%. This shows that as the percent mass loss increases, the surface roughness of the specimens also increases.

However, for cutter heads A and B, the statistical analysis of the average difference in percent roughness between the top and bottom of the specimens were found to be statistically similar.
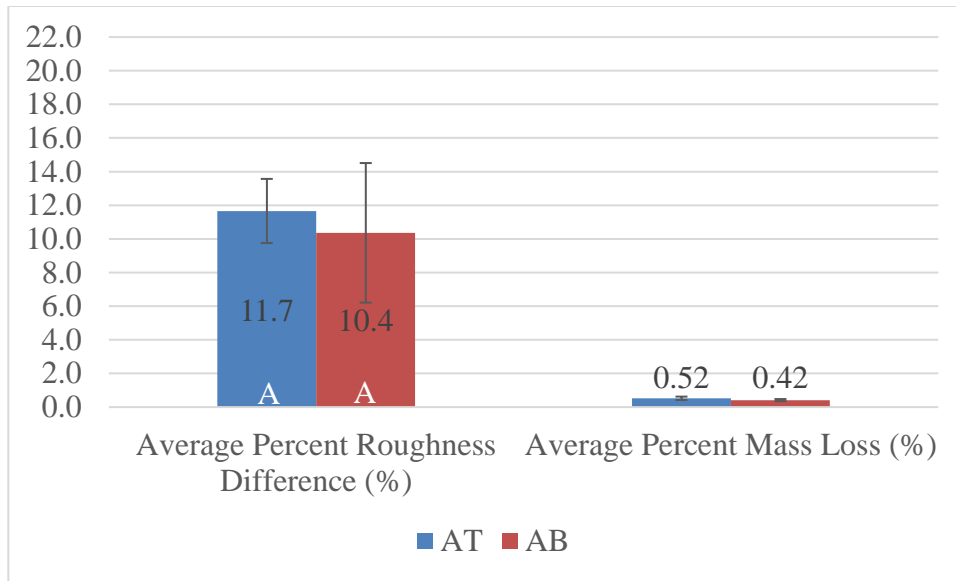
(a)
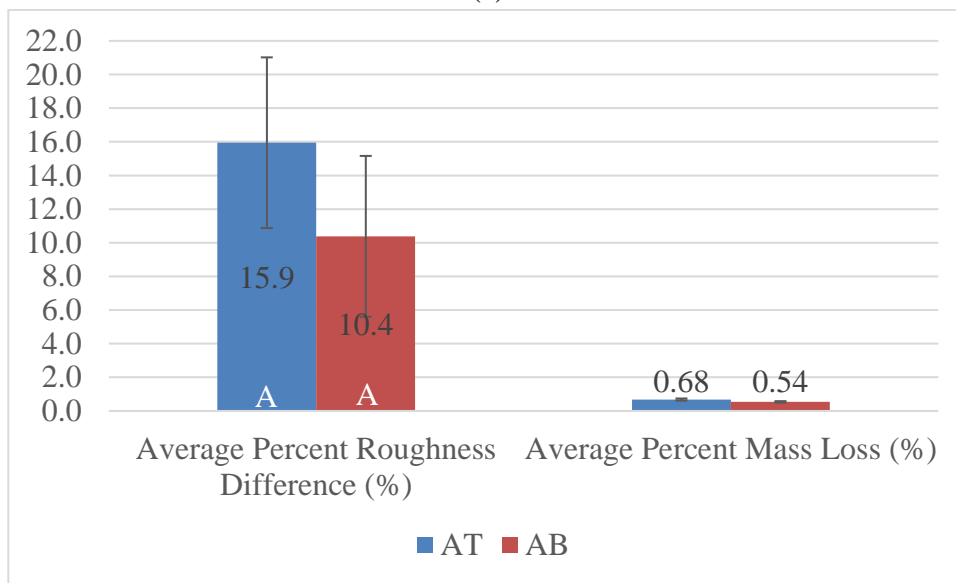
(b)

Figure 4.16- Singular Motion Average Percent Roughness Difference for the Aged Specimens and Average Percent Mass Loss for Cutter Head A (a) and Cutter Head B (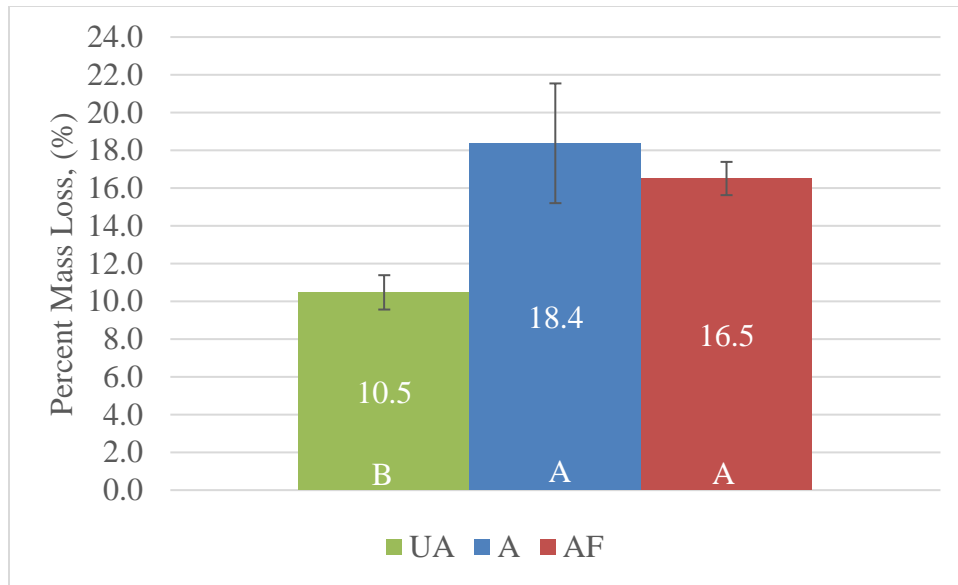b) (The White Letters Represent the Statistical Analysis of the Data as Analyzed by the Letter Report. Alike Letters are Statistically Similar)

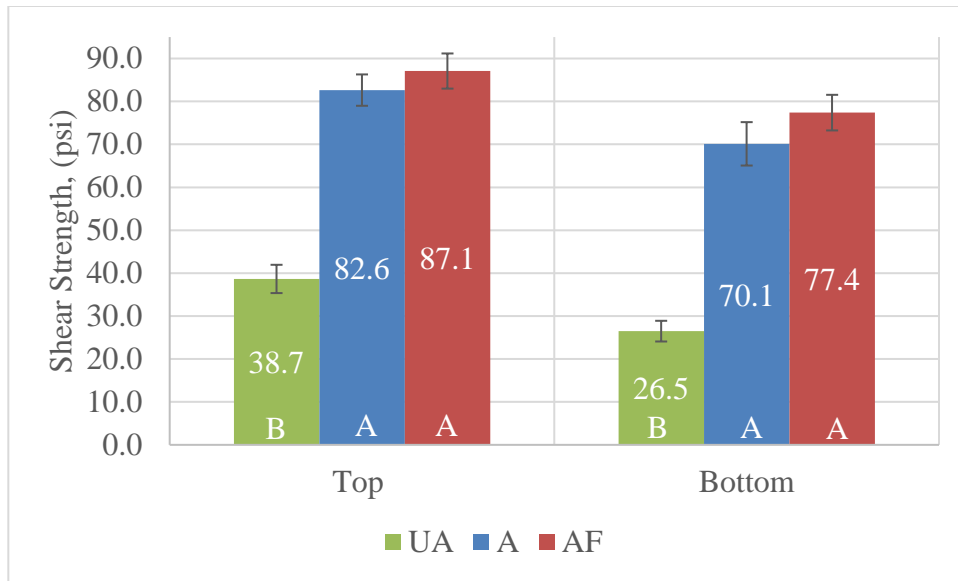The statistical analysis of the percent mass loss for cutter head A (Table 4.3) was conducted by comparing the specimens by their conditioning type. The top of the un-aged and aged specimens were significantly similar. This means that there was not a significant difference between the percent mass loss between the tops of the un-aged and aged specimens for cutter head A. The bottoms of the un-aged and aged specimens were also found to be significantly similar, which indicates that there was not a significant difference between the percent mass loss between the bottom of the un-aged and aged specimens for cutter head A.

Statistical analysis comparing the top of the specimens to the bottom of the specimens for each aging condition found that the top of the specimens for the un-aged and aged specimens were significantly similar to the bottom of the specimens. This means that there was not a significant difference between the percent mass loss between the top and bottom of the specimens for cutter head A for both conditioning types.

The statistical analysis of the percent mass loss for cutter head B (Table 4.4) was conducted by comparing the specimens by their conditioning type. The tops of the un-aged and aged specimens were found to be significantly different. This means that there was a significant difference between the percent mass loss between the top of the un-aged and aged specimens for cutter head B. The bottoms of the un-aged and aged specimens were found to be significantly different. This means that there was a significant difference between the percent mass loss between the bottom of the un-aged and aged specimens for cutter head B.

84

Statistical analysis comparing the tops of the specimens to the bottoms of the specimens for each aging condition indicated that the tops of the specimens for the un-aged and aged specimens were significantly different for cutter head B. The bottoms of the specimens for the un-aged and aged specimens were found to be significantly different for cutter head B as well. This means that there is a significant difference between the percent mass loss between the top and bottom of the specimens for cutter head B for both conditioning types.

Table 4.3- Statistical Analysis by Specimen Condition Type for the Singular Motion Abrasion Test Method for Cutter Head A (Alike Letters Indicate that the Data is Statistically Similar)

Statistical Analysis by Conditioning		
Cutter Head A		
Location	Conditioning Type	
	Un-Aged	Aged
Top	A	A
Bottom	A	A

Table 4.4- Statistical Analysis by Specimen Condition Type for the Singular Motion Abrasion Test Method for Cutter Head B(Alike Letters Indicate that the Data is Statistically Similar)

Statistical Analysis by Conditioning		
Cutter Head B		
Location	Conditioning Type	
	Un-Aged	Aged
Top	A	B
Bottom	A	B

Figures 4.17 and 4.18 show the tops and bottoms, respectively, of the un-aged and aged specimens using the singular motion surface abrasion test method before and after testing using cutter head A. A visible difference in the top of the specimens after testing can be seen for both conditioning types. Completely whole aggregate particles can be seen missing from the top of the specimens after testing shown by green circles (Figure 4.17 (b) and (d), and Figure 4.18 (b) and (d)). The singular motion surface abrasion test method wears the specimens in more of a grinding, circular pattern during testing.

(a)	(b)
(c)	(d)
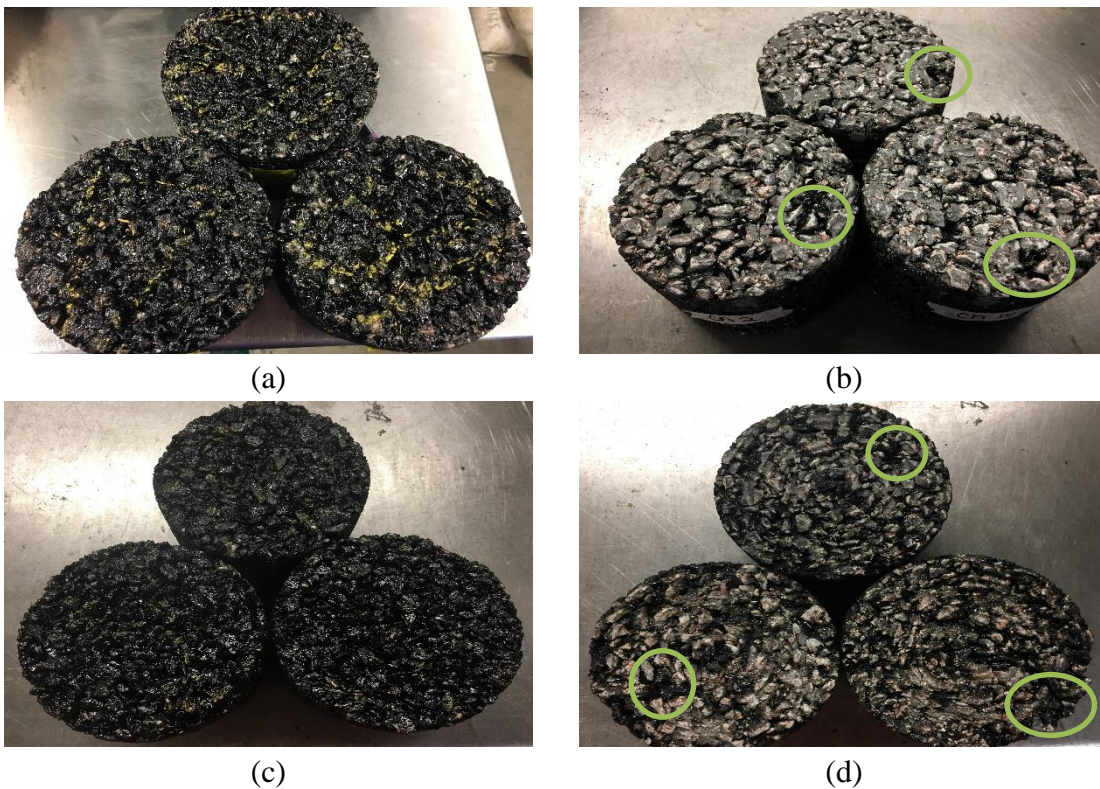
Figure 4.17- Singular Motion Surface Abrasion Test on the Top of the Specimen Using Cutter A (a) Un-Aged Before, (b) Un-Aged After, (c) Aged Before, and (d) Aged After
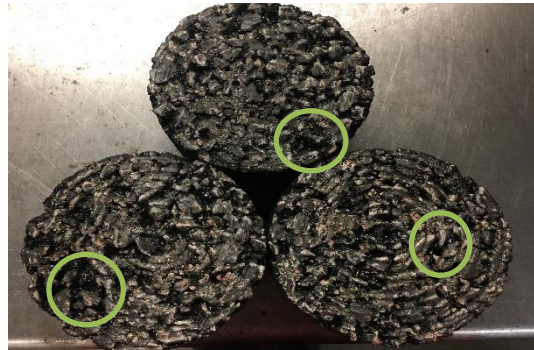
Figure 4.18- Singular Motion Surface Abrasion Test on the Bottom of the Specimen Using Cutter A (a) Un-Aged Before, (b) Un-Aged After, (c) Aged Before, and (d) Aged After

Figures 4.19 and Figure 4.20 shows the tops and bottoms, respectively, of the un-aged and aged specimens using the singular motion surface abrasion test method before and after testing using cutter head B. A visible difference in the top of the specimens after testing can be seen for both conditioning types. Completely whole aggregate particles can be seen missing from the top of the specimens after testing shown by green circles (Figure 4.9 (b) and (d)). Cutter head B had larger and more aggregate particles dislodged during testing from visual inspection.

<div align="center">(a)   (b)</div>

<div align="center">(c)   (d)</div>
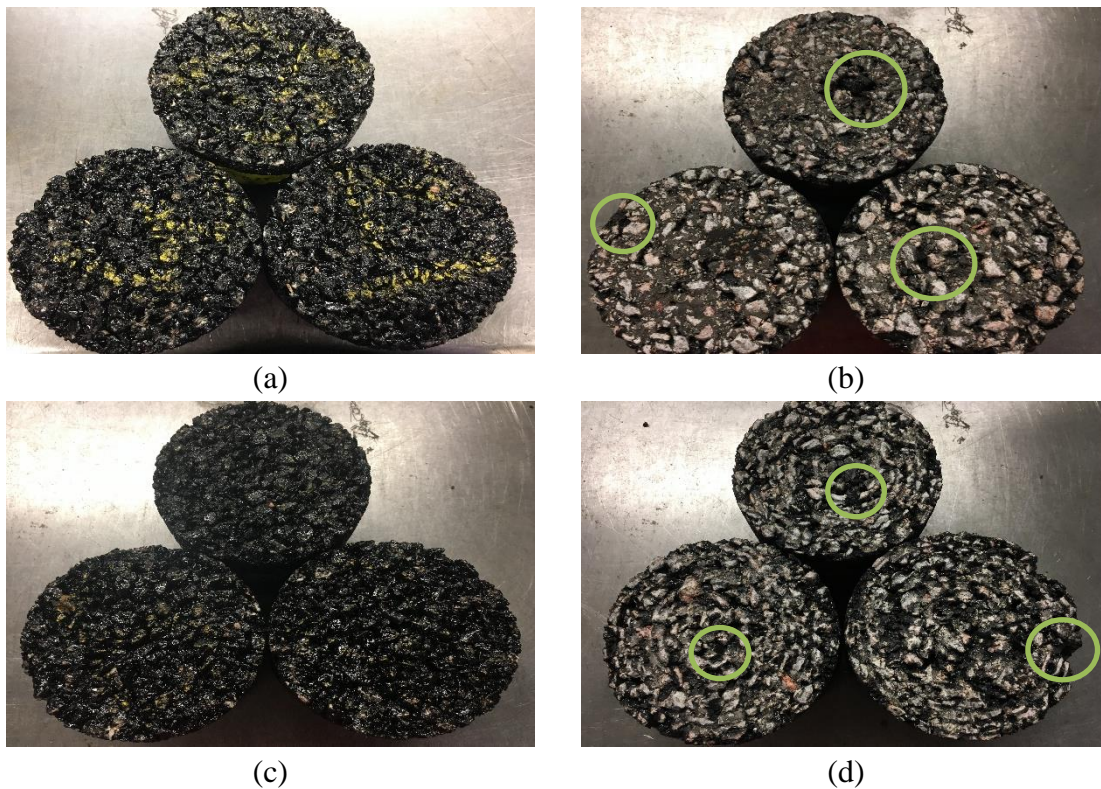
Figure 4.19- Singular Motion Surface Abrasion Test on the Top of the Specimen Using Cutter B (a) Un-Aged Before, (b) Un-Aged After, (c) Aged Before, and (d) Aged After

Figure 4.20- Singular Motion Surface Abrasion Test on the Bottom of the Specimen Using Cutter B (a) Un-Aged Before, (b) Un-Aged After, (c) Aged Before, and (d) Aged After

Planetary Motion Surface Abrasion Test

Figure 4.21 shows the percent mass loss versus the number of cycles for the top and bottom of each specimen using cutter head A (Figure 4.21(a)) and cutter head B (Figure 4.21 (b)). Three specimens for three conditioning types, (un-aged, aged and aged flipped) were subjected to a planetary motion surface abrasion test on the top and bottom of each specimen for cutter head A (Figure 4.21 (a)). The top of the un-aged specimens had the highest percent mass loss, whereas the bottom of the flipped specimens had the lowest with the aged specimens being in-between the two conditioning types for cutter head A. The planetary motion surface abrasion test for cutter head A had a similar trend as the singular motion surface abrasion test. The top of the specimens for each conditioning type had a higher percent mass loss.

Three specimens for two conditioning types, (un-aged and aged) were subjected to a planetary motion surface abrasion test on the top and bottom of each specimen for cutter head B (Figure 4.21 (b)). The top of the un-aged specimens had the highest percent mass loss, whereas the bottom of the aged specimens had the lowest. The top of the specimens for each conditioning type had a higher percent mass loss than the bottom of the specimen.

Figure 4.21- Planetary Motion Surface Abrasion Test Method Data for Cutter Head A (a) and Cutter Head B (b) (Ran for 5 Minute Cycles)

When comparing the slopes of the trendlines for each of the specimens, the tops

of the un-aged specimens had the highest slope for cutter head A (Table 4.5). The tops of

the aged specimens had the highest slope for cutter head B. Cutter head B had higher

slope values for all specimen types except for the un-aged top and bottom specimens

when compared to cutter head A. The un-aged bottom slope for cutter head A had the

same slope as cutter head B. Cutter head B was not used on the aged flipped conditioned

specimens. The slope of these data points indicate that the rate of the percent mass loss

per cycle of cutter head B is higher than cutter head A for the aged specimens; therefore

cutter head B is more abrasive on the aged specimens than cutter head A. The slopes also

represent the rate of raveling for each set of specimens. For the aged specimens using

cutter head B, the rate of raveling was much higher than the aged specimens that were

tested using cutter head A.

Table 4.5- Slope of Trendlines of Cutter Head A and B for Planetary Motion Abrasion Test

Slope of Trendlines (% Mass Loss/Cycle)		
Specimen Type	Cutter Head A	Cutter Head B
UAT	0.19	0.11
UAB	0.18	0.18
AT	0.16	0.29
AB	0.13	0.27
AFT	0.11	-
AFB	0.05	-

The surface roughness of the aged specimens before and after testing was measured and the percent difference in the roughness was calculated. The planetary motion average percent difference in roughness and average percent mass loss after cycle six for cutter head A of the aged (Figure 4.22 (a)) and aged flipped (Figure 4.22 (b)) specimens can be seen in Figure 4.22. The average difference in percent roughness of the top and bottom of the aged specimens were statistically similar, even though the top of the aged specimens (14.4%) had a higher change in roughness than the bottom (8.5%) of the specimens (Figure 4.22 (a)). The change in roughness of the tops and bottoms of the aged specimens had a similar correlation as the average percent mass loss; the tops of the aged specimens (1.14%) had a higher average percent mass loss than the bottoms of the aged specimens (0.86%) after six testing cycles.

The average difference in percent roughness of the tops and bottoms of the aged flipped specimens were statistically different, the tops of the aged specimens (20.5%) had a higher change in roughness than the bottoms (5.5%) of the specimens (Figure 4.22 (b)). The change in roughness of the tops and bottoms of the aged specimens had a similar correlation as the average percent mass loss; the tops of the aged specimens (0.82%) had a higher average percent mass loss than the bottoms of the aged specimens (0.56%) after six testing cycles.
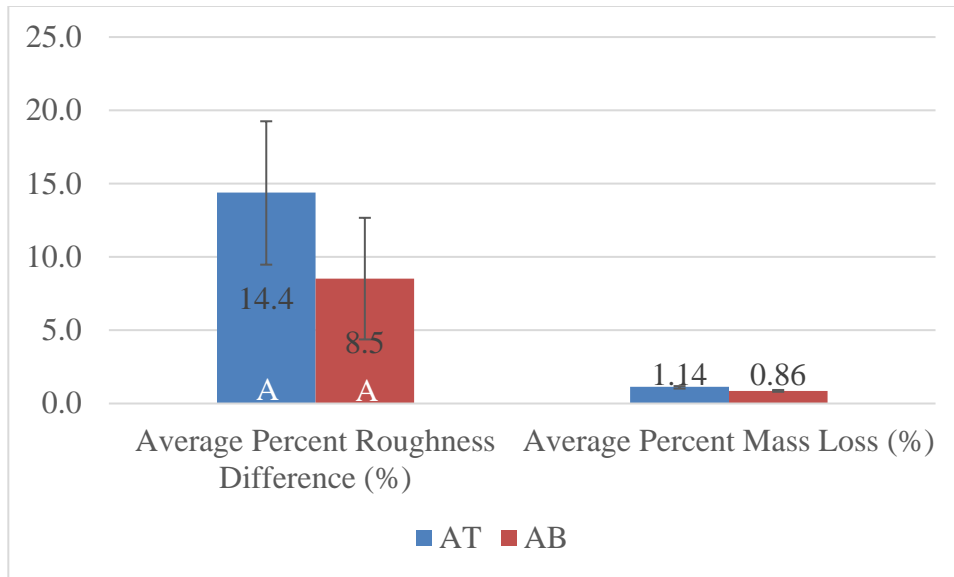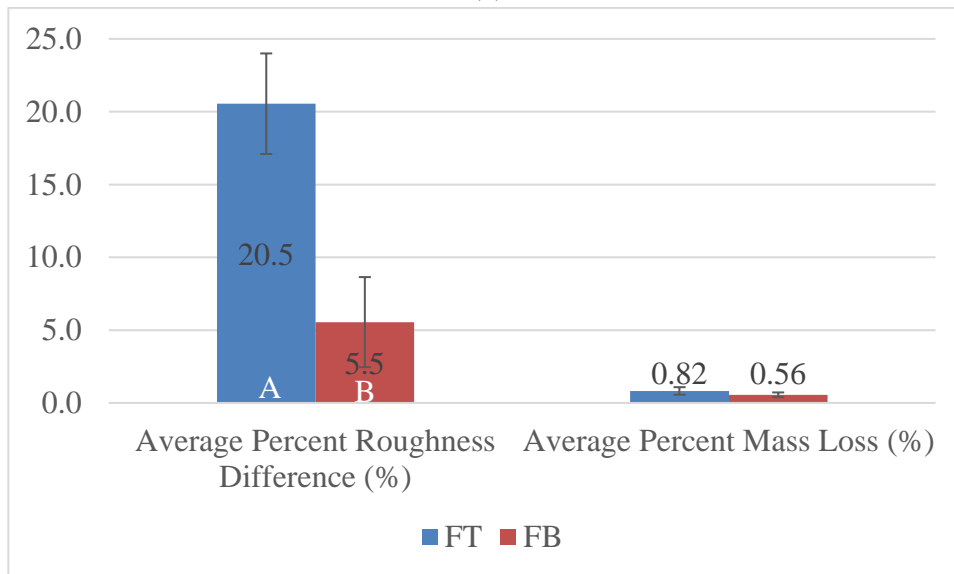
Figure 4.22- Planetary Motion Average Percent Roughness and Average Percent Mass Loss for the Aged (a) and Flipped (b) Specimens for Cutter Head A (The White Letters Represent the Statistical Analysis of the Data as Analyzed by the Letter Report. Alike Letters are Statistically Similar)

The planetary motion average difference in percent roughness and average percent mass loss after six cycles for cutter head B of the aged specimens can be seen in Figure 4.23. The average difference in percent roughness of the tops and bottoms of the aged specimens were statistically different, the tops of the aged specimens (11.6%) had a lower change in roughness than the bottoms (24.1%) of the specimens. The change in roughness of the tops and bottoms of the aged specimens had a different correlation than the average percent mass loss; the tops of the aged specimens (2.02%) had a higher average percent mass loss than the bottoms of the aged specimens (1.70%) after six testing cycles.
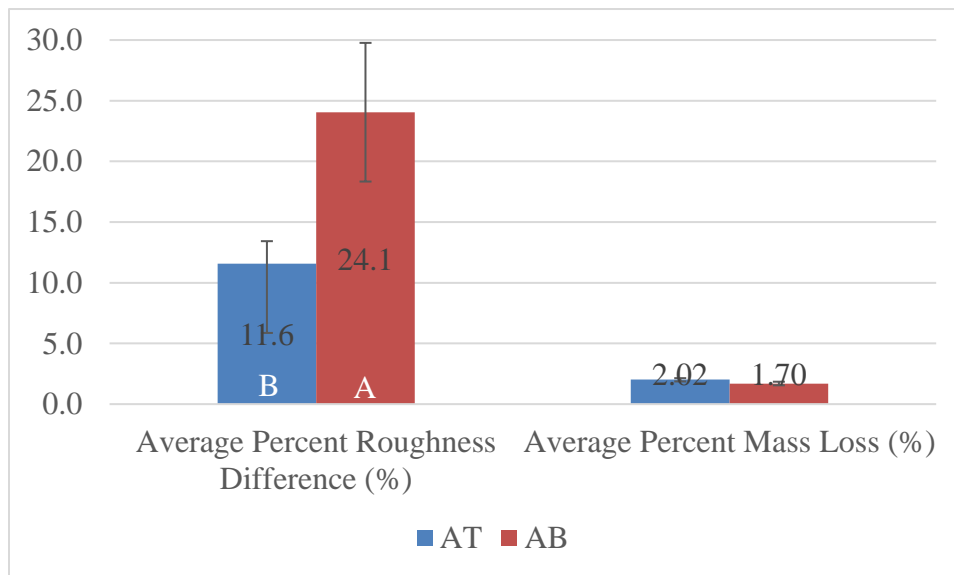
Figure 4.23- Planetary Motion Average Percent Roughness and Average Percent Mass Loss for the Aged Specimens for Cutter Head B (The White Letters Represent the Statistical Analysis of the Data as Analyzed by the Letter Report. Alike Letters are Statistically Similar)

The statistical analysis of the percent mass loss for cutter head A (Table 4.6) was conducted by comparing the specimens by their conditioning type. The tops of the un-aged and aged specimens were significantly similar, but the un-aged was significantly different from the tops of the aged flipped conditioned specimens. However, the tops of aged and aged flipped specimens were significantly similar, but the aged flipped conditioned specimens were significantly different from the un-aged. This means that there was not a significant difference between the percent mass loss of the tops of the un-aged and aged specimens; as well as the tops of the aged and aged flipped conditioned specimens for cutter head A. There was a significant difference between the percent mass loss of the un-aged and aged flipped conditioned specimens for cutter head A. The bottoms of the specimens followed the same statistical trend as the tops of the specimens for cutter head A when comparing by conditioning type.

Statistical analysis comparing the tops of the specimens to the bottoms of the specimens for each aging condition found that the tops of the specimens for the un-aged and aged flipped conditioned specimens were significantly similar to the bottom of the specimens. There was a significant difference between the tops and bottoms of the aged specimens for cutter head A. This means that there was not a significant difference between the percent mass loss between the tops and bottoms of the specimens for cutter head A for the un-aged and aged flipped specimens, and a significant difference between the tops and bottoms of the aged specimens.

The statistical analysis of the percent mass loss for cutter head B (Table 4.7) was conducted by comparing the specimens by their conditioning type. The tops of the un-aged and aged specimens, as well as the bottoms of the un-aged and aged specimens were found to be significantly different.

Statistical analysis comparing the tops of the specimens to the bottoms of the specimens for each aging condition found that the top of the specimens for the un-aged specimens were significantly similar for cutter head B. The aged specimens were found to be significantly different for cutter head B.

Table 4.6- Statistical Analysis by Specimen Condition Type for the Planetary Motion Abrasion Test Method for Cutter Head A (Alike Letters are Statistically Similar)

Statistical Analysis by Conditioning		
Cutter Head A		
Location	Conditioning Type	
	Un-Aged	Aged	Flipped
Top	A	AB	B
Bottom	A	AB	B

Table 4.7- Statistical Analysis by Specimen Condition Type for the Planetary Motion Abrasion Test Method for Cutter Head B (Alike Letters are Statistically Similar)

Statistical Analysis by Conditioning		
Cutter Head B		
Location	**Conditioning Type**	
	Un-Aged	Aged
Top	A	B
Bottom	A	B

Figures 4.24 and 4.25 show the tops and bottoms, respectively, of the un-aged, aged and aged flipped specimens using the planetary motion surface abrasion test method before and after testing using cutter head A. A visible difference in the tops of the specimens after testing can be seen for all conditioning types. Whole aggregate particles that were removed for the specimen's surface during testing are shown by green circles (Figure 4.24 (b), (d) and (f); and Figure 4.25 (b), (d) and (f)). From visual inspection, the planetary motion surface abrasion test method had larger and more aggregate particles dislodged during testing for both cutter heads when compared to the singular motion surface abrasion test method. This could be due to the planetary motion of the cutter heads on the surface of the specimens.
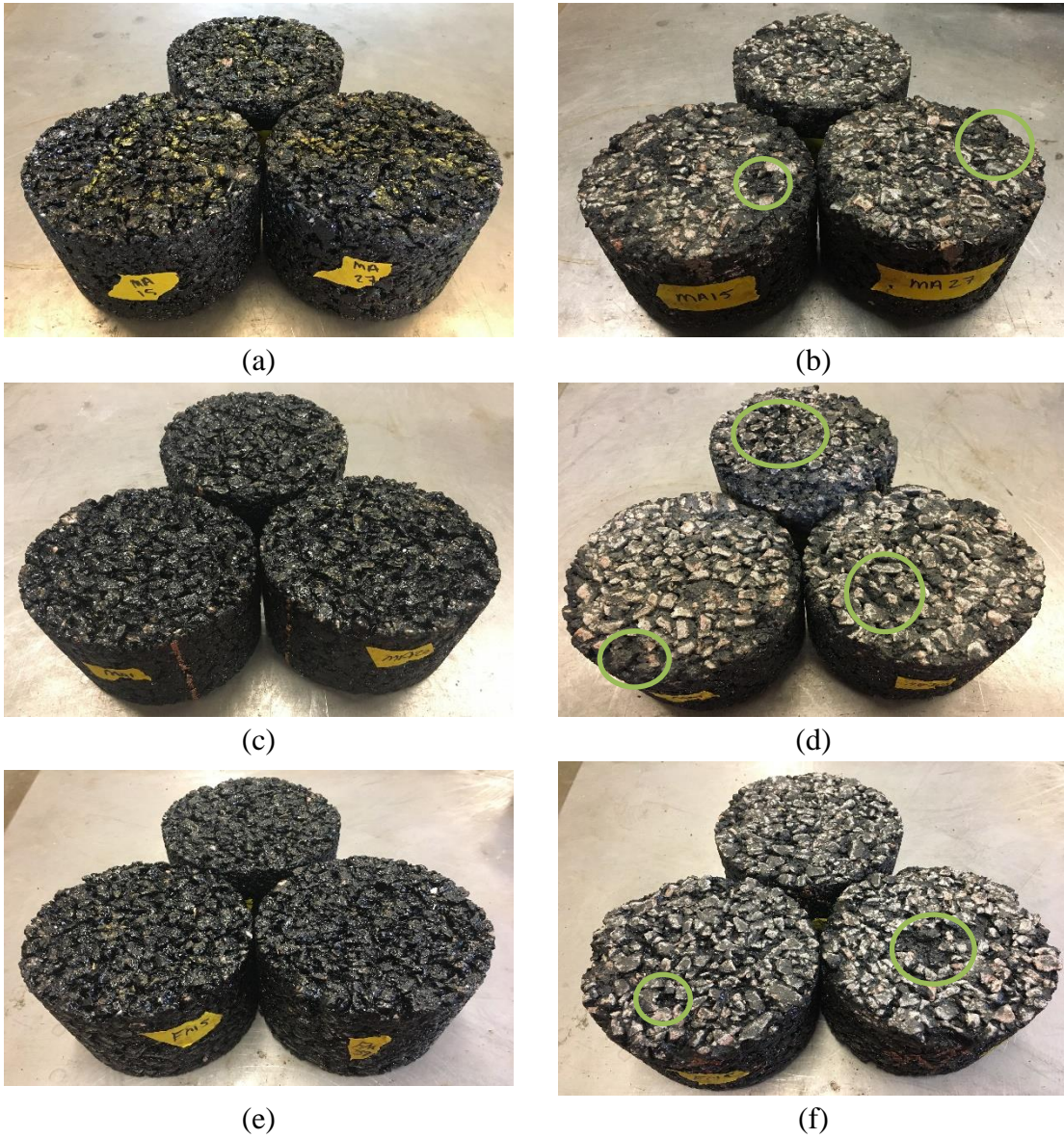
Figure 4.24- Planetary Motion Surface Abrasion Test on the Top of the Specimen Using Cutter A (a) Un-Aged Before, (b) Un-Aged After, (c) Aged Before, (d) Aged After, (e) Flipped before, and (f) Flipped after
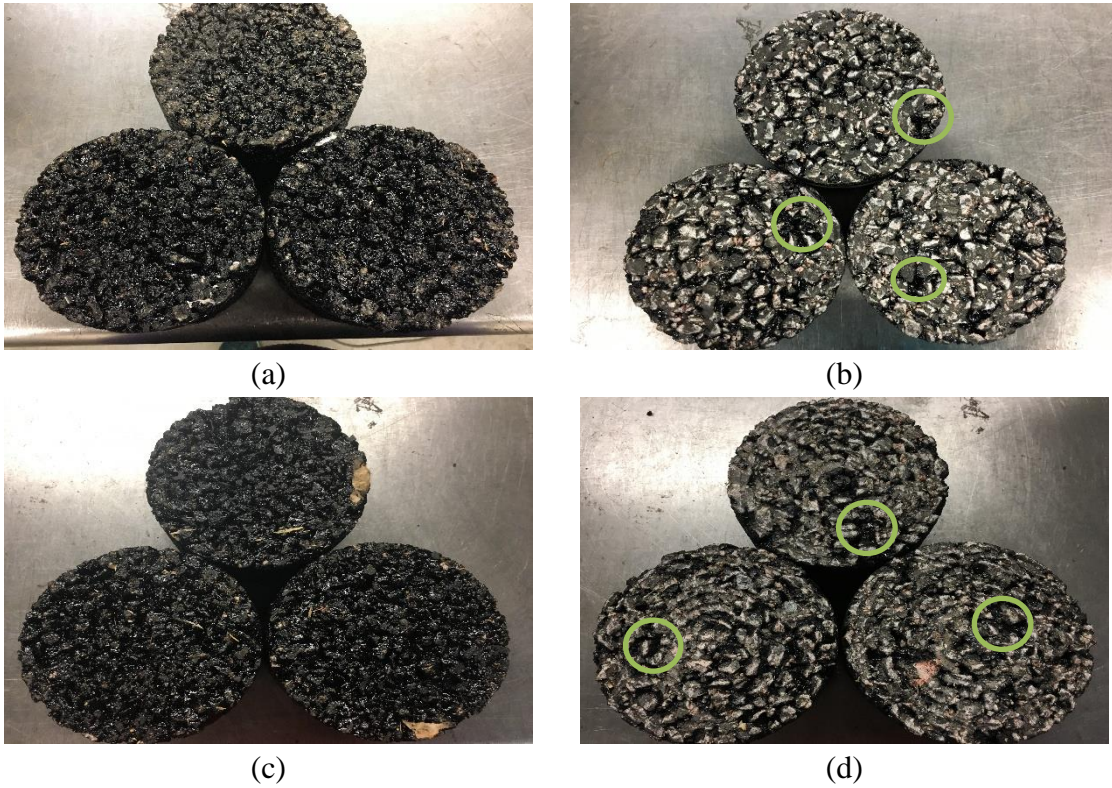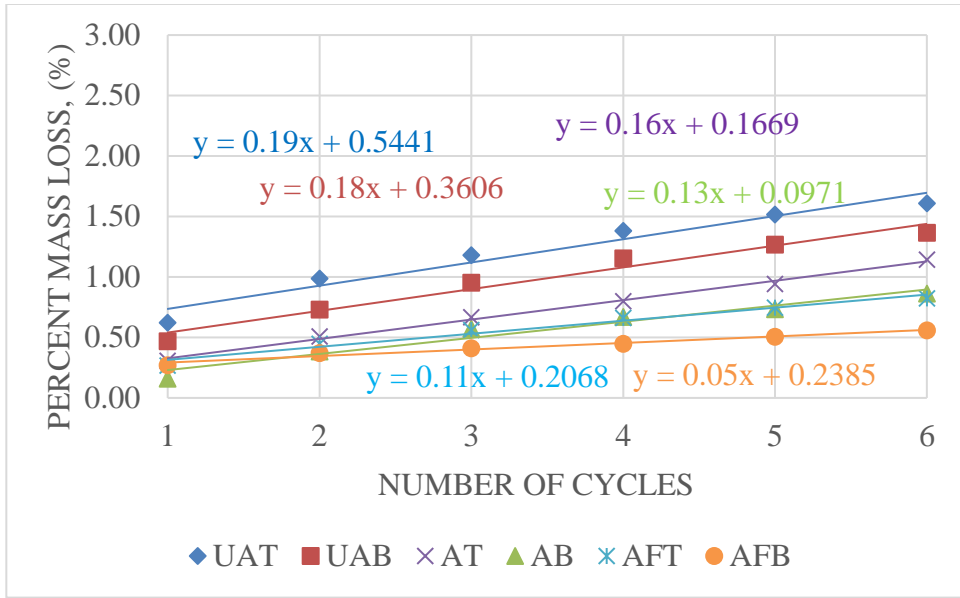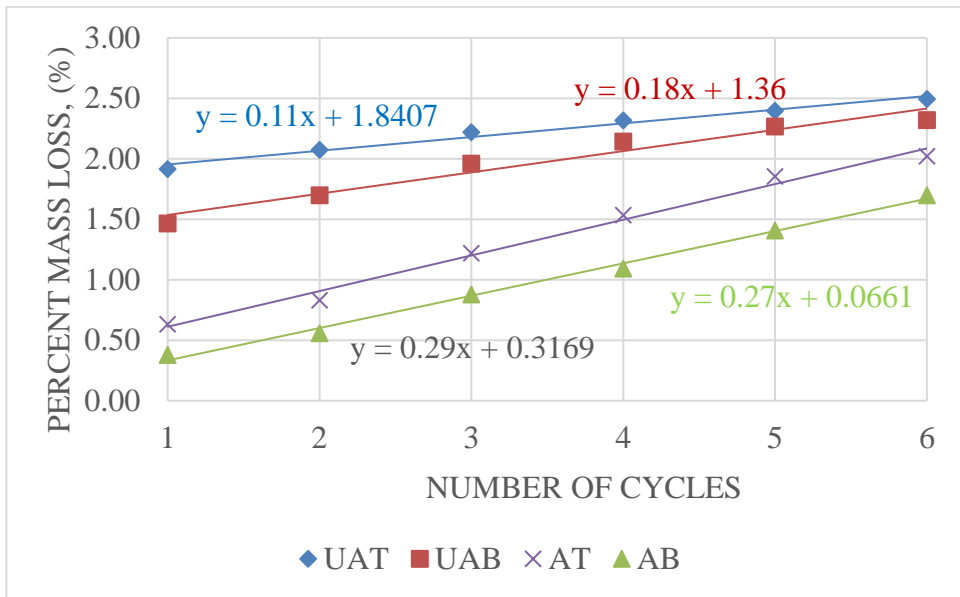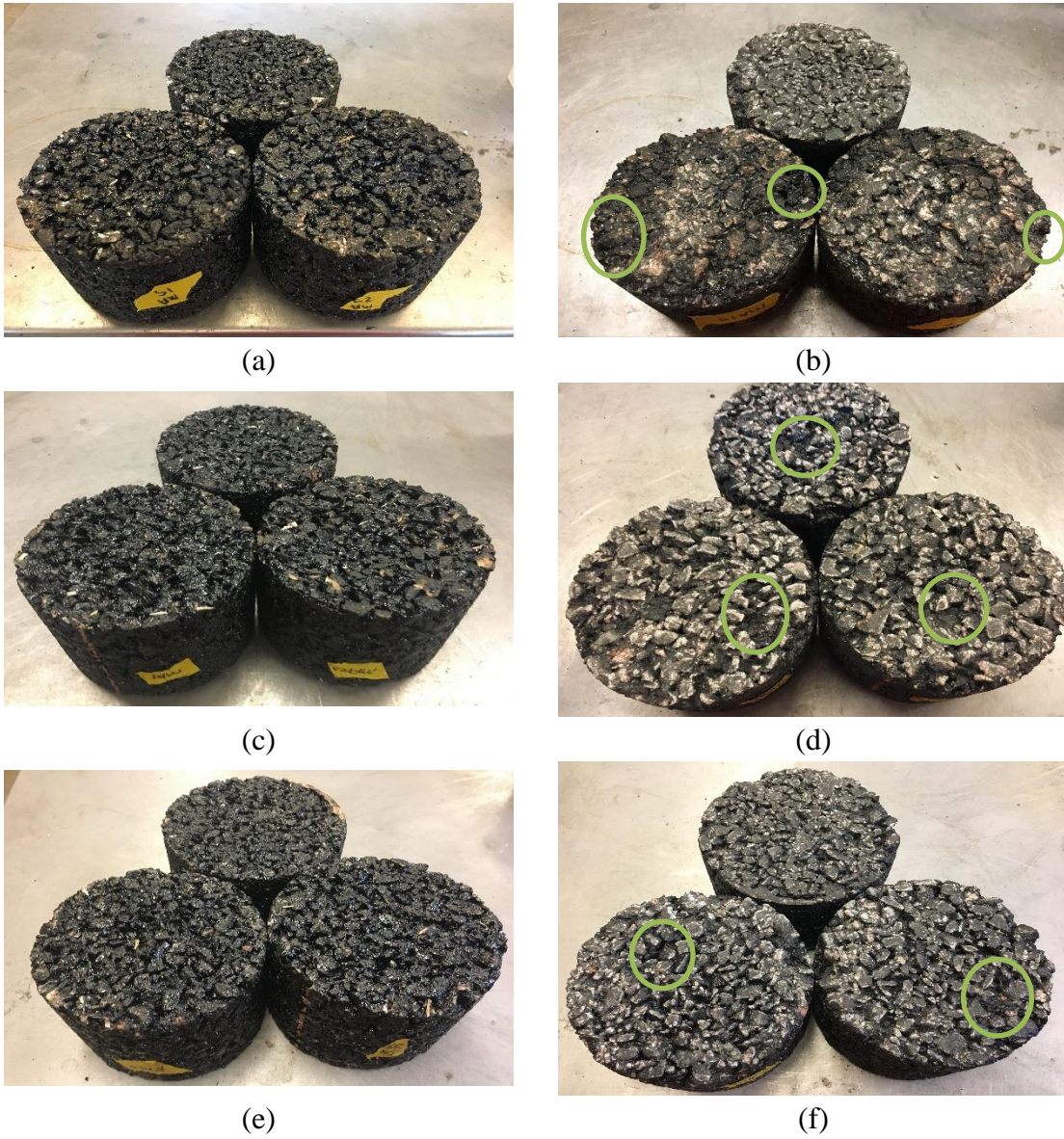
Figure 4.25- Planetary Motion Surface Abrasion Test on the Bottom of the Specimen Using Cutter A (a) Un-Aged Before, (b) Un-Aged After, (c) Aged Before, (d) Aged After, (e) Flipped Before, and (f) Flipped After

Figures 4.26 and 4.27 shows the tops and bottoms, respectively, of the un-aged and aged specimens using the planetary motion surface abrasion test method before and after testing using cutter head B. The larger aggregate particles that were removed during testing are highlighted by green circles (Figure 4.26 (b) and (d); Figure 4.27 (b) and (d)).

(a)   (b)

(c)   (d)
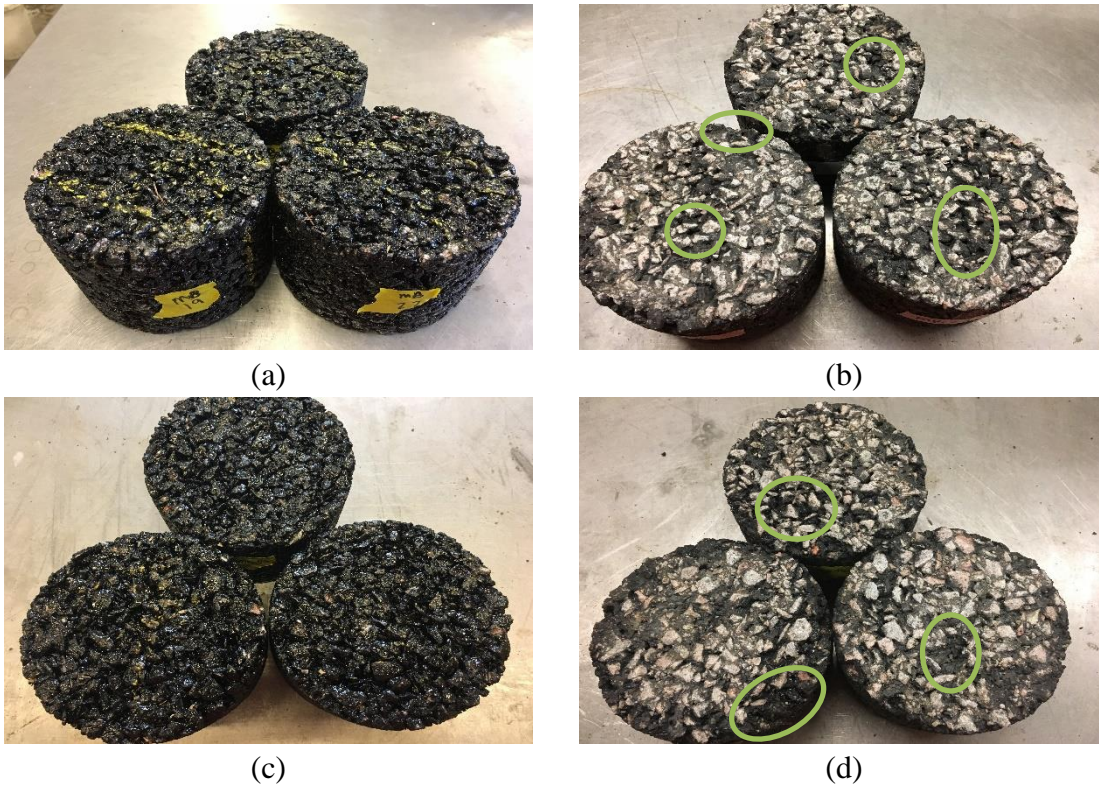
Figure 4.26- Planetary Motion Surface Abrasion Test on the Top of the Specimen Using Cutter B (a) Un-Aged Before, (b) Un-Aged After, (c) Aged Before, and (d) Aged After

Figure 4.27- Planetary Motion Surface Abrasion Test on the Bottom of the Specimen Using Cutter B (a) Un-Aged Before, (b) Un-Aged After, (c) Aged Before, and (d) Aged After

Indirect Tensile Strength

Three un-aged and aged specimens were subjected to an indirect tensile test. The indirect tensile strength (ITS) of the un-aged (74.3 psi) was lower than the indirect tensile strength of the aged specimen (99.9 psi) as illustrated in Figure 4.28 (a). The un-aged specimens were found to be significantly different from the aged specimens when comparing their ITS values.

The area under the load-deformation curve between zero load and the peak was calculated as the toughness. The average toughness for each aging condition is summarized in Figure 4.28 (b). The modulus of toughness for the aged specimens (16.6 lbf/in) was higher than the modulus of toughness for the un-aged specimens (14.8 lbf/in). However, the un-aged and aged specimens were found to be statistically similar. The calculated toughness modulus of the specimens indicates the ability of the specimens to absorb energy and plastically deform without failure.
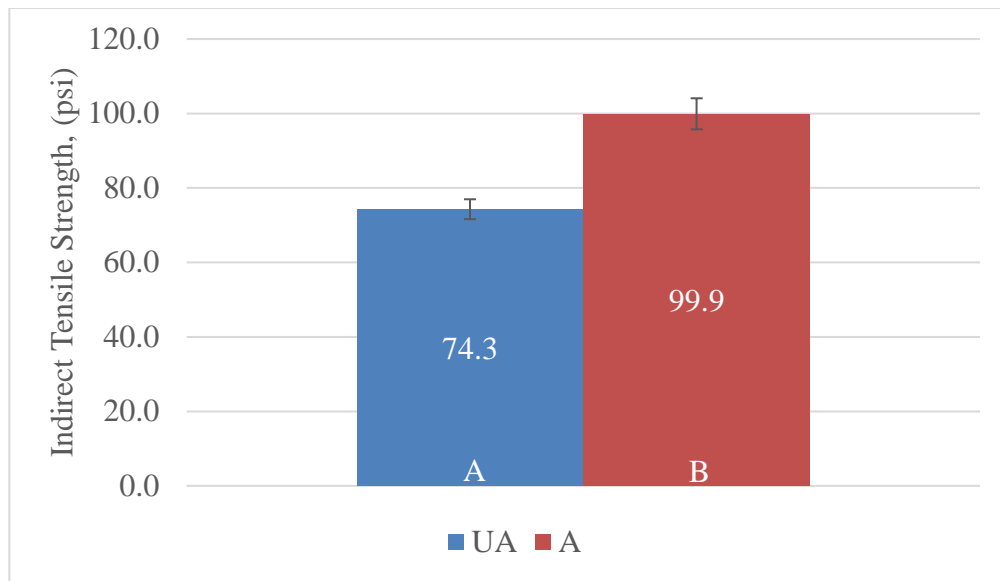
(a)
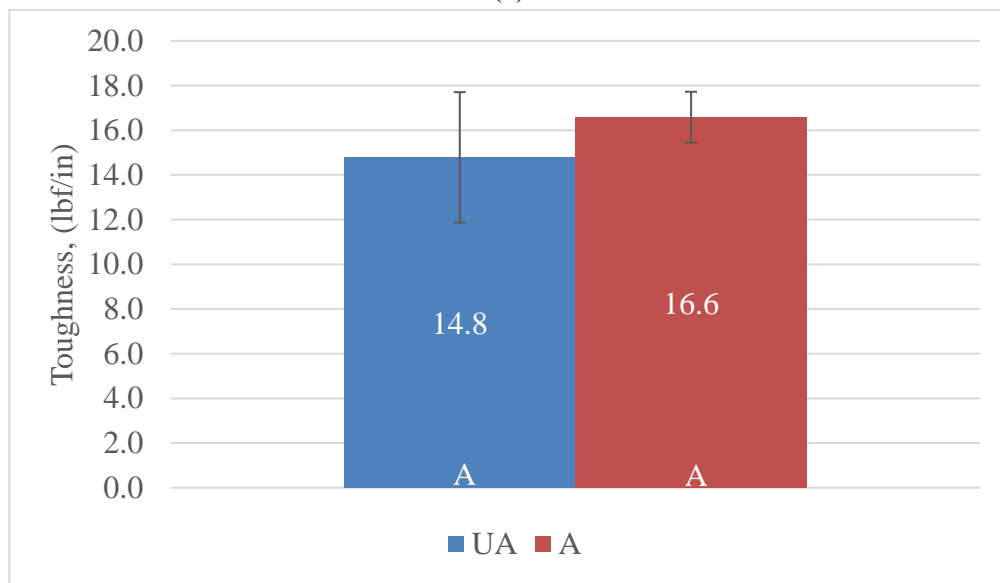
(b)

Figure 4.28- Indirect Tensile Strength (a) and Modulus of Toughness (b) of the Un-Aged and Aged Conditioned Specimens

Figure 4.29 shows the stiffness of the un-aged (a) and aged specimens (b), as well as the average pre and post peak slopes (rate of change). The aged specimens (Figure 4.29 (b)) have a higher average pre and post peak slope than the un-aged specimens. Higher pre and post peak slope means an increase in stiffness therefore could be an increase in the raveling susceptibility with continued aging.
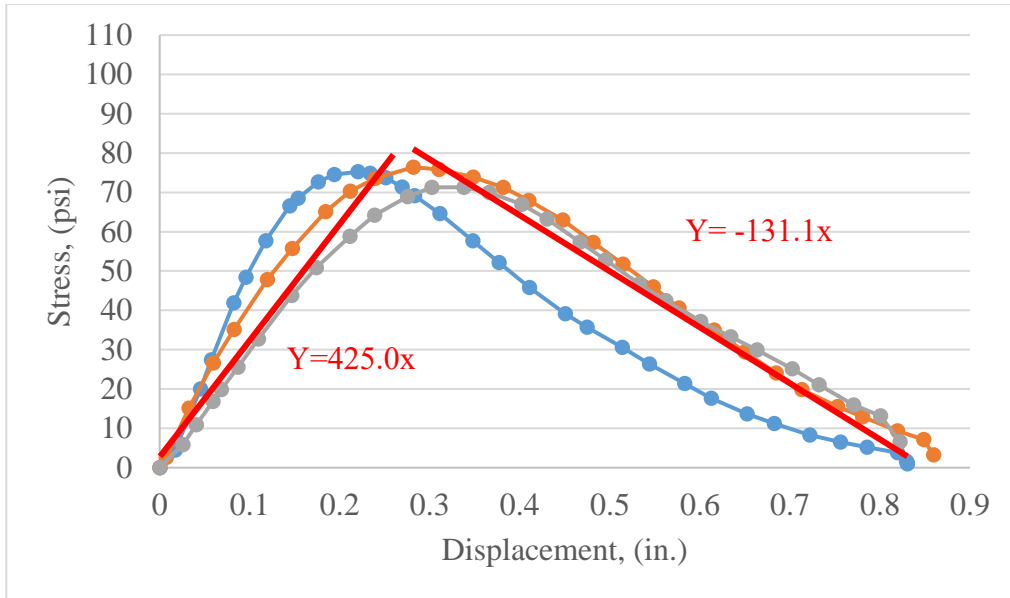
(a)
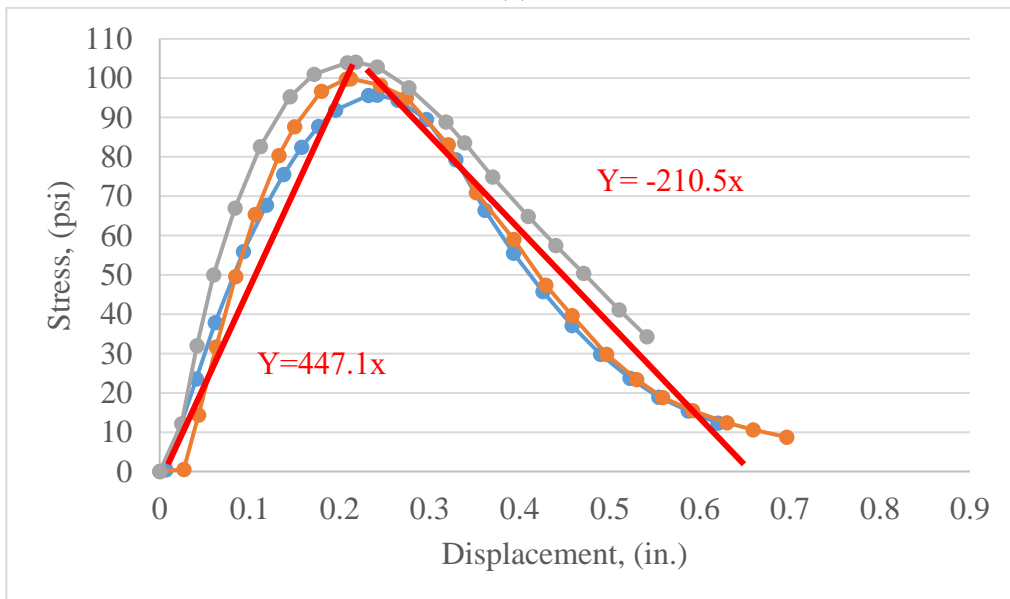
(b)

Figure 4.29- Indirect Tensile Stiffness for the Un-aged (a) and Aged (b) Specimens Showing the Average Pre and Post Peak Slopes

107

<u>Binder Properties</u>

Table 4.8 shows the binder properties for the asphalt binder collected from the plant (prior to mixing), extracted from compacted un-aged specimens (after plant mixing and lab compaction), and extracted from compacted 56 day aged specimens (after plant mixing, lab compaction, and aging). The viscosity and G*/sinδ of the binder tested at 76⁰C increases with aging, indicating an increase in stiffness of the binder. This increase in stiffness of the binder effects the raveling susceptibility of the OGFC over its service life.

Table 4.8- Binder Properties

	Binder Condition		
Property	Plant	Compacted Un-Aged (Extracted)	Compacted Aged (Extracted)
Original Viscosity @ 135**°C** G*/sinδ @ 76**°C** DSR Test Temp. (**°C**)	1.140 Pa·s 1.219 kPa 76°C	1.890 Pa·s 2.381 kPa 76°C	3.160 Pa·s 5.035 kPa 76°C
RTFO Aged DSR Test Temp. (**°C**) Mass Change G*/sinδ @ 76°C	76°C -0.337% 2.702 kPa	N/A N/A N/A	N/A N/A N/A
PAV Aged G*sinδ @ 31⁰C **Stiffness @ -12°C** **m-value @ -12°C**	1477 kPa 143 MPa 0.358	1496 kPa 135 MPa 0.359	2213 kPa 174 MPa 0.321

Evaluation of Test Procedures

When comparing the test methods that were developed (singular and planetary motion abrasion test method) to look at the raveling susceptibility of OGFC to the current standard used (Cantabro test method); the new surface abrasion test methods (singular and planetary motion) showed different trends than the Cantabro test method. Indirect tensile strength and shear testing was conducted on the specimens and showed a similar trend to the new test methods. Table 4.9 summarizes the results of the direct shear, indirect tensile strength, Cantabro, singular motion abrasion, and planetary motion abrasion test methods. The singular and planetary methods results are from the completion of six cycles for the top and bottom of the specimens for all aging conditions.

Table 4.9- Comparison of the Singular Motion Abrasion Test Method, Planetary Motion Abrasion Test Method, and the Direct Shear Test Method Data

Test Method		Specimen Conditioning Type					
		Un-Aged		Aged		Aged Flipped	
		Specimen Test Location					
		Top	Bottom	Top	Bottom	Top	Bottom
Singular Motion (% Mass Loss)	Cutter Head A	0.57	0.52	0.52	0.42	-	-
	Cutter Head B	1.01	0.94	0.68	0.54	-	-
Planetary Motion (% Mass Loss)	Cutter Head A	1.61	1.36	1.14	0.86	0.82	0.56
	Cutter Head B	2.49	2.32	2.02	1.70	-	
Direct Shear (psi)	-	38.7	26.5	82.6	70.1	87.1	77.4
Indirect Tensile (psi)	-	74.3		99.9		-	
Cantabro (% Mass Loss)	-	10.5		18.4		16.5	

In the Cantabro test method, the un-aged specimens had a lower percent mass loss that was statistically different from the aged and aged flipped conditioned specimens. The Canatbro test method is more of an impact test instead of a surface abrasion test method. The new surface abrasion test methods (singular and planetary motion) simulate the friction between the pavement surface and the tire of a vehicle over the service life of OGFC pavements.

The indirect tensile strength and the direct shear strength tests evaluate cohesive failure. These tests measure the cohesive bond between the asphalt binder molecules. The indirect tensile strength of the un-aged and aged specimens showed that the aged specimens had a higher indirect tensile strength (99.9 psi) than the un-aged specimens (74.3 psi) and were statistically different from one another. This is opposite of the Cantabro data, where the un-aged specimens outperformed the aged specimens.

The singular and planetary abrasion methods show the same trends as the ITS and direct shear strength test methods. The tops and bottoms of the aged specimens of the singular abrasion test method had a lower percent mass loss than the top and bottom of the un-aged specimens for both cutter heads. The tops and bottoms of the aged specimens of the planetary abrasion test method have a lower percent mass loss than the tops and bottoms of the un-aged specimens for both cutter heads. For the direct shear strength test data as well as the ITS data, the aged specimens have a higher value than the un-aged. This indicates that the binder of the aged specimens got stiffer with aging.

The singular and planetary motion surface abrasion test methods follow the same trend as the direct shear strength test and the indirect tensile strength test. The singular and planetary motion surface abrasion test methods are simulating more of a cohesive failure between the asphalt binder-to-binder interaction on the surface of the specimens since the data aligns with the indirect tensile strength and direct shear strength test data.

Figure 4.30 shows the dislodged aggregate particles from the Cantabro test, the planetary, and singular motion surface abrasion test methods with the Cantabro aggregate on the left, planetary test method particles in the middle, and the singular test method particles on the right. The Cantabro test method crushes the aggregate particles resulting in more dust particles than the singular and planetary motion surface abrasion test methods.

When comparing the singular motion test method to the planetary motion test, the singular motion test resulted in smaller aggregate particles being dislodged during testing. One can see that the singular and planetary aggregate particles that have been dislodged have less damage to the aggregate particles themselves, along with less dust being present. Through visual inspection during testing, the singular and planetary motion surface abrasion test methods show more of a cohesive failure rather than an impact test like the Cantabro test method that fractures aggregate particles during testing.

Figure 4.30- Dislodged Aggregate Particle from the Cantabro Test Method, Planetary Motion Abrasion Test Method, and Singular Motion Abrasion Test Method (Left to Right)

PHASE B: QUANTIFYING LONG-TERM DRAINDOWN

Figure 4.31 shows the binder content and air content by percent of pixels for the un-aged specimens using image analysis. The specimens that were compacted at 50 gyrations had a higher binder content when comparing slices (Figure 4.31(a)) than the specimens compacted at 20 gyrations. The top of the specimens had a higher binder content by percent pixels than the bottom of the specimens for each compaction level (20, 35, and 50).

When looking at the air void content by percent pixels of the un-aged specimens (Figure 4.31(b)), the 50 gyration specimens had less air voids than the 20 gyration specimens did. This makes sense because the 20 gyration specimens were compacted for fewer gyrations, therefore increasing the air void content of the specimens. The top of the specimens had a lower air content by percent pixels than the bottom of the specimens for the 20 and 35 compaction level specimens except for the 50 gyration specimens, which had the same air void content by image analysis.

Even though Figure 4.31 (a) shows a difference in binder content per slice by percent pixels for each gyration type, the statistical analysis comparing slice one through four for each compaction level (20, 35 and 50 gyration) were found to be significantly similar. The same trend can be seen in Figure 4.31 (b) for the air void content by percent pixels for each gyration type. This means that for the 50 gyration specimens, slice one through four are significantly similar to one another. The same statistical trend can be seen for the 20 and 35 gyration specimens.
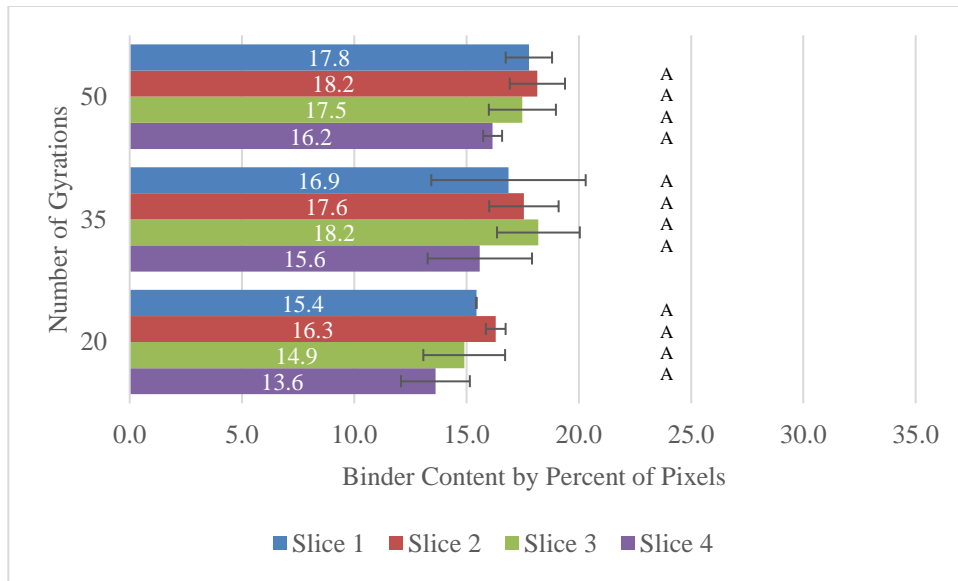
(a)
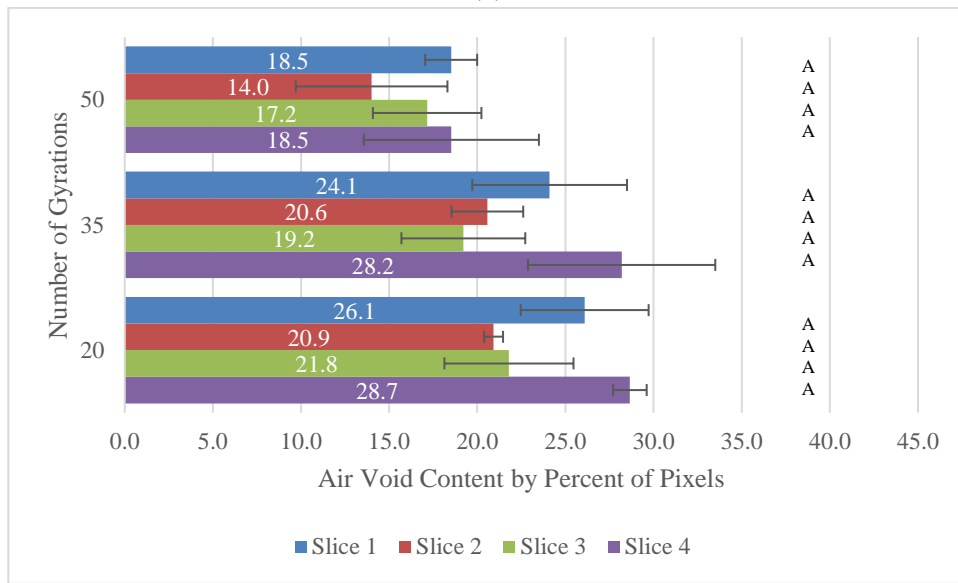
(b)

Figure 4.31- The Binder Content (a) and Air Content (b) by Percent of Pixels for the Un-Aged Specimens Using Image Analysis (The Black Letters Represent the Statistical Analysis of the Data as Analyzed by the Letter Report. Alike Letters are Statistically Similar)

114

Figure 4.32 shows the binder content and air content by percent of pixels for the 28 day aged specimens using image analysis. The specimens that were compacted at 50 gyrations had a higher binder content when comparing slices (Figure 4.32(a)) than the specimens compacted at 20 gyrations. The top of the specimens had a higher binder content by percent pixels than the bottom of the specimens for each compaction level (20, 35, and 50).

Even though the Figure 4.32 (a) shows a difference in binder content per slice by percent pixels for each gyration type, the statistically analysis by slice for each compaction level (20, 35 and 50 gyration) were found to be significantly similar. This means that for the 20 gyration specimens, slice one through four are significantly similar to one another. The same statistical trend can be seen for the 35 and 50 gyration specimens.

When looking at the air void content by percent pixels of the 28 day aged specimens (Figure 4.32 (b)), the 50 gyration specimens had less air voids than the 20 gyration specimens did. This make sense because the 20 gyration specimens were compacted for fewer gyrations, therefore increasing the air void content of the specimens. The top of the specimens had a lower air content by percent pixels than the bottom of the specimens for the all compaction levels (20, 35 and 50).
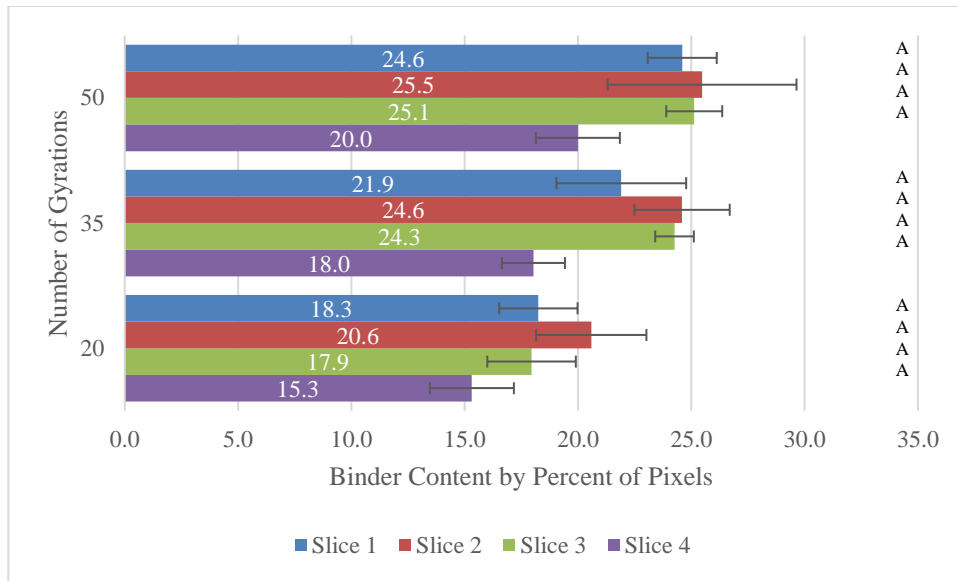
(a)
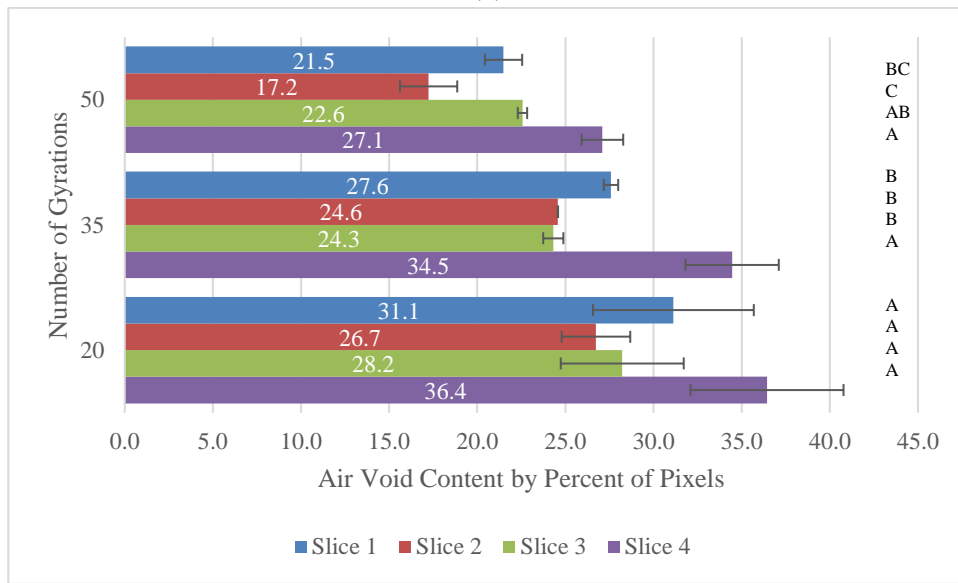
(b)

Figure 4.32- The Binder Content (a) and Air Content (b) by Percent of Pixels for the 28 Day Aged Specimens Using Image Analysis (The Black Letters Represent the Statistical Analysis of the Data as Analyzed by the Letter Report. Alike Letters are Statistically Similar)

Figure 4.33 shows the binder content and air content by percent of pixels for the 56 day-aged specimens using image analysis. The specimens that were compacted at 50 gyrations had a higher binder content when comparing slices (Figure 4.33 (a)) than the specimens compacted at 20 gyrations. The top of the specimens had a higher binder content by percent pixels than the bottom of the specimens for each compaction level (20, 35, and 50).

Even though the Figure 4.33 (a) shows a difference in binder content per slice by percent pixels for each gyration type, the statistically analysis by slice for the 20 gyration specimens were found to be significantly similar. The 50 gyration specimens follows this same trend. This means that for the 50 gyration specimens, slice one through four are significantly similar to one another. The specimens that were compacted at a compaction level of 35 gyrations showed a different trend. The statistically analysis of the 35 gyration specimens by slice showed that slice one is statistically similar to slice two, three and four. However, slice four is significantly different from slice two and three.

When looking at the air void content by percent pixels of the 56 day aged specimens (Figure 4.33 (b)), the 50 gyration specimens had less air voids than the 20 gyration specimens did. This make sense because the 20 gyration specimens were compacted for fewer gyrations, therefore increasing the air void content of the specimens. The top of the specimens had a lower air content by percent pixels than the bottom of the specimens for the all compaction levels (20, 35 and 50).

117

The statistical analysis by slice for each compaction level found that the 20 and 35 gyration specimens follow the same trends. When looking at slice one for the 20 and 35 gyration specimens, they were found to be statistically similar to slice two, three and four. However, slice four for both gyrations (20 and 35) was found to be significantly different from slice two and three. When analyzing the 50 gyration specimens by slices, slice one was found to be significantly similar to two and three, but significantly different from slice four. When comparing slice four for the 50 gyration specimens, slice one and three were found to be significantly similar to one another, while slice two was found to be significantly different.
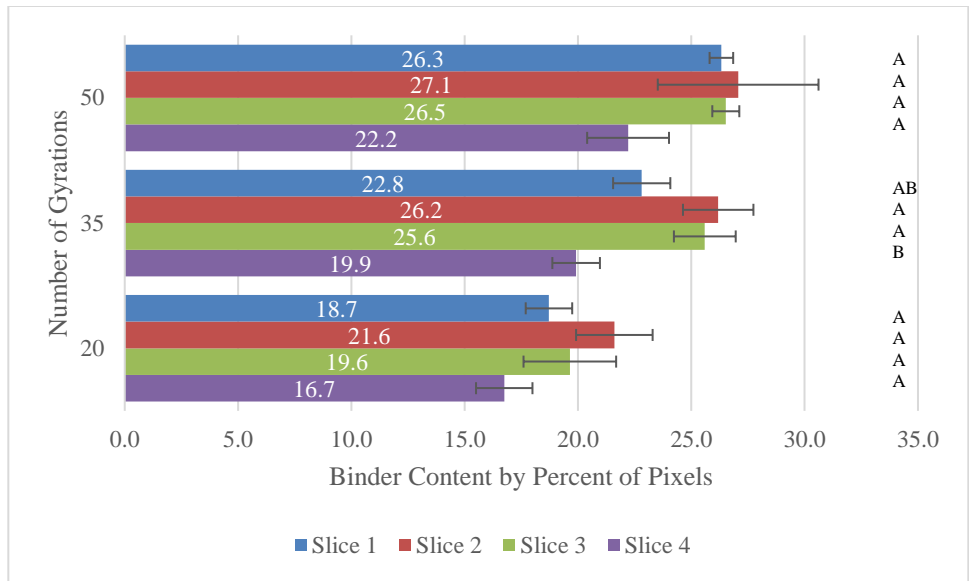
(a)
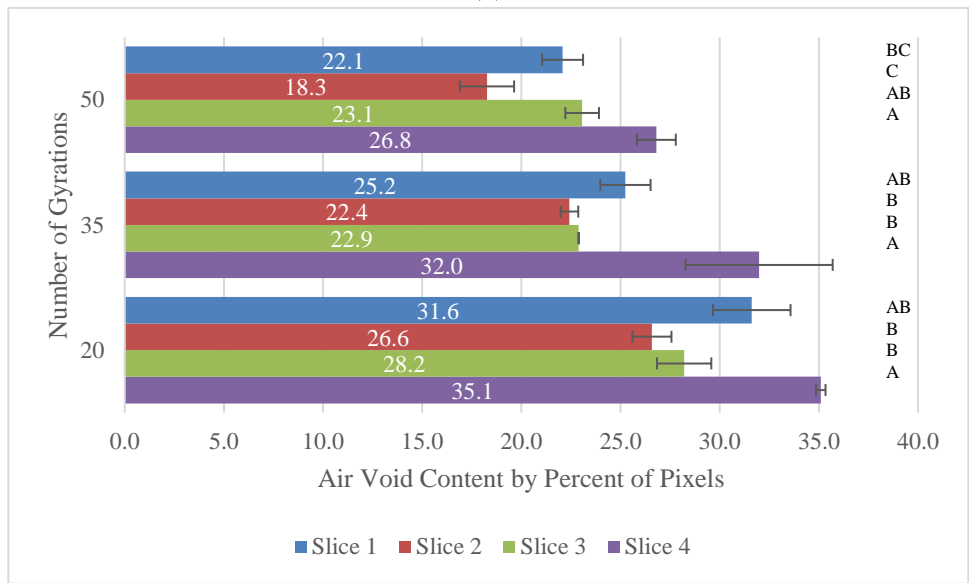
(b)

Figure 4.33- The Binder Content (a) and Air Content (b) by Percent of Pixels for the 56 Day Aged Specimens Using Image Analysis (The Black Letters Represent the Statistical Analysis of the Data as Analyzed by the Letter Report. Alike Letters are Statistically Similar)

119

Figure 4.34 shows the average binder content by percent of pixels for the top slice of the 50 gyration aged specimens with a depth of 28.75 mm sectioned into 10 slices (1 Slice≈ 2.875 mm). The binder content increases from zero days aged to the 28 days aged for all ten slices. Slice one and six resulted in a decrease in binder content when comparing the 28 day aged binder content to the 56 day aged. The other slices showed an increase in the binder content by percent pixels from the 28 day aged to the 56 day aged specimens.

Figure 4.34- The Average Binder Content by Percent of Pixels for the Top 28.75 mm of the 50 Gyration Aged OGFC Image Analysis Specimens (1 Slice≈ 2.875 mm)

Figure 4.35 shows the average air voids by percent of pixels for the top of the 50 gyration aged specimens with a depth of 28.75 mm sectioned into 10 slices (1 Slice≈ 2.875 mm). The air void content increases from zero days aged to the 28 days aged for all ten slices. Slice one, four, and eight decreased in air content when comparing the 28 day aged air void content to the 56 day aged. The other slices showed an increase in the air void content by percent pixels from the 28 day aged to the 56 day aged specimens.

Figure 4.35- The Average Air Void Content by Percent of Pixels for the Top 28.75 mm of the Aged OGFC Image Analysis Specimens (1 Slice≈ 2.875 mm)

Figure 4.36 shows the average change in binder and air content (by percent pixels) between the 0 and 56 days of aging for the 20 gyration specimens. This figure shows the top 28.75 mm (Slice 1) of the specimen sliced into 10 sections with zero representing the surface of the specimen (1 Slice≈ 2.875 mm). An increase in the average change in binder content (by percent of pixels) can be seen between slices 1-2 and 6-10. This indicates an increase in the binder migration between these slices. Between slices 2 and 6, the change in binder content (by percent pixels) remains relatively consistent. This could be due to the fact that the binder is draining downward from slice to slice at a similar rate.
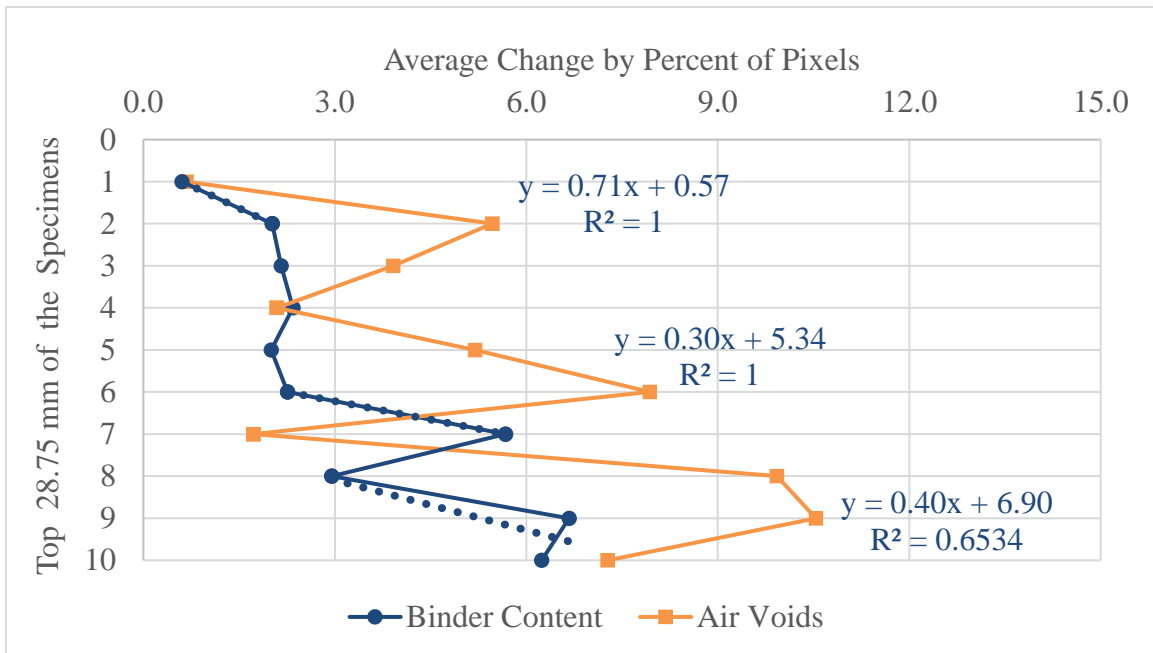
Figure 4.36- Average Change in Binder Content and Air Voids by Percent Pixels between 0 and 56 Days Aged Specimens for the 20 Gyration Specimens

Figure 4.37 shows the average change in binder and air content (by percent pixels) between the 0 and 56 days of aging for the 35 gyration specimens. An increase in the average change by percent of pixels of the binder content are seen between slices 1-2 and 4-6 which indicates an increase in the binder migration.
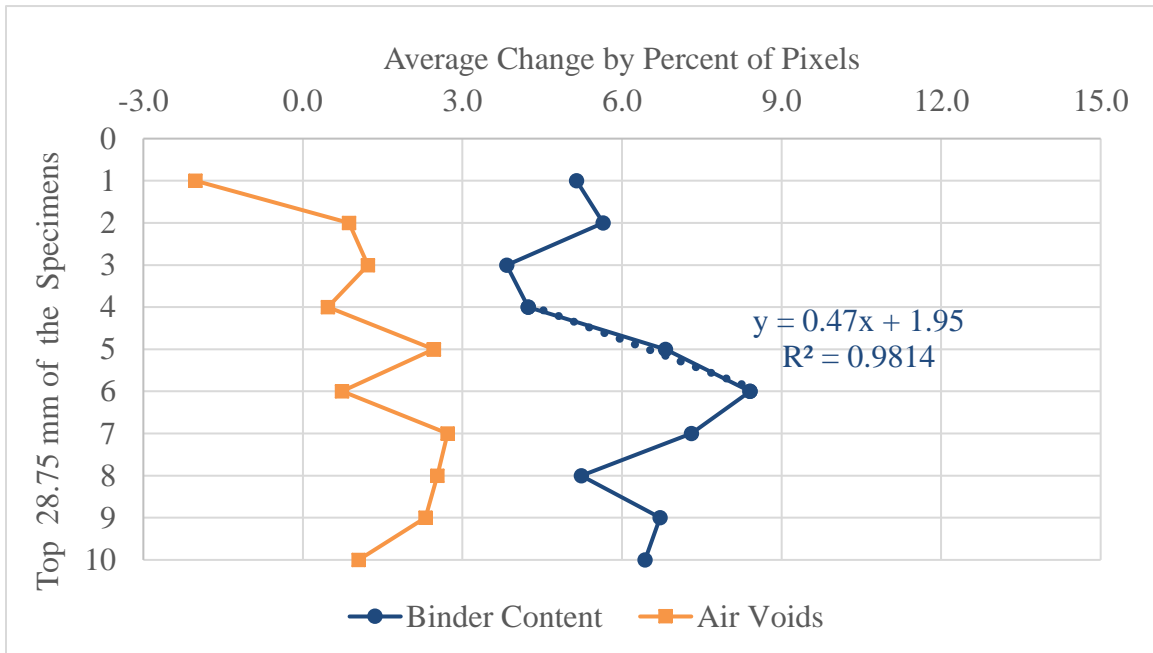
Figure 4.37- Average Change in Binder Content and Air Voids by Percent Pixels between 0 and 56 Days Aged Specimens for the 35 Gyration Specimens

Figure 4.38 shows the average change in binder and air content (by percent pixels) between the 0 and 56 days of aging for the 50 gyration specimens. The binder content has a greater average change by percent of pixels than the 20 and 35 gyration specimens. Between slices 1 and 4, and 5 and 10, the average binder content by percent of pixels increases. This indicates an increase in the binder migration between these slices.
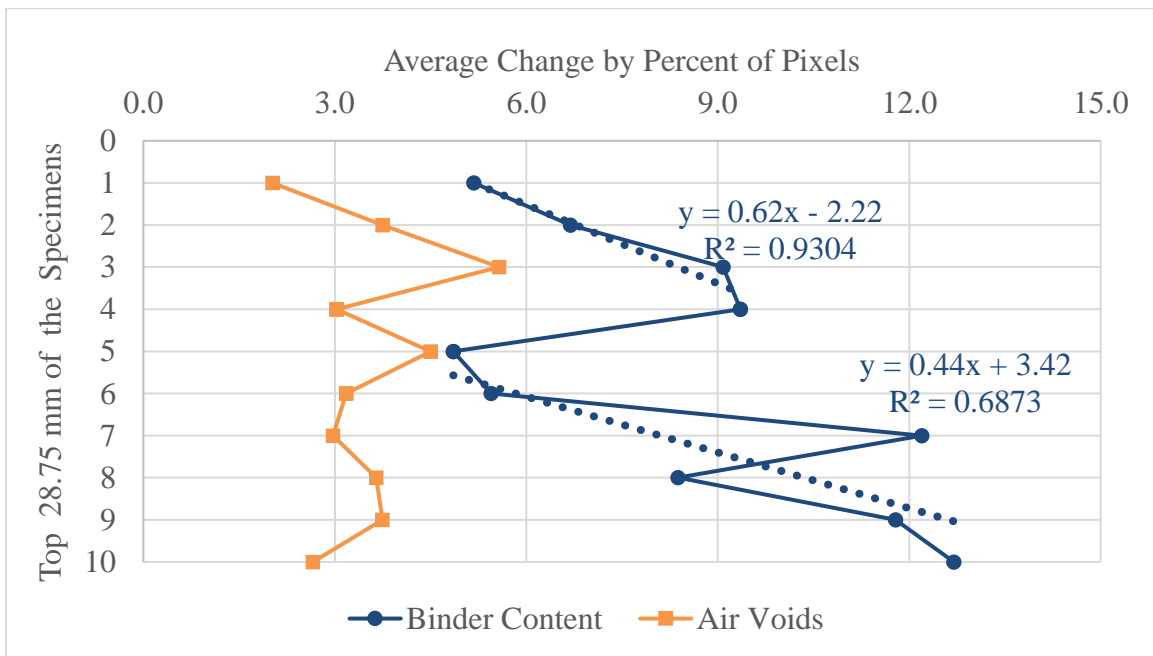
Figure 4.38- Average Change in Binder Content and Air Voids by Percent Pixels between 0 and 56 Days Aged Specimens for the 50 Gyration Specimens

Due to image analysis procedure used to analyze the specimens, the binder migrated from around the aggregate particles onto the surface of the aggregate particles along the cut face of the specimen instead of draining into the air voids in some cases as seen in Figure 4.39. The reason the binder drained over the cut face of the specimen instead of into the air voids surrounding the aggregate particles was the lack of resistance to flow of the binder over the exposed surface. This was the path of least resistance for the binder to flow. The percentage of aggregates does not change in the specimens and this has to be taken into consideration during the analysis of the draindown of the asphalt binder using image analysis. Therefore, the average change by percent pixels of the binder content and air voids over 56 days were evaluated.

(a)

(b)

Figure 4.39 – Before (a) and After (b) Aging of the Long-term Draindown Specimen

<u>Long-term Draindown Evaluation of the Flipped Aged Specimens</u>

Figure 4.40 shows the binder content and air content by percent of pixels for the flipped aged specimens using image analysis for 0, 28 and 56 days aged. Figure 4.40 (a) shows that the binder content increased per slice as the specimens aged. The 0, 28 and 56 day aged specimens have a similar trend, where the top of the specimens had a higher binder content by percent of pixels than the bottom of the specimens, with the middle two slices having a higher binder content by percent of pixels than the top and bottom slices of the specimen.

The statistical analysis of the 0 day aged specimens showed that all four slices were significantly similar to one another. When comparing the slices of the 28 day aged specimens, slice one was found to be significantly similar to slice two, three and four. However, slice four was found to be significantly different from slice two and three for the 28 day aged specimens. When comparing the slices of the 56 day aged specimens, slice one was found to be significantly similar to slice two, three and four. However, slice four was found to be significantly different from slice three for the 56 day aged specimens.

Figure 4.40 (b) shows the air content by percent of pixels for the flipped aged specimens using image analysis for 0, 28 and 56 days aged. The top and bottom of the specimens for all aging conditioning times had a higher air void content than the two middle slices (three and four); with the bottom slice having the highest percent air voids by percent pixels.

The statistical analysis of the air void content of the 0 and 28 day aged specimens showed that slices one, two, and three were statistically similar to each other, but slice four was statistically different from slices one, two and three. When comparing the slices of the 56 day aged specimens, slice one was found to be significantly similar to slices two, three and four. However, slice four was found to be significantly different than slices two and three for the 56 day aged specimens.
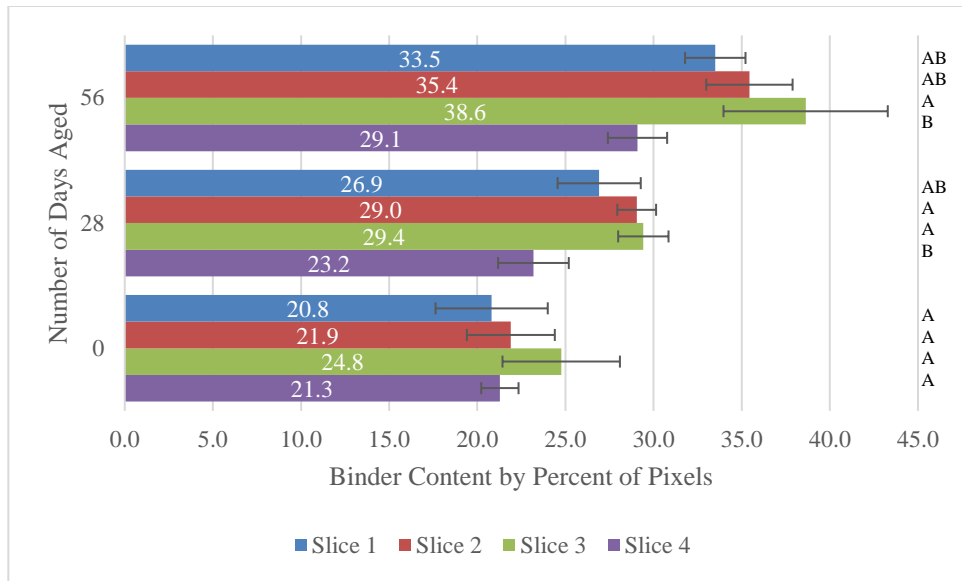
(a)
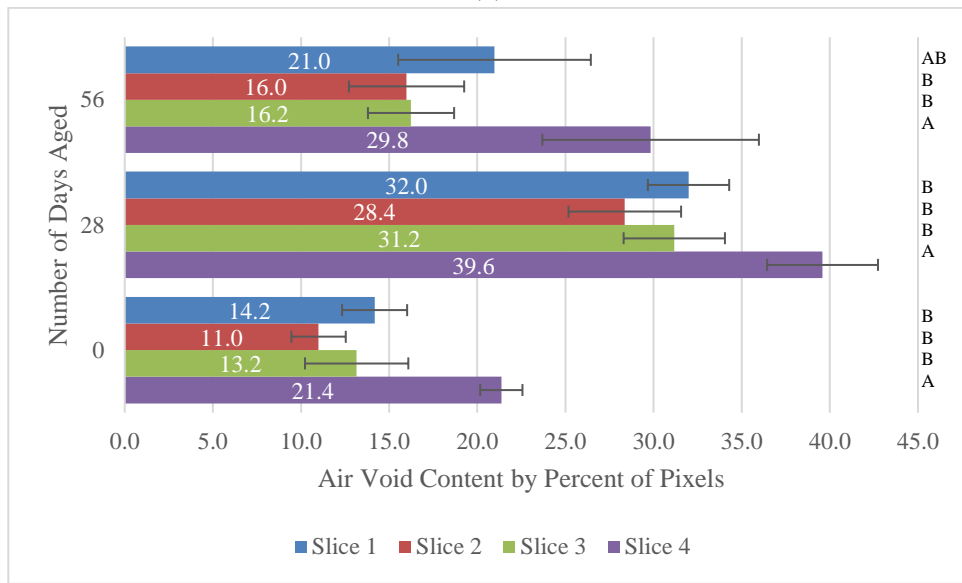
(b)

Figure 4.40- The Binder Content (a) and Air Content (b) by Percent of Pixels for the Flipped Aged Specimens Using Image Analysis

131

Figure 4.41 shows the average binder content by percent of pixels for the top of the 50 gyration flipped aged specimens with a depth of 28.75 mm sectioned into 10 slices (1 Slice≈ 2.875 mm). The binder content increases from zero days aged to the 56 days aged for all ten slices. The figure shows that the average binder content by percent of pixels for each slice increases with aging.
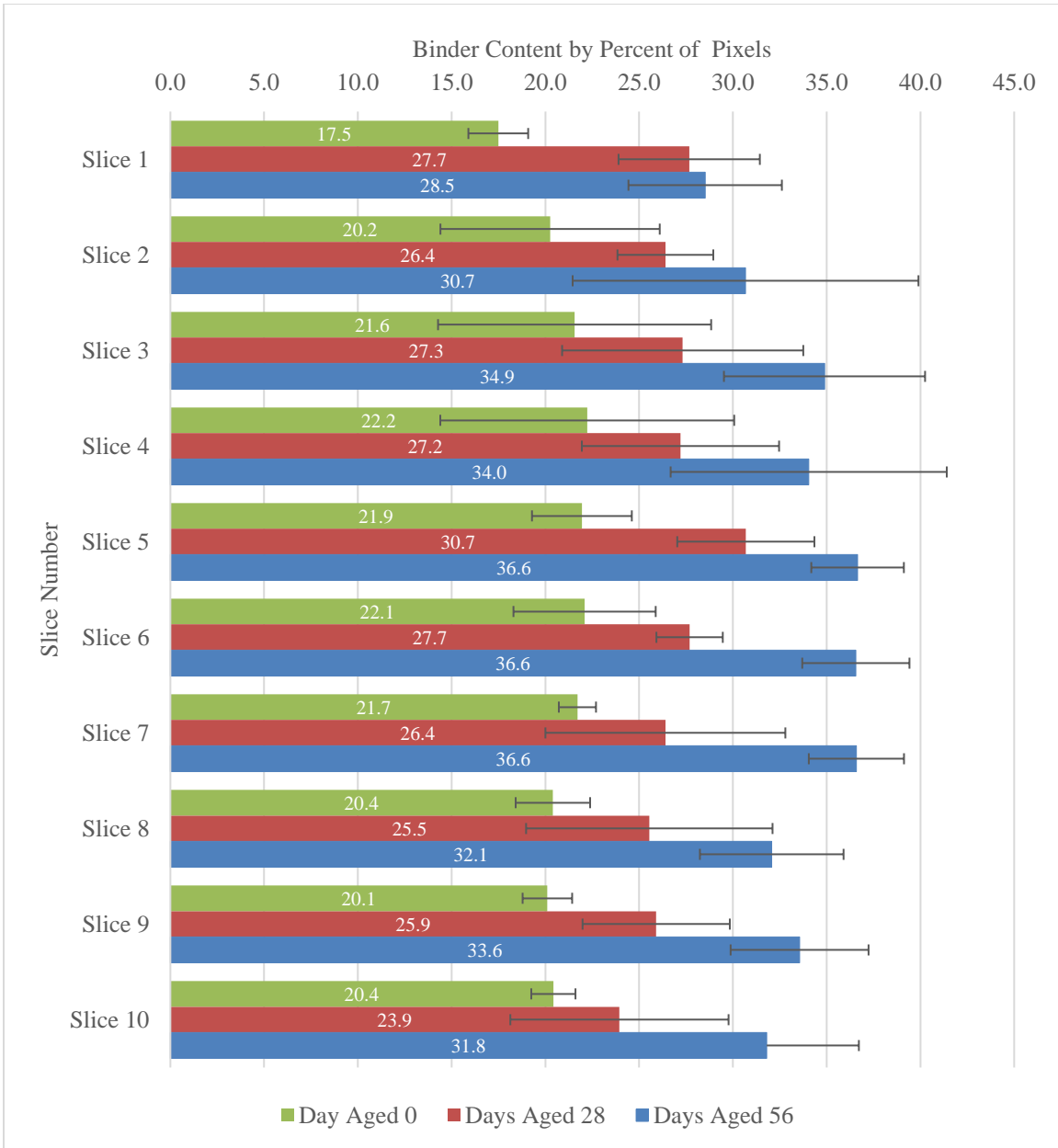
Figure 4.41- The Average Binder Content by Percent of Pixels for the Top 28 mm of the 56 Day Flipped Aged OGFC Image Analysis Specimens (1 Slice≈ 2.875 mm)

Figure 4.42 shows the average air voids by percent of pixels for the top of the 50 gyration flipped aged specimens with a depth of 28.75 mm sectioned into 10 slices (1 Slice≈ 2.875 mm). The air void content increases from zero days aged to the 28 days aged for all ten slices, then decreases for the 56 day aged slices. The 56 day aged slices all had a higher average air void content than the zero day aged slices. This means that the air void content increased from zero to 28 days of aging then decreased from 28 to 56 days of aging, with the 56 day aged still having a higher air void content than the unaged.
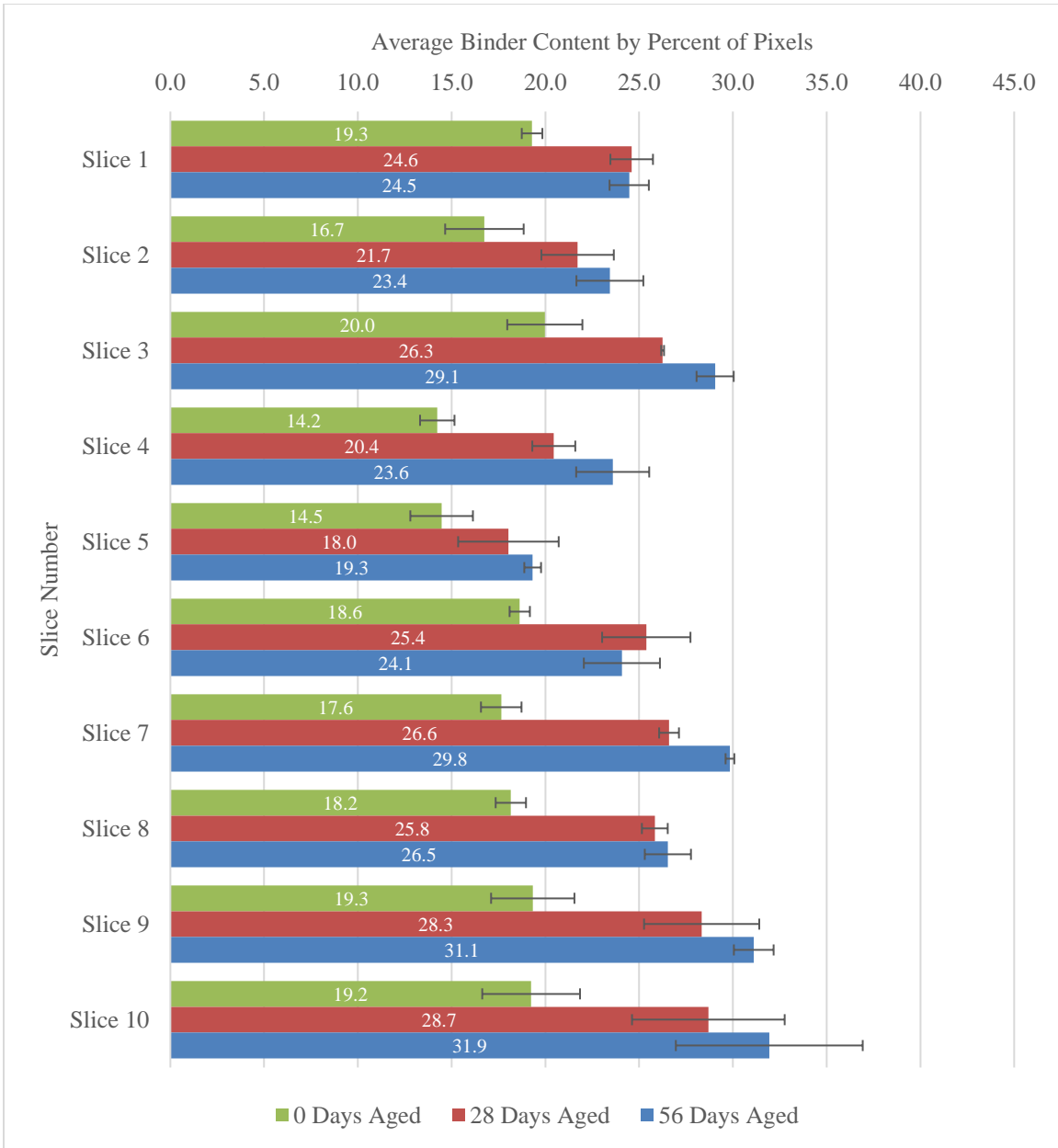
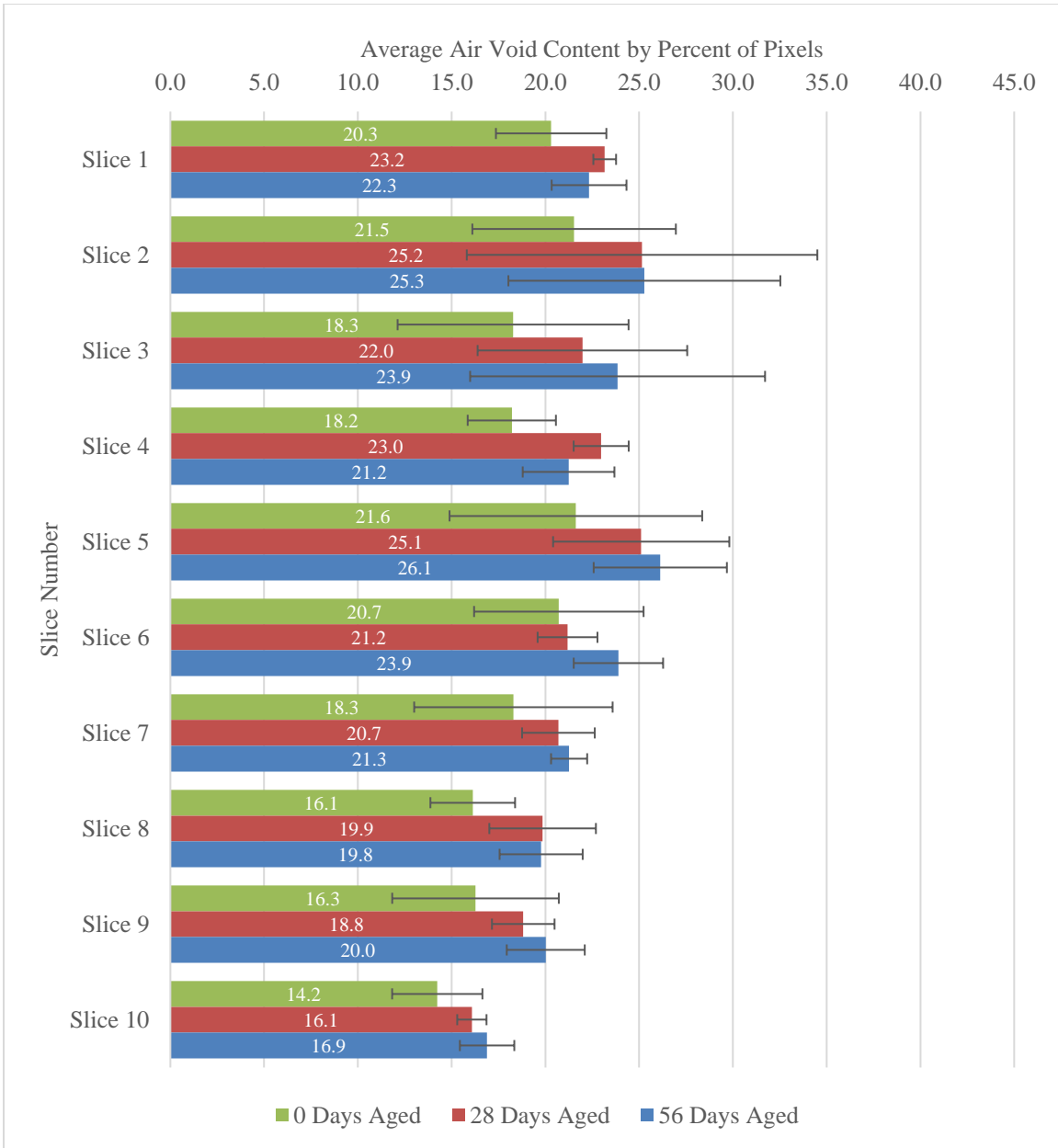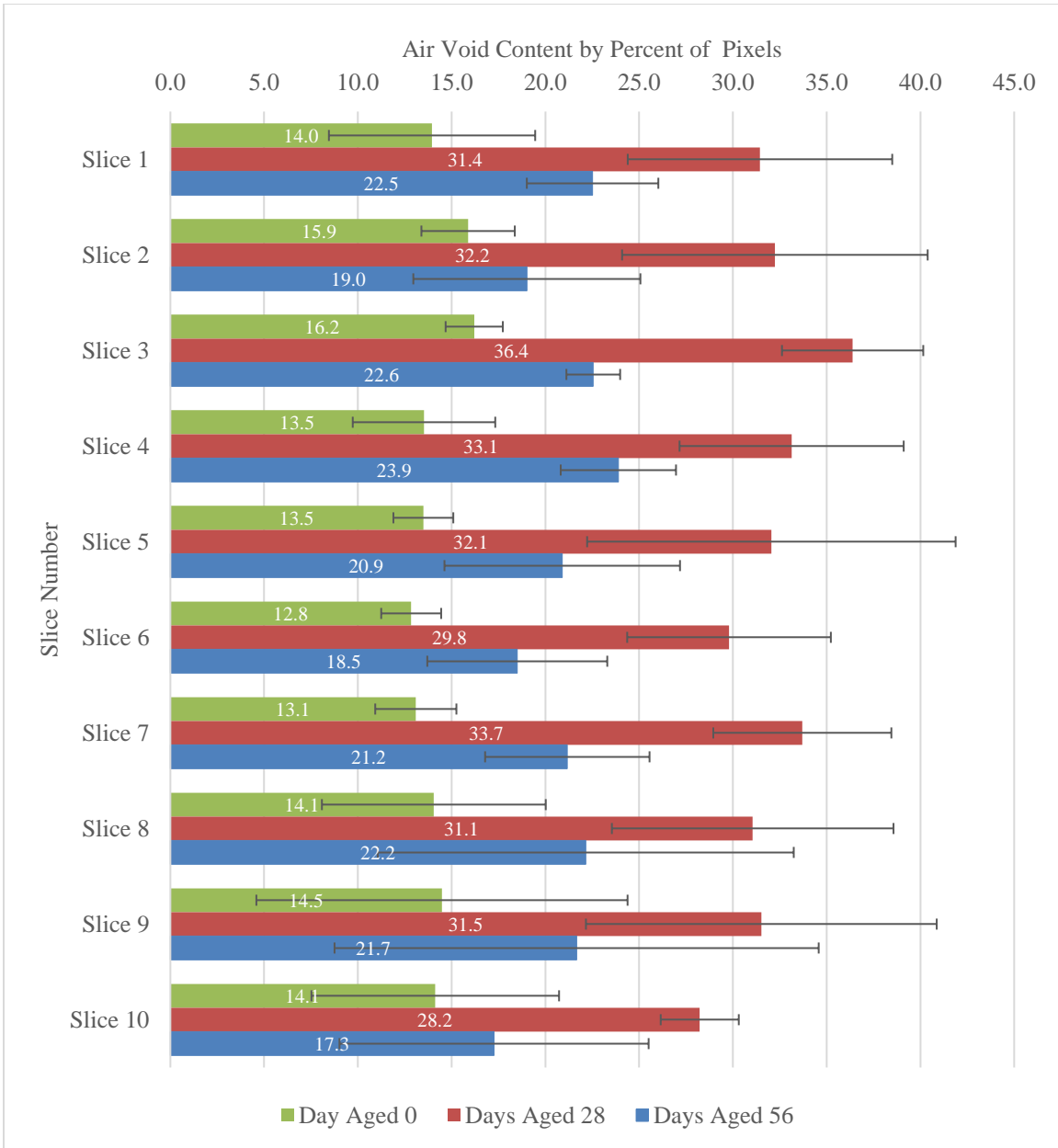**Figure 4.42- The Average Air Void Content by Percent of Pixels for the Top 28 mm of the 56 Day Flipped Aged OGFC Image Analysis Specimens (1 Slice≈ 11.5 mm)**

Figure 4.43 shows the average change in binder and air content by percent pixels over the 56 day aging period for the flipped aged specimens. This figure shows the top 28.75 mm of the specimen with zero representing the surface of the specimen (1 Slice≈ 2.875 mm). The binder content has a greater average change by percent of pixels than the air voids. Between slices 1and 5, which is approximately a depth of 2.875 mm to 14.375 mm from the top of the specimen, the average change in binder content by percent of pixels increases. When comparing the flipped (Figure 4.43) to the un-flipped specimens (Figure 4.38), the flipped specimens have a smaller range of change in binder content over the specimen depth compared to the unflipped specimens.
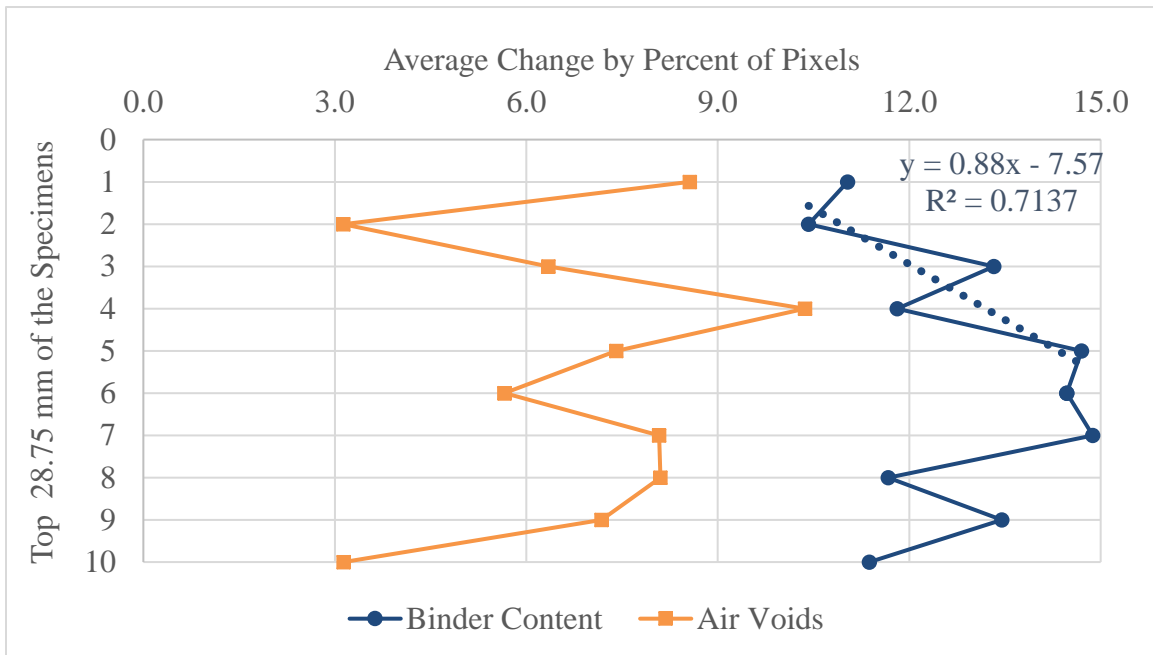
Figure 4.43- Average Change in Binder Content and Air Voids by Percent Pixels between 0 Days Aged and 56 Days Flipped Aged Specimens

136

Table 4.10 displays the Draindown Factor [D_F] for the aged and flipped aged specimens. The Draindown Factor was calculated by multiplying the positive slope of the average change in binder content (by percent of pixels) over time (from 0 to 56 days) for a given specimen (e.g., Figure 4.43) by the slice thickness (2.875 mm) then taking the inverse of that value to get units of ΔP_b/mm. The flipped aged specimens had the lowest D_F compared to the aged specimens because the specimens were inverted every 2 days during aging, which allowed the binder to migrate back and forth.

Table 4.10 – Draindown Factor [D_F] (ΔP_b/mm)

Specimen	Gyrations	Draindown Factor [D_F] (ΔP_b/mm)	Thickness (mm)	Slice
Aged	20	0.49	2.875	1-2
		1.16	5.75	4-6
		0.87	5.75	8-10
	35	0.74	8.625	4-7
	50	1.78	11.5	1-4
		0.79	14.375	5-10
Flipped Aged	50	0.395	14.375	1-5

Binder Content

Figure 4.44 shows the binder content of the image analysis specimens by use of ignition oven (a) and image analysis by pixels (b) for both the aged and flipped aged specimens. The image analysis specimens were sliced into four equal slices and the binder content was determined by ignition oven after image analysis was complete. Figure 4.44 (a) shows the binder content of each slice by ignition oven for both the aged and flipped aged specimens. When evaluating the aged specimens, the percent average binder content of slice one (5.2%) was slightly higher than slice four (4.9%). The two middle slices had the same average binder content (5.3%). Slices one through four were found to be statistically similar for the aged specimens even though there was a difference in binder content of the slices.

When evaluating the flipped aged specimens by ignition oven, the percent average binder content of slice one (5.0%) was higher than slice four (4.9%). The two middle slices had the same average binder content (5.2%). Slices one through four were found to be statistically similar for the flipped aged specimens even though there was a difference in binder content of the slices.

Figure 4.44 (b) shows the average binder content of the slices by pixels using image analysis. For the aged specimens, the top (26.3%) slice had a higher average binder content than the bottom (22.2%). The binder content increases from slice one to slice two, with slice two (27.1%) and slice three (26.5%) having similar average binder contents, then decreases in slice four. Slices one and two were found to be statistically

similar to all four slices for the aged specimens. However, slices three and four were found to be statistically different to each other for the aged specimens.

For the flipped aged specimens, the top slice had a higher average binder content (33.5%) than the bottom (29.1%). The binder content increases from slice one to slice three, with slice three having an average binder content of (35.4%) and slice three (38.6%) having similar average binder contents, then decreases in slice four. All four slices were found to be statistically similar, even though there is a change in the average binder content of the slices by percent of pixels.
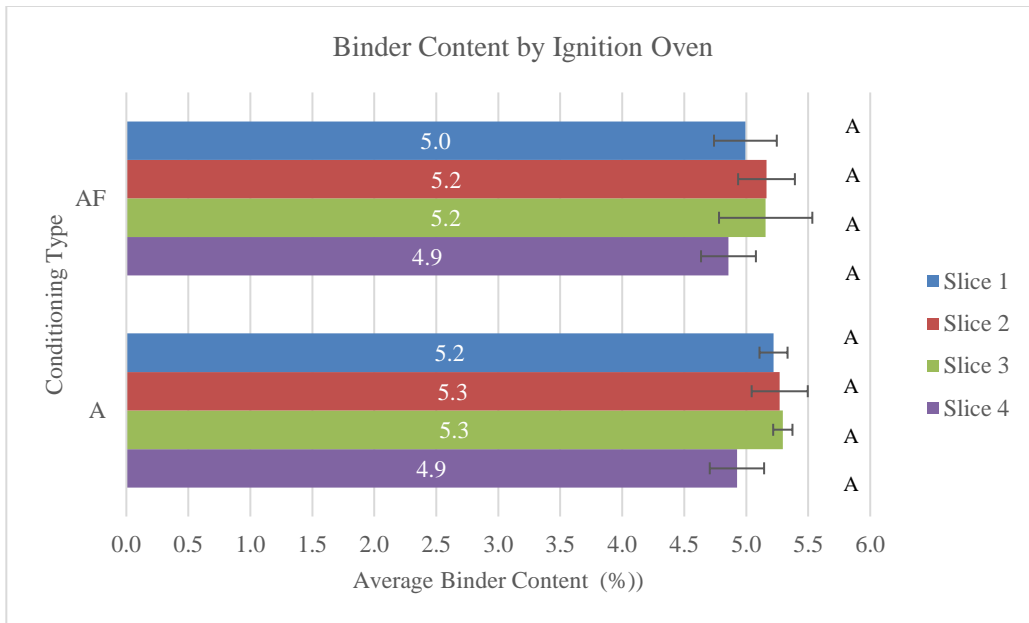
(a)
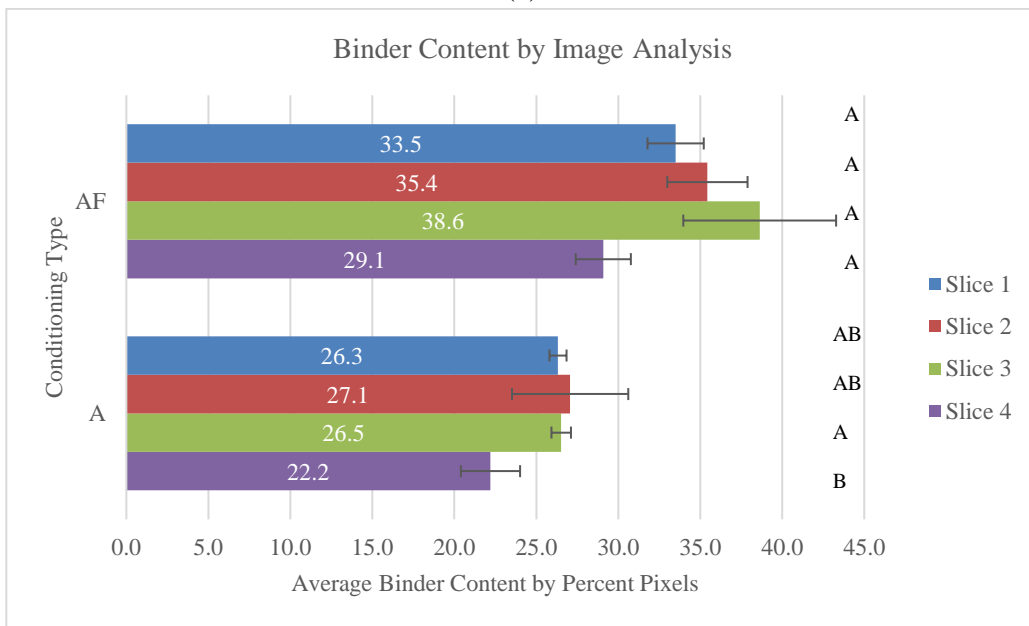
(b)

Figure 4.44- Binder Content of the Image Analysis Specimens by use of Ignition Oven (a) and Image Analysis by Pixels (b)

COMPARISON OF LONG-TERM DRAINDOWN TO THE RAVELING

SUSCEPTIBILITY OF OGFC

Table 4.11 shows the comparison between the, Draindown Factor [D_F], binder content (using both the ignition oven and image analysis) to the raveling susceptibility testing methods including the direct shear strength and indirect tensile strength test methods. The long-term draindown examination by image analysis showed similar results to the binder content of the slices by ignition oven. The binder content using both methods showed that the top of the specimens had a higher binder content than the bottom of the specimens for all aging conditions.

This follows the same trend as the singular and planetary motion surface abrasion test methods, where the top had a lower percent mass loss than the bottom of the specimens for all of the aging conditions. The direct shear also showed that the top of the specimens had a higher strength than the bottom of the specimens for all aging conditions. This can be explained by the fact that the top of the specimens had a higher binder content than the bottom of the specimens. Higher binder content should show an increase in the strength of the specimen.

When comparing the average Draindown Factor [D_F] to the surface abrasion test results of the top surface of the aged and aged flipped specimens, there was a correlation indicating that a higher D_F value resulted in a lower resistance to abrasion. This correlation was identified as the aged specimens had the highest D_F (1.285 ΔP_b/mm) exhibited the highest percent mass loss (1.14%, planetary motion, cutter head A)

141

compared to the aged flipped specimens which had a lower D_F (0.395 ΔP_b/mm) and

percent mass loss (0.82%). This indicates that long-term draindown does have an

influence on the raveling susceptibility of OGFC. The mixture becomes more susceptible

to raveling as draindown increases (i.e., higher the D_F).

Table 4.11- Comparison of the Binder Content of the Specimens to the Raveling Susceptibility of OGFC (*Image Analysis is Average Binder Content by Percent of Pixels)

Test Method		Specimen Conditioning Type					
		Un-Aged		Aged		Aged Flipped	
		Specimen Test Location					
		Top	Bottom	Top	Bottom	Top	Bottom
Singular Motion (% Mass Loss)	Cutter Head A	0.57	0.52	0.52	0.42	-	-
	Cutter Head B	1.01	0.94	0.68	0.54	-	-
Planetary Motion (% Mass Loss)	Cutter Head A	1.61	1.36	1.14	0.86	0.82	0.56
	Cutter Head B	2.49	2.32	2.02	1.70	-	
Direct Shear (psi)	-	38.7	26.5	82.6	70.1	87.1	77.4
Average Draindown Factor (ΔP_b/mm)	-	-	-	1.285	-	0.395	-
Indirect Tensile (psi)	-	74.3		99.9		-	
Cantabro (% Mass Loss)	-	10.5		18.4		16.5	
Binder Content (%)	Ignition Oven	-	-	5.2	4.9	5.0	4.9
	*Image Analysis	17.8	16.2	26.3	22.2	33.5	29.1

CHAPTER FIVE

SUMMARY, CONCLUSIONS, AND RECOMMENDATIONS

Summary

A porous pavement is a type of sustainable pavement that allows stormwater to infiltrate through the pavement into the natural soil bed. An open-graded friction course (OGFC) is a type of porous asphalt mixture that is commonly used as a sacrificial wearing course, typically less than 1.5-in thick, constructed over a conventional asphalt pavement. This sacrificial wearing course is used to improve the frictional resistance of pavements and minimize hydroplaning on highways. The use of OGFC provides major advantages to the asphalt pavement surface such as improvements in safety, economy, and the environment. The goal of this research was to:

a. Evaluate and quantify long-term draindown, and investigate how long-term draindown influences the raveling susceptibility of OGFC.

b. Identify the underlining mechanism using newly designed laboratory test methods compared to the existing test method that is used to evaluate the raveling susceptibility of OGFC.

This evaluation was based on the comparison of two OGFC mixtures (a lab prepared mix and WMA plant-mix) using five main criteria: image analysis of long-term draindown, binder content by use of ignition oven, indirect tensile strength, direct shear strength, and abrasion resistance test methods on un-aged, aged and flipped aged specimens.

CONCLUSIONS

Based on the results of this study on the effects of long-term draindown and the raveling susceptibility of OGFC asphalt mixtures, the following conclusions were made based on the two primary objectives of this study: (1) Evaluation of Raveling Susceptibility Test Methods and (2) Quantification of Binder Long-term Draindown

Evaluation of Raveling Susceptibility Test Methods

- The planetary and singular motion surface abrasion test methods showed similar trends to the direct shear strength and indirect tensile strength tests. These test methods showed a lower percent mass loss for the aged specimens while the direct shear and indirect tensile tests showed higher strengths for the aged specimens when compared to the unaged specimens.

- The Cantabro test method showed different results than the other test methods. The unaged specimens exhibited the lowest percent mass loss and the aged specimens had the highest percent mass loss.

- Based on visual observation of the tested specimens, the Cantabro test method is an impact based test procedure, which results in fracturing of aggregate particles

rather than a surface abrasion test. This mode of failure is not typical in OGFC pavements over its service life. However, the surface abrasion test methods used in this study experienced more aggregate particle dislodgement from the pavement surface.

- The planetary motion surface abrasion test method was more abrasive than the singular motion surface abrasion test method. The planetary motion surface abrasion test dislodged larger aggregate particles when compared to the singular motion surface abrasion test method due to the compound rotation of the testing head over the surface of the specimen.

- Cutter head B (triangular) was more abrasive than cutter head A (square) for both test methods (Singular and Planetary) due to its sharper, triangular cutter head, which allowed it to dig deeper into the pavement surface. However, the trends of the results for both cutter heads were similar.

<u>Quantification of Long-term Binder Draindown</u>

- Image analysis of the cut faces of test specimens conditioned at high temperature (60°C) showed that binder does migrate downward over time (i.e., long-term draindown). The analysis procedure used in this study provided the ability to quantify the change in binder content (percent by area) of a particular horizontal slice over time. Appendix F shows the visual inspection of the long-term draindown over the 56 days of aging for all aging conditions, and draindown is visible over the 56 day aging period in 28 day intervals.

145

- The analysis procedures allowed for higher resolution of the specimen, therefore enabling better visualization of binder draindown and how it is influenced by the void structure of the specimen.

- The Draindown Factor [D_F] was the term assigned to quantify the long-term draindown. The D_F is calculated as inverse of the slope profile of the average change in binder content with specimen depth from 0 to 56 days of aging. The area of interest for long-term draindown is the top 1 to 1.5 inches of a specimen as this is the typical thickness of an OGFC layer.

- When comparing the Draindown Factor [D_F] to the raveling susceptibility of the aged specimens, a direct correlation could be seen between the long-term binder draindown and the raveling susceptibility of OGFC. The higher the D_F, the higher the percent mass loss of the specimens, therefore binder draindown directly effects the raveling susceptibility of the specimens.

- The flipped aged specimens had the lowest Draindown Factor [D_F] when compared to the aged specimens at all three compaction levels (20, 35, and 50 gyrations). Inverting the specimen allowed gravity to move the flow of binder in a reversing effect.

The Effect of Long-term Binder Draindown on the Raveling Susceptibility of OGFC

- An increase in Draindown Factor [D_F] resulted in a higher percent mass loss in the surface abrasion test methods, indicating a higher susceptibility to raveling of OGFC. The flipped aged specimens had the lowest percent mass loss and D_F, indicating a lower susceptibility to raveling.

Recommendations for Implementation

- This study shows that the Cantabro abrasion test method may not be best test method to evaluate the raveling susceptibility of OGFC because it is more of an impact test and not representative of the abrasion seen on OGFC pavements in the field during its service life. The planetary and singular motion surface abrasion test methods are more representative of the raveling susceptibility of OGFC pavements and could be consider a test method used to evaluate raveling susceptibility in the laboratory.

- The binder content of the mix design could be increased in order to minimize the effects of long-term draindown and raveling susceptibility of OGFC.

Recommendations for Future Work

- Expand this study to evaluate longer conditioning durations, mix design variables and their effects on the draindown factor [D_F]. (e.g. look at different binder types and contents; and evaluate their effect on the surface abrasion of OGFC).

- Further, refine the image analysis process of long-term draindown by improving the imaging process and setup.

- Correlate the surface abrasion lab results of OGFC to field performance.

147

APPENDICES

APPENDIX A

Abrasion Resistance

Table A.1 – Cantabro Abrasion Data for the Un-Aged Specimens, 56 Day Aged Un-

Flipped Specimens, and the 56 Day Aged Flipped Specimens

Specimen Conditioning Type	Specimen	Porosity	Raveling (%)	Average Raveling (%)	Standard Deviation
Un-aged	34	15.0	9.6	10.5	0.91
	40	15.5	11.4		
	47	12.5	10.4		
Aged 56 Day	13	17.2	22.0	18.4	3.2
	24	15.2	17.2		
	42	10.6	15.9		
Flipped 56 Day	6	15.4	17.4	16.5	0.88
	11	16.1	16.5		
	36	11.5	15.6		

APPENDIX B

Direct Shear Strength Test

Table B.1 – Direct Shear Strength Test Data for the Un-Aged Specimens

Location of Specimen Testing	Specimen	Porosity (%)	Stress (psi)	Average Stress (psi)	Standard Deviation
Top of Specimen	12	16.6	42.4	36.3	6.9
	41	13.4	28.9		
	49	13.2	37.6		
Bottom of Specimen	12	16.6	29.3	26.4	2.4
	41	13.4	25.9		
	49	13.2	24.8		

Table B.2 – Direct Shear Strength Test Data for the 56 Day Aged Specimens

Location of Specimen Testing	Specimen	Porosity (%)	Stress (psi)	Average Stress (psi)	Standard Deviation
Top of Specimen	14	16.5	86.9	82.6	3.7
	31	15.1	80.5		
	52	11.6	80.6		
Bottom of Specimen	14	16.5	75.2	70.1	5.1
	31	15.1	65.1		
	52	11.6	70.1		

Table B.3 – Direct Shear Strength Test Data for the Flipped 56 Day Aged Specimens

Location of Specimen Testing	Specimen	Porosity (%)	Stress (psi)	Average Stress (psi)	Standard Deviation
Top of Specimen	16	17.5	82.5	87.1	4.1
	54	12.3	88.4		
	58	13.2	90.3		
Bottom of Specimen	16	17.5	81.7	77.4	4.1
	54	12.3	73.5		
	58	13.2	77.0		

APPENDIX C

<u>Circular Motion Surface Abrasion Test</u>

Table C.1 –Circular Motion Surface Abrasion Data for the Zero Day Aged

Specimens (Cutter Head A)

Location of Specimen Testing	Specimen	Porosity (%)	Percent Mass Loss per Cycle					
			1	2	3	4	5	6
Top of Specimen	2	15.8	0.26	0.34	0.39	0.43	0.47	0.58
	18	15.3	0.19	0.40	0.45	0.51	0.61	0.65
	43	11.9	0.18	0.25	0.29	0.40	0.44	0.48
Top Average Percent Mass Loss (psi)	2 18 43	N/A	0.21	0.33	0.38	0.44	0.51	0.57
Top Standard Deviation	2 18 43	N/A	0.04	0.08	0.08	0.06	0.09	0.08
Bottom of Specimen	2	15.8	0.11	0.20	0.27	0.32	0.40	0.46
	18	15.3	0.22	0.37	0.44	0.50	0.57	0.60
	43	11.9	0.14	0.22	0.31	0.40	0.44	0.48
Bottom Average Percent Mass Loss (psi)	2 18 43	N/A	0.16	0.26	0.34	0.40	0.44	0.48
Bottom Standard Deviation	2 18 43	N/A	0.06	0.09	0.09	0.09	0.09	0.08

Table C.2 –Circular Motion Surface Abrasion Data for the Zero Day Aged

Specimens (Cutter Head B)

Location of Specimen Testing	Specimen	Porosity (%)	Percent Mass Loss per Cycle					
			1	2	3	4	5	6
Top of Specimen	3	14.9	0.27	0.45	0.64	0.75	0.88	0.99
	21	12.7	0.30	0.57	0.69	0.77	0.86	1.01
	25	15.5	0.43	0.58	0.70	0.76	0.87	1.02
Top Average Percent Mass Loss (psi)	3 21 25	N/A	0.33	0.53	0.68	0.76	0.87	1.01
Top Standard Deviation	3 21 25	N/A	0.08	0.07	0.04	0.01	0.01	0.02
Bottom of Specimen	3	14.9	0.26	0.43	0.69	0.78	0.82	0.92
	21	12.7	0.27	0.46	0.60	0.73	0.83	0.94
	25	15.5	0.26	0.42	0.58	0.70	0.84	0.94
Bottom Average Percent Mass Loss (psi)	3 21 25	N/A	0.27	0.44	0.62	0.73	0.83	0.94
Bottom Standard Deviation	3 21 25	N/A	0.01	0.02	0.06	0.04	0.01	0.01

Table C.3 – Circular Motion Surface Abrasion Data for the 56 Day Aged Specimens

(Cutter Head A)

Location of Specimen Testing	Specimen	Porosity (%)	Percent Mass Loss per Cycle					
			1	2	3	4	5	6
Top of Specimen	9	15.1	0.06	0.16	0.29	0.40	0.49	0.63
	35	15.1	0.07	0.14	0.27	0.32	0.40	0.51
	44	12.7	0.08	0.12	0.23	0.28	0.38	0.43
Top Average Percent Mass Loss (psi)	9 35 44	N/A	0.07	0.14	0.26	0.33	0.42	0.52
Top Standard Deviation	9 35 44	N/A	0.01	0.02	0.03	0.06	0.06	0.10
Bottom of Specimen	9	15.1	0.07	0.16	0.20	0.27	0.34	0.48
	35	15.1	0.09	0.15	0.19	0.25	0.31	0.41
	44	12.7	0.08	0.12	0.16	0.23	0.28	0.36
Bottom Average Percent Mass Loss (psi)	9 35 44	N/A	0.08	0.14	0.19	0.25	0.31	0.42
Bottom Standard Deviation	9 35 44	N/A	0.01	0.02	0.02	0.02	0.03	0.06

Table C.4 – Circular Motion Surface Abrasion Data for the 56 Day Aged Specimens

(Cutter Head B)

Location of Specimen Testing	Specimen	Porosity (%)	Percent Mass Loss per Cycle					
			1	2	3	4	5	6
Top of Specimen	8	15.8	0.17	0.29	0.39	0.46	0.56	0.75
	26	14.8	0.16	0.25	0.36	0.45	0.55	0.67
	56	12.4	0.12	0.22	0.27	0.41	0.49	0.62
Top Average Percent Mass Loss (psi)	8 26 56	N/A	0.15	0.26	0.34	0.44	0.53	0.68
Top Standard Deviation	8 26 56	N/A	0.03	0.04	0.06	0.02	0.04	0.07
Bottom of Specimen	8	15.8	0.16	0.25	0.32	0.36	0.47	0.58
	26	14.8	0.13	0.20	0.29	0.35	0.46	0.55
	56	12.4	0.11	0.17	0.23	0.30	0.35	0.49
Bottom Average Percent Mass Loss (psi)	8 26 56	N/A	0.13	0.21	0.28	0.34	0.42	0.54
Bottom Standard Deviation	8 26 56	N/A	0.03	0.04	0.05	0.03	0.07	0.04

Planetary Motion Surface Abrasion Test

Table D.1 –Planetary Motion Surface Abrasion Data for the Zero Day Aged

Specimens (Cutter Method A)

Location of Specimen Testing	Specimen	Porosity (%)	Percent Mass Loss per Cycle					
			1	2	3	4	5	6
Top of Specimen	15	15.9	0.88	1.31	1.40	1.61	1.75	1.87
	27	15.0	0.56	0.94	1.25	1.48	1.73	1.79
	60	12.2	0.43	0.72	0.89	1.06	1.07	1.16
Top Average Percent Mass Loss (psi)	15 27 60	N/A	0.62	0.99	1.18	1.38	1.52	1.61
Top Standard Deviation	15 27 60	N/A	0.24	0.30	0.27	0.29	0.39	0.39
Bottom of Specimen	15	15.9	0.60	1.00	1.40	1.59	1.69	1.75
	27	15.0	0.41	0.68	0.90	1.16	1.29	1.42
	60	12.2	0.40	0.51	0.56	0.71	0.82	0.93
Bottom Average Percent Mass Loss (psi)	15 27 60	N/A	0.47	0.73	0.95	1.15	1.27	1.36
Bottom Standard Deviation	15 27 60	N/A	0.11	0.25	0.42	0.44	0.44	0.41

Table D.2 –Planetary Motion Surface Abrasion Data for the Zero Day Aged

Specimens (Cutter Method B)

Location of Specimen Testing	Specimen	Porosity (%)	Percent Mass Loss per Cycle					
			1	2	3	4	5	6
Top of Specimen	19	15.1	1.81	2.05	2.31	2.40	2.49	2.55
	22	13.9	1.80	1.86	1.93	2.01	2.09	2.23
	37	14.1	2.14	2.30	2.41	2.55	2.60	2.71
Top Average Percent Mass Loss (psi)	19 22 37	N/A	1.92	2.07	2.22	2.32	2.40	2.49
Top Standard Deviation	19 22 37	N/A	0.20	0.22	0.25	0.28	0.27	0.24
Bottom of Specimen	19	15.1	1.31	1.59	1.84	1.99	2.08	2.13
	22	13.9	1.62	1.82	2.18	2.42	2.49	2.54
	37	14.1	1.46	1.69	1.86	2.01	2.23	2.29
Bottom Average Percent Mass Loss (psi)	19 22 37	N/A	1.47	1.70	1.96	2.14	2.27	2.32
Bottom Standard Deviation	19 22 37	N/A	0.15	0.11	0.19	0.24	0.21	0.21

Table D.3 –Planetary Motion Surface Abrasion Data for the 56 Day Aged

Specimens (Cutter Method A)

Location of Specimen Testing	Specimen	Porosity (%)	Percent Mass Loss per Cycle					
			1	2	3	4	5	6
Top of Specimen	1	13.1	0.30	0.54	0.72	0.85	0.99	1.18
	20	13.8	0.31	0.48	0.59	0.70	0.83	1.09
	30	16.2	0.32	0.51	0.69	0.85	1.01	1.16
Top Average Percent Mass Loss (psi)	1 20 30	N/A	0.31	0.51	0.67	0.80	0.94	1.14
Top Standard Deviation	1 20 30	N/A	0.01	0.03	0.06	0.08	0.10	0.05
Bottom of Specimen	1	13.1	0.14	0.45	0.58	0.74	0.81	0.95
	20	13.8	0.19	0.36	0.53	0.61	0.63	0.72
	30	16.2	0.15	0.34	0.60	0.67	0.75	0.92
Bottom Average Percent Mass Loss (psi)	1 20 30	N/A	0.16	0.38	0.57	0.67	0.73	0.86
Bottom Standard Deviation	1 20 30	N/A	0.03	0.06	0.04	0.06	0.09	0.12

Table D.4 –Planetary Motion Surface Abrasion Data for the 56 Day Aged

Specimens (Cutter Method B)

Location of Specimen Testing	Specimen	Porosity (%)	Percent Mass Loss per Cycle					
			1	2	3	4	5	6
Top of Specimen	7	15.9	0.67	0.86	1.20	1.41	1.98	2.16
	33	15.6	0.77	1.03	1.38	1.70	1.85	1.97
	46	11.7	0.46	0.61	1.08	1.49	1.73	1.93
Top Average Percent Mass Loss (psi)	7 33 46	N/A	0.63	0.83	1.22	1.53	1.86	2.02
Top Standard Deviation	7 33 46	N/A	0.16	0.21	0.15	0.15	0.12	0.12
Bottom of Specimen	7	15.9	0.39	0.66	0.90	1.19	1.48	1.77
	33	15.6	0.40	0.54	0.89	1.06	1.29	1.53
	46	11.7	0.34	0.47	0.84	1.03	1.45	1.79
Bottom Average Percent Mass Loss (psi)	7 33 46	N/A	0.38	0.56	0.88	1.09	1.41	1.70
Bottom Standard Deviation	7 33 46	N/A	0.03	0.09	0.03	0.09	0.10	0.15

Table D.5 –Planetary Motion Surface Abrasion Data for the Flipped 56 Day Aged

Specimens (Cutter Method A)

Location of Specimen Testing	Specimen	Porosity (%)	Percent Mass Loss per Cycle					
			1	2	3	4	5	6
Top of Specimen	5	15.9	0.28	0.39	0.50	0.65	0.76	0.80
	39	15.5	0.20	0.54	0.72	0.83	0.94	1.10
	55	11.5	0.32	0.41	0.46	0.51	0.54	0.58
Top Average Percent Mass Loss (psi)	5	N/A	0.27	0.45	0.56	0.66	0.75	0.82
	39							
	55							
Top Standard Deviation	5	N/A	0.06	0.09	0.14	0.16	0.20	0.26
	39							
	55							
Bottom of Specimen	5	15.9	0.30	0.44	0.49	0.52	0.56	0.62
	39	15.5	0.35	0.46	0.50	0.55	0.65	0.69
	55	11.5	0.16	0.21	0.24	0.27	0.31	0.37
Bottom Average Percent Mass Loss (psi)	5	N/A	0.27	0.37	0.41	0.45	0.51	0.56
	39							
	55							
Bottom Standard Deviation	5	N/A	0.10	0.14	0.15	0.16	0.17	0.16
	39							
	55							

Indirect Tensile Strength (Modulus of Toughness)

Table E.1 – Indirect Tensile Strength and Modulus of Toughness Data for both the

Un-Aged and 56 Day Aged Specimens

Un-Aged				Aged			
Specimen	Porosity (%)	Modulus of Toughness (lbf/in)	Indirect Tensile Strength (psi)	Specimen	Porosity (%)	Modulus of Toughness (lbf/in)	Indirect Tensile Strength (psi)
17	17.5	11.5	75.2	**10**	16.2	16.9	95.8
50	12.4	15.9	76.4	**38**	14.7	15.3	99.9
57	13.1	17.0	71.3	**59**	12.1	17.5	104.1
Average	14.3	14.8	74.3	**Average**	14.3	16.6	99.9
Standard Deviation	2.7	2.9	2.7	**Standard Deviation**	2.1	1.1	4.2

Evaluation of Long-Term Draindown

(20-1) Before Aging

(20-2) Before Aging

(20-1) After Aging 28 Days

(20-2) After Aging 28 Days

(20-1) After Aging 56 Days

(20-2) After Aging 56 Days
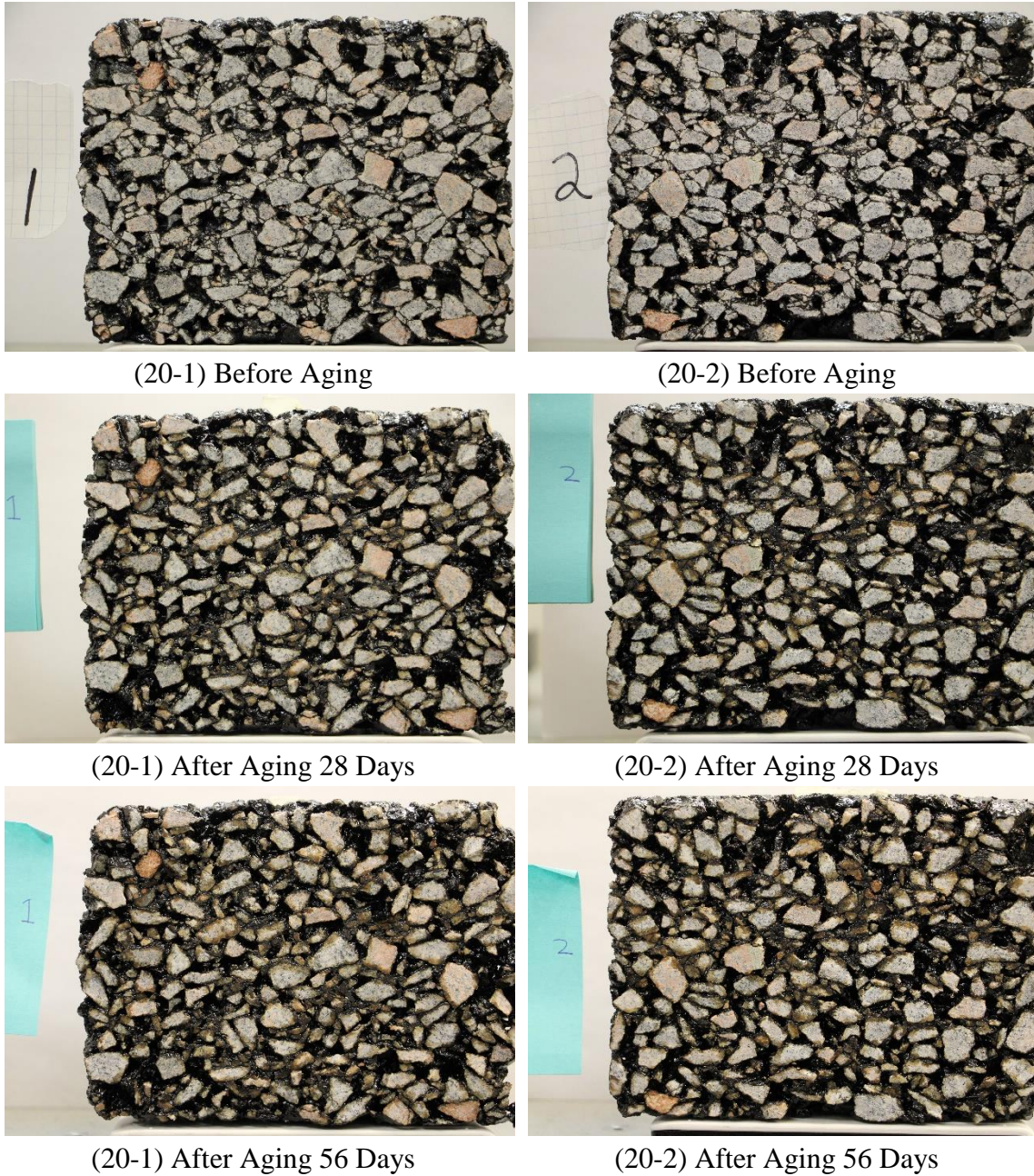
Figure F.1 – Long-Term Draindown Over Time of the Specimen with 20 Gyrations
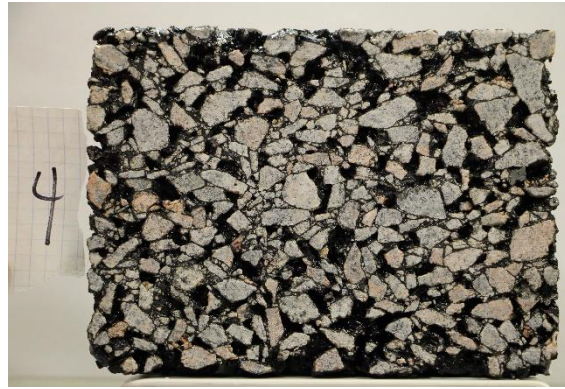
(35-1) Before Aging   (35-2) Before Aging

(35-1) After Aging 28 Days   (35-2) After Aging 28 Days

(35-1) After Aging 56 Days   (35-2) After Aging 56 Days

Figure F.2 – Long-Term Draindown Over Time of the Specimen with 35 Gyrations

(50-1) Before Aging   (50-2) Before Aging

(50-1) After Aging 28 Days   (50-2) After Aging 28 Days

(50-1) After Aging 56 Days   (50-2) After Aging 56 Days
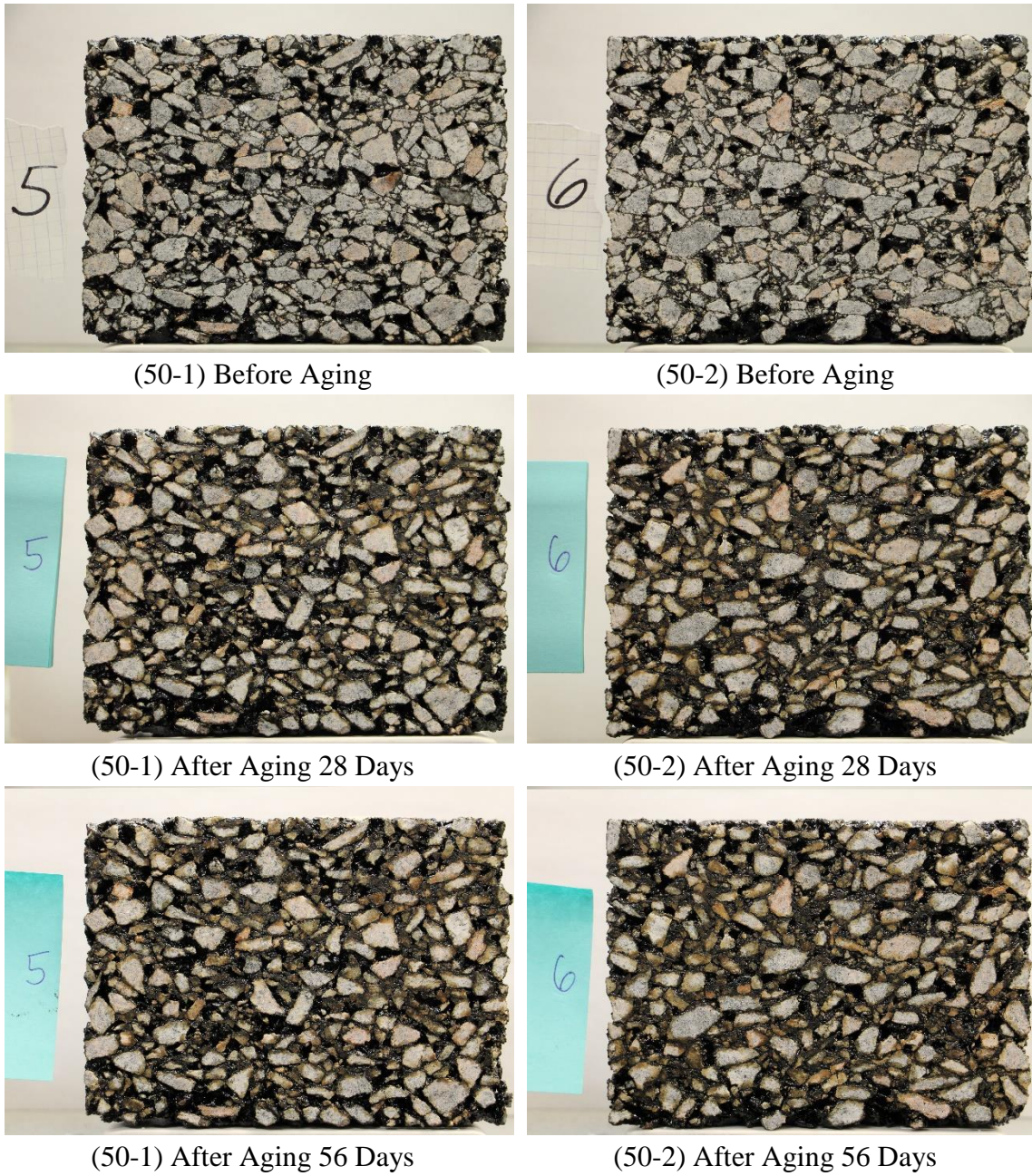
Figure F.3 – Long-Term Draindown Over Time of the Specimen with 50 Gyrations

(50-1-F) Before Aging

(50-2-F) Before Aging

(50-1-F) After Aging 28 Days

(51-2-F) After Aging 28 Days

(50-1-F) After Aging 56 Days

(50-2-F) After Aging 56 Days

Figure F.4 –Long-Term Draindown Over Time of the Flipped Specimen Number 4 with 50 Gyrations

(50-3-F) Before Aging

(50-4-F) Before Aging

(50-3-F) After Aging 28 Days

(50-4-F) After Aging 28 Days

Failed During Conditioning
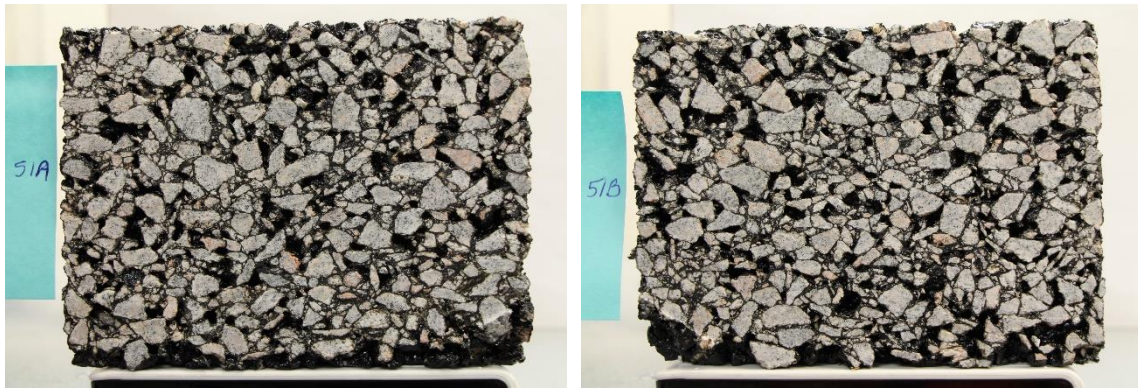

(50-3-F) After Aging 56 Days

(50-4-F) After Aging 56 Days

**Figure F.5 – Long-Term Draindown Over Time of the Flipped Specimen Number 51
with 50 Gyrations**

Binder Content

Table G.1 – Binder Content for Un-Aged, 56 Day Aged, and Flipped Specimens

Un-Aged											
Specimen	23				48				62			
Slice	1	2	3	4	1	2	3	4	1	2	3	4
Binder Content (%)	5.22	5.35	5.13	5.55	5.13	5.75	5.51	5.25	5.69	5.85	5.83	5.82
Slice	**1**				**2**				**3**			**4**
Average Binder Content (%)	5.35				5.65				5.49			5.54
Standard Deviation	0.30				0.26				0.35			0.29
Aged												
Specimen	32				53				N/A			
Slice	1	2	3	4	1	2	3	4				
Binder Content (%)	5.16	5.26	5.15	5.01	5.45	5.78	5.57	5.15				
Slice	**1**				**2**				**3**			**4**
Average Binder Content (%)	5.31				5.52				5.36			5.08
Standard Deviation	0.21				0.37				0.30			0.10
Flipped-Aged												
Specimen	28				61				N/A			
Slice	1	2	3	4	1	2	3	4				
Binder Content (%)	4.95	5.36	5.19	4.99	5.84	5.85	5.54	5.64				
Slice	**1**				**2**				**3**			**4**
Average Binder Content (%)	5.40				5.61				5.37			5.32
Standard Deviation	0.63				0.35				0.25			0.46

REFERENCES

Alvarez, A. E. et al. 2009. "Determination of Volumetric Properties for Permeable Friction Course Mixtures." *Journal of Testing and Evaluation* (2009): Vol. 37. pp. 1–10. Print.

Caltrans. "Open Graded Friction Course Usage Guide." California Department of Transportation Report. Feb. 8, 2006.

Hamzah, M.O., et al. "The Effects of Initial Conditioning and Ambient Temperatures on Abrasion Loss and Temperature Change of Porous Asphalt." *Construction and Building Materials* (2012): 108-113. Print.

Hardiman, C . "The Improvement of Water Drainage Function and Abrasion Loss of Conventional Porous Asphalt." *Eastern Asia Society for Transportation Studies* (2005): Vol 5. Pp. 671-678. Print.

Hirst, K. "The Ancient Uses of Asphalt - 40,000 Years of Bitumen." Archaeology.about.com.14 Mar. 2016. Web. 12 Dec. 2016.

Huber, G. "Performance Survey on Open-Graded Friction Course Mixes." *NCHRP Synthesis of Highway Practice 284. Transportation Research Board, National Research Council*. Washington, D.C.; 2000.

Ferguson, Bruce K. "Porous Pavements." *Boca Raton, FL: Taylor & Francis*, 2005. Print.

Kandhal, P.,and Mallick, R. "Open-graded friction course: State of the practice."

Transportation Research Board of the National Academies, Washington, DC

(1998).

Kandhal, P., and National Asphalt Pavement Association. *Design, Construction,*

and Maintenance of Open-graded Asphalt Friction Courses. National Asphalt

Pavement Association, Lanham MD. 2002.

Kluttz. "An Introduction to Modified Asphalt Binders." *Nebraska Asphalt Paving*

Conference. 2012.

Lavin, Patrick. *Asphalt Pavement: A Practical Guide to Design, Production, and*

Maintenance for Engineers and Architects. Spon Press. London and New York.

 2003.

Lu, X. and Isacsson, U. "Chemical and Rheological Evaluation of Ageing Properties of

SBS Polymer Modified Bitumen." *Elsevier Science: Fuel.* Volume 77: pp 961-

972. 1998.

Lu, X. and Isacsson, U. "Effect of Ageing on Bitumen Chemistry and Rheology."

Construction and Building Materials. Volume 16. Pp. 15-22. 2002.

Mallick, Rajib B. et al. 2000 "Design, Construction, and Performance of New-Generation

 Open-graded Friction Courses." *Asphalt Paving Technology* 69 (2000): 391-423.

Mansour, T.N., and Putman, B.J. "Influence of Aggregate Gradation on the Performance Properties of Porous Asphalt Mixtures." *Journal of Materials in Civil Engineering* (2013): 281-288. Print.

Martinez-Boza, F. et al. "Rheology and Microstructure of Asphalt Binders." *Springer-Verlag: Rheological Acta.* Volume 40: pp135-141. 2001.

Mathavan, S., Rahman, M.M., Stonecliffe-Jones, M. and Kamal, K. "Pavement Raveling Detection and Measurement from Synchronized Intensity and Range Images." *Journal of the Transportation Research Board,* Washington, D.C., 2014, No. 2457, pp. 3-11.

Mitchell, R., Woodward, D., and Maguire, C. "Development of an Asphalt Durability Raveling Test." *Sustainability, Eco-efficiency and Conservation in Transportation Infrastructure Asset Management,* Taylor & Francis Group, London, 2014.

Mogawer, W. et al 2011. "Evaluation of Binder Elastic Recovery on HMA Fatigue Cracking Using Continuum Damage and Overlay Test Based Analyses." *Road Material and Pavement Design.* Volume 12, pp. 345-376. 2011.

"Porous Pavement: Pavement That Leaks." *POROUS PAVEMENT: Pavement That Leaks*. Web. 27 Sept. 2012. http://www.millermicro.com/porpave.html.

Poulikakos, L.D., and M.N. Partl. "Evaluation of Moisture Susceptibility of Porous Asphalt Concrete Using Water Submersion Fatigue Tests." *Construction and Building Materials*. 2009: 3475-3484.

Putman, B.J. "Evaluation of Open-Graded Friction Courses: Construction, Maintenance, and Performance." South Carolina Department of Transportation-Final Report, October 2012.

Putman, B.J. and Lyons, K.R. "Laboratory Evaluation of Long-Term Draindown of Porous Asphalt Mixtures." *Journal of Materials in Civil Engineering.* 2015.

"Raveling" 7 April 2009. *Pavement Interactive: Raveling.* Web. 7 Nov 2016 http://www.pavementinteractive.org/article/raveling/.

Shaowen, D.U. and Shanshan, L.I. "The Raveling Characteristics of Porous Asphalt Mixture." ICTE, 2011, pp.1880-1885.

Shirodkar, P. et al. 2012. "Characterization of Creep and Recovery Curve of Polymer Modified Binder." *Construction and Building Materials.* Volume 34, pp 504-511. 2012.

"Warm Mix Asphalt" 14 November 2016. *U.S. Department of Transportation: Federal Highway Administration.* Web. 2 Feb 2017. https://www.fhwa.dot.gov

Yildirim, Y. "Polymer Modified Asphalt Binders." *Construction and Building Materials.* Issue 21, Volume 1, pp: 66-72. 2007.